The Dissertation Committee for Hsing-Yu Tuan Certifies that this is the approved version of the following dissertation

Synthesis and Characterization of Silicon and Germanium Nanowires, Silica Nanotubes, and Germanium Telluride/Tellurium Nanostructures

Committee:

Brian A. Korgel, Supervisor

James R. Chelikowsky

Paulo Ferreira

Roger T. Bonnecaze

Miguel Jose Yacaman

Synthesis and Characterization of Silicon and Germanium Nanowires, Silica Nanotubes, and Germanium Telluride/Tellurium Nanostructures

by

Hsing-Yu Tuan, B.S.

Dissertation

Presented to the Faculty of the Graduate School of

The University of Texas at Austin

in Partial Fulfillment

of the Requirements

for the Degree of

Doctor of Philosophy

The University of Texas at Austin

May 2007

Dedication

To my family and loved ones

Acknowledgements

I would like to acknowledge all of the people who assisted in my graduate study. I thank all of the members of the Korgel group for motivating, enjoyable and supportive research environment. Especially, I would like to thank Doh Change Lee for sharing me his priceless research experience and leading me to the right track during my Ph.D trip, Tobias Hanrath for instructing me on the supercritical fluid synthesis, Ali Ghezelbash for learning funny American idioms, Xianmao Lu for research sharing, Dayne Fanfair for useful research discussion and critics, Danielle Smith for making me warm in the big cold office and other group members, Michael Sigman, Cindy Stowell, April Schricker, Aaron Saunders, Felice Shieh, Preeti Sood, Tripp Davidson, Bonil Koo, Damon Smith, Andy Heitsch, Vince Holmberg, Matt Panthani, Michael Rasch and Vahid Akhavan.

The TEM is the most important tool in my research. I would especially thank Dr. Zhou for his assistance and training on the operation with this microscope.

I also thank my committee – Dr. James R. Chelikowsky, Dr. Ferreira, Dr. Bonnecaze, and Dr. Yacaman for their suggestions; especially, my advisor Dr. Korgel for his advice and guidance. Finally I want to thank my parents and family for their encouragement, love, patience and support.

Synthesis and Characterization of Silicon and Germanium Nanowires, Silica Nanotubes, and Germanium Telluride/Tellurium Nanostructures

Publication No._____

Hsing-Yu Tuan, Ph.D.

The University of Texas at Austin, 2007

Supervisor: Brian A. Korgel

A supercritical fluid-liquid solid (SFLS) nanowire growth process using alkanethiol-coated Au nanoparticles to seed silicon nanowires was developed for synthesizing silicon nanowires in solution. The organic solvent was found to significantly influence the silicon precursor decomposition in solution. 46.8 mg of silicon nanowires with 63% yield of silicon nanowire synthesis were achieved while using benzene as a solvent.

The most widely used metal for seeding Si and Ge nanowires is Au. However, Au forms deep trap in both Si and Ge and alternative metal seeds are more desirable for electronic applications. Different metal nanocrystals were studied for

Si and Ge nanowire synthesis, including Co, Ni, CuS, Mn, Ir, $MnPt_3$, Fe_2O_3, and FePt. All eight metals have eutectic temperatures with Si and Ge that are well above the nanowire growth temperature. Unlike Au nanocrystals, which seed nanowire growth through the formation of a liquid Au:Si (Au:Ge) alloy, these other metals seed nanowires by forming solid silicide alloys, a process we have called "supercritical fluid-solid-solid" (SFSS) growth. Moreover, Co and Ni nanoparticles were found to catalyze the decomposition of various silane reactants that do not work well to make Si nanowires using Au seeds. In addition to seeding solid nanowires, CuS nanoparticles were found to seed silica nanotubes via a SFSS like mechanism. 5% of synthesized silica nanotubes were coiled.

Heterostructured nanomaterials are interesting since they merge the properties of the individual materials and can be used in diverse applications. GeTe/Te heterostructures were synthesized by reacting diphenylgermane (DPG) and TOP-Te in the presence of organic surfactants. Aligned Te nanorods were grown on the surface facets of micrometer-size germanium telluride particles.

Table of Contents

List of Tables

List of Figures

Chapter 1: Introduction

1.1 ONE-DIMENSIONAL NANOSTRUCTURES

Intensive efforts of materials science focus on dealing with nanoscale materials, i.e., with characteristic dimensions between 1 and 100 nm. The advance of synthetic strategies and characterization techniques help researchers precisely control and utilize these tiny materials. When the size shrinks to the nanoscale, the large surface-to-volume ratio and quantum size effects of materials give rise to unique electrical, optical, magnetic, mechanical and chemical properties and can be used in diverse applications such as optoelectronics, sensing, catalysts, medical cures and have been proposed as the building blocks of future electronics.

In addition to size, the dimensionality of the nanostructures has strong affects material properties. One-dimensional (1D) nanostructures, such as nanowires, nanorods, and nanotubes, have attracted attention because of their possible use as electronic channels, interconnects and functional building blocks in electronic, optoelectronic and nanofluidic devices. For example, semiconductor nanowires can be used to fabricate various prototype nanoscale electronic devices such as field effect transistors, photodetectors, and chemical sensors.[1-5] Hollow inorganic nanotubes might serve as nanoscale pipes to transport fluid and molecular species and have been proposed as building blocks for nanofluidic systems.[6-9]

Semiconductor nanorods have been explored for use in efficient solar cell devices.[10-12]

Group IV semiconductors such as silicon, germanium and their compounds, germanium telluride, and silica are interesting because of their importance in the semiconductor industry. Therefore, understanding, the effect of dimensionality and size control on nanostructures is of great interest and robust synthetic methods of these nanomaterials are desired.

1.2 NANOWIRE SYNTHESIS

Vapor-liquid-solid (VLS) growth is an effect approach to synthesize group IV nanowires that are single crystalline, straight with a narrow size distribution, and free of defects. The VLS growth mechanism was first discovered by Wagner and Ellis in the 1960s.[13] In the first VLS experiments, silicon atoms from degradation of a silicon precursor from vapor phase by chemical vapor decomposition were deposited on an Au-film coated silicon substrate (CVD). Because the substrate temperature is above the Au:Si eutectic point, the silicon dissolves into the Au to form a liquid Au:Si eutectic droplets instead of depositing on the surface. C ontinuous feeding of silicon atoms into this liquid Au:Si eutectic droplets leads to supersaturation and nucleation of solid Si from the droplet and sequential wire growth. In conclusion, VLS nanowire growth involves four stages: (1) alloying, (2) liquidation, (3) supersaturation, and (4) nanowire nucleation

Figure 1.1 illustrated the VLS growth mechanism of Au-seeded Si nanowires. Successful wire growth by VLS requires crystallization and a sufficient concentration of semiconductor to sustain growth. The growth temperature must exceed the metal/semiconductor eutectic temperature.[14] The concentration of the semiconductor must be large enough to sustain nanowire growth. In binary metal-semiconductor systems such as Au-Si, Fe-Si, Co-Si, and Ni-Si…etc., offering a reaction condition with high temperature over binary eutectic temperatures and high concentration of feeding semiconductor atoms can promote the whisker growth.

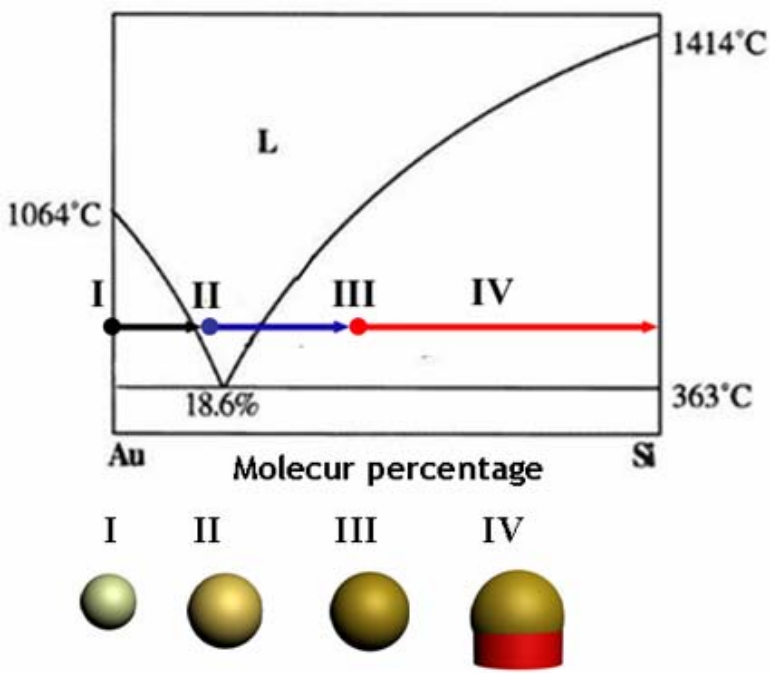

Figure 1.1: Phase diagram of Au:Si and a schematic illustration of a VLS type Au seeded silicon nanowire growth which involves (I) alloying, (II) liquidation, (III) supersaturation, and (IV) nanowire crystallization.

The use of nanosize metal particles to seed nanowire growth is critical to obtaining wires with nanometer scale distrbution. In 1995, Buhro et al. used a solution-liquid-solid (SLS) method to synthesize GaAs and GaP nanowires in organic solvent. In 1998, Morales and Lieber used a laser ablation method to produce nanoscale nanoparticles to seed Si and Ge nanowire with diameters less than 30 nm via VLS mechanism.[15] They later used this laser catalyzed growth (LCG) method to synthesize various semiconductors including, Si, Ge, GaAs, and GaP. Followed their work, chemical vapor depositon (CVD) and supercritical fluid synthesis were later developed to produce other semiconductor nanowires such as GaAs, InAs and GaP nanowires. [15-25]

The problem with laser ablation is that a very broad size distribution of nanoparticles is generated, leading to a broad nanowire distribution. In 2000, Holmes et al., reported using dodecanethiol-coated monodisperse Au nanoparticles to seed nanowires with diameters smaller than 10 nm and relatively narrow size distributions by using a supercritical fluid at a high temperature and a high pressure. Lieber and co-workers later reported controlling the diameter Si and InP grown by VLS nanowires with a narrow distribution of Au nanoparticles by combing CVD using size-monodisperse Au particles.[26]

Although CVD based nanowire synthesis allows high temperature reaction conditions and can be used to produce many different semiconductor nanowires, the throughput of one-batch nanowires is much less than the solution-based method. In a

solution-based synthesis, a larger reaction volume and higher precursor concentration gives much larger quantities of nanowires. Buhro and co-workers have shown various III-V nanowires can be synthesized in high boiling point organic solvents; however, this method can not applied to synthesize Si and Ge nanowires because the boiling points of most organic solvents are lower than the eutectic temperatures of Si and Ge.[16] Organic solvents, however, can be pressuried and heated above their critical points to access very high temperatures (up to 600 ˚C), offering reaction conditions suitable for Si and Ge nanowire synthesis. Nanowire growth in supercirtical conditions using metal nanocrystals as seeds is called supercritical fluid-liquid-solid growth mechanism (SFLS).

The SFLS method has been developed to produce crystalline Si and Ge nanowires with diameters less than 30 nm and length longer than 10μm in solution. Moreover, as shown in Chapter 2, the SFLS method is proven to produce silicon nanowires of ~50mg in a single reaction.

1.3 SUPERCRITICAL FLUIDS

A supercritical fluid (SCF) is a substance with a pressure and temperature above its critical point. Figure 1.2 shows the general pressure-temperature phase diagram and shows that a single phase fluid exists beyond the critical point where the vapor-liquid coexistence curve disappears. SCFs have the properties such as density and diffusivity intermediate between those of liquids and gas and can be

modulated gas-like to liquid-like behavior by tiny changes in temperature and pressure.[27-28] As shown in Figure 1.3, the density of the solvent can be changed from 0.1g/m to 0.6 g/m by adjusting temperature and pressure, which causes big different statuses of the same solvent. High diffusivity and low viscosity of SCFS also provide an idea platform for transporting reactants which is usually limited in conventional liquid phase.

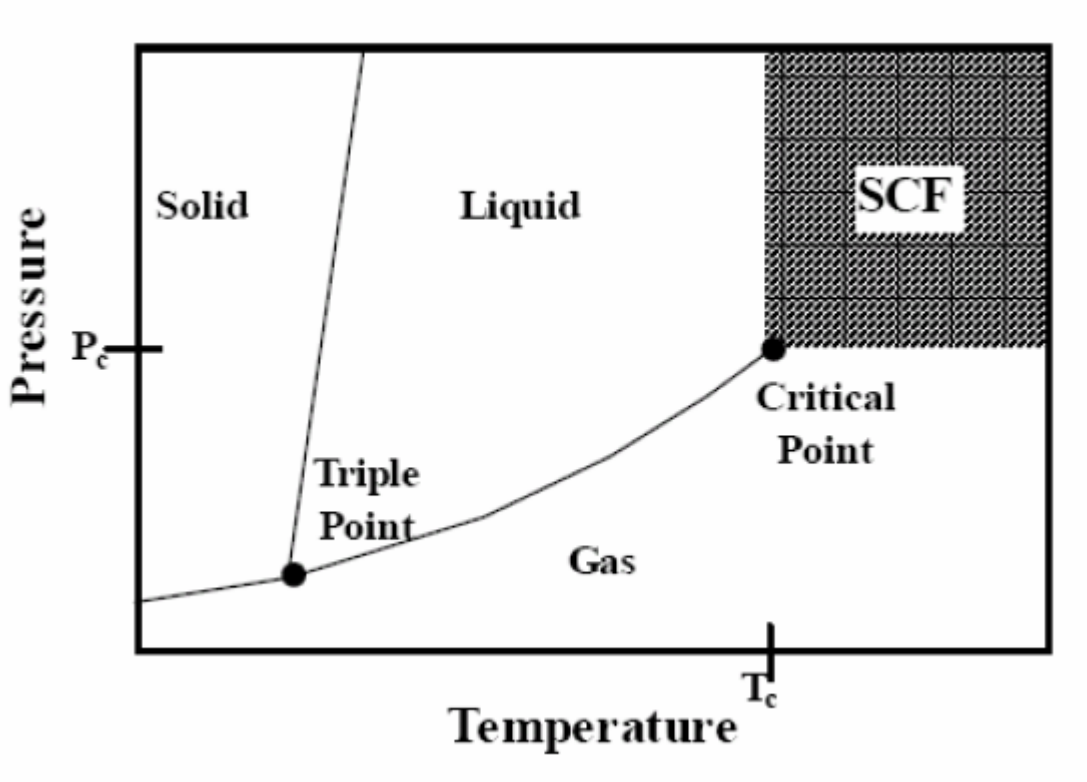

Figure 1.2: Schematic pressure-temperature equilibrium phase diagram showing the triple point, the critical point and the supercritical region.

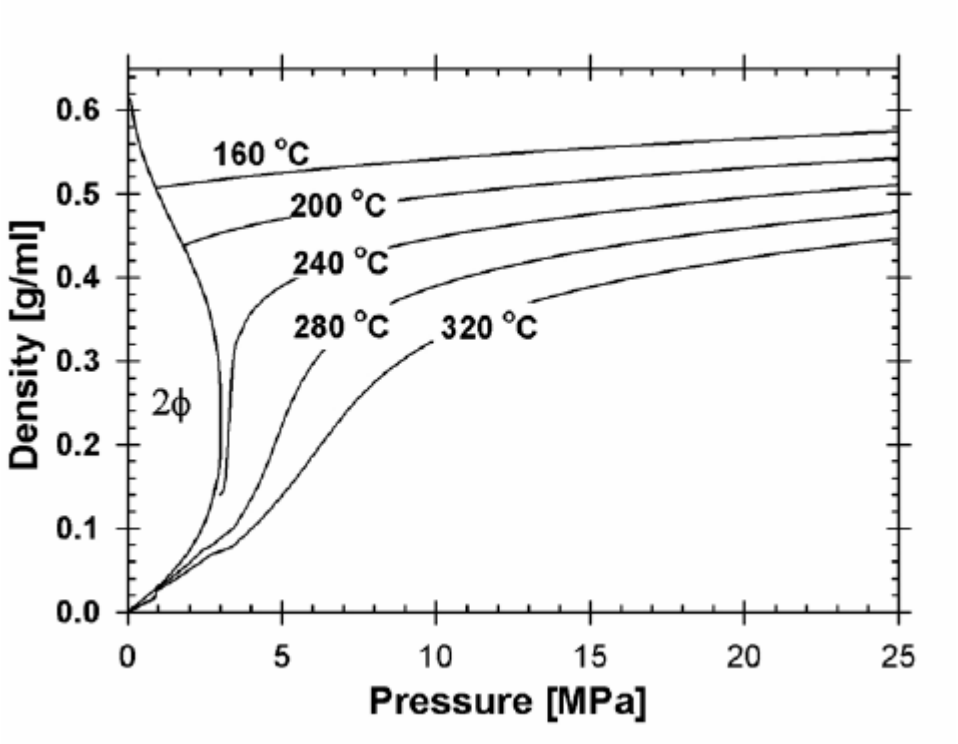

Figure 1.3: Equilibrium phase diagram of n-hexane showing density as a function of temperature and pressure

Supercritical carbon dioxide and water are the most common supercritical media and are used in industrial processes such as extraction, chromatography, and cleaning. A few years ago, researchers start to apply SCFs as part of the synthetic strategies to produce different nanomaterials. For example, Cu and CuO nanoparticles were synthesized in supercritical water and semiconductor Si and Ge nanoparticles were synthesized in supercritical hexane.[29-32] Arrested precipitation methods using organic surfactants were used to stabilize the nanoparticles and control their sizes. In the Korgel group, one dimensional nanomaterials such as

silicon and germanium nanowires and carbon nanotbues were also synthesized via a supercritical fluid-liquid-solid growth mechanism.

In conclusion, supercritical fluid is considered as a useful platform for preparing one-dimensional nanomaterials, providing access to high reaction temperatures (up to 600 ˚C) for degradation of precursors and crystallization.

1.4 SURFACTANT-MEDIATED COLLOIDAL NANOCRYSTAL SYNTHESIS

Colloidal nanocrystal synthesis in solution often involves the interactions between inorganic nanoparticles and organic surfactants to control the size and shape of nanoparticles. Surfactant molecules adhere to the surfaces of growing nanocrystals and act as stabilizing agents (also called capping ligands) to control the size and shape of nanocrystals. Murray, Norris and Bawendi in 1993[33] synthesized monodisperse CdSe nanoparticles using trioctylphosphine oxide (TOPO) as surfactants. These organic surfactants such as alkyl phosphine oxide, alky phosphonic acids, alkyl posphines, fatty acids and amines have a bonding head group and a hydrocarbon chain with hydrophobic character.

In addition to nanocrystals with nearly spherical shapes, nanocrystals with anisotropic crystallographic characteristics have different energies in different surfaces. Since the growth rate of surfaces is exponentially proportional to the surface energy, highly anisotropic shapes of nanocrystals such as nanorods, nanodisks are obtained. The surface energy of the nanocrystals can be changed by introducing surfactants undergo selective adhesion on the nanocrystal's surface. The

surface energy of the particular facets selectively stabilized by organic surfactants is lower and grows slower than the other facets. Selective adhesion of surfactants can not only direct elongation along one axis but it can also compress the plane growth along other axes as shown in Figure 1.4b.[34] More complicated shapes of nanocrystals can be obtained by this selective adhesion mechanism of organic surfactants.

. Organic surfactant-mediated synthesis of nanocrystals can be extended to hybrid nanocrystal synthesis. When some materials such as cadmium chalcogenide nanoparticles form in the wurtzite structure in the presence of some surfactants, the polar facets grow much faster than non-polar facets and form rods or tetrapods. The polar facets have higher reactivity and can allow a second material nucleate at the location, forming hybrid nanoparticles in some cases as shown in Figure 1.5.[35-36]

As described above, by interaction with inorganic nanoparticle surface, organic surfactants have been proposed as useful tools to manipulate the growth of colloidal nanocrystals. Moreover, organic surfactants are expected to have more structural and compositional control over the colloidal nanocrystal synthesis. For example, Chapter 6 respresents GeTe/Te heterostructure synthesis as one illustration of organic surfact mediated growth of colloidal nanomaterial heterostructures

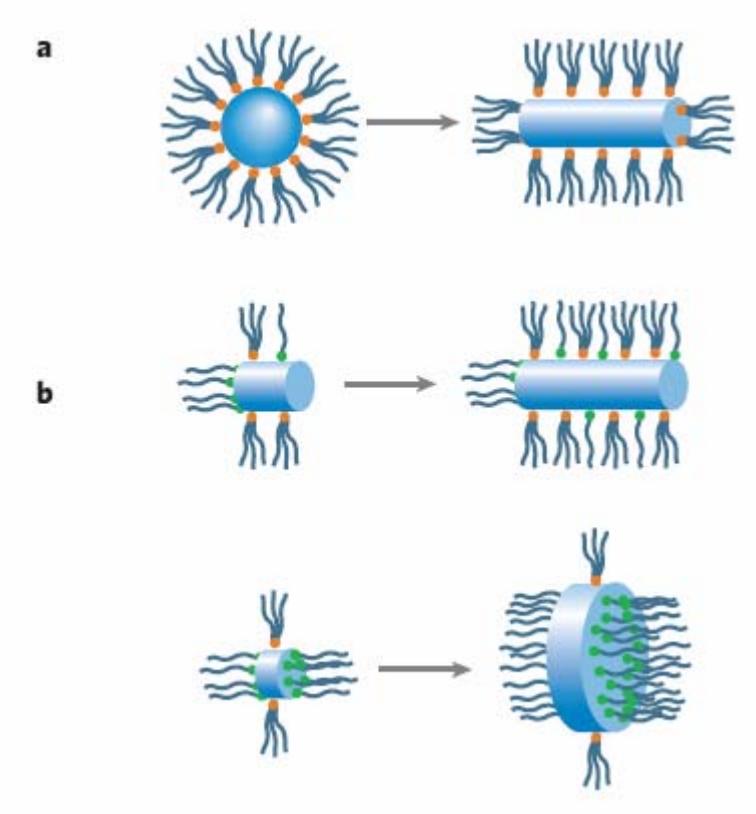

Figure 1.4: Shape control of colloidal nanocrystals via kinetic control of anisotropic crystal growth or selective adhesion of organic surfactants. a. The high-energy facets grow faster than low energy facets. b. kinetic shape control by selective adhesion of organic surfactants.(images taken from ref 34)

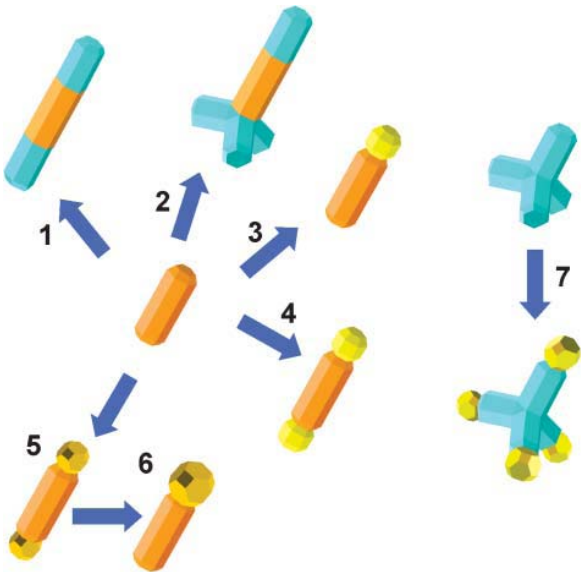

Figure 1.5: Hybrid nanocrystal heterostructures starting from rod-like seeds: a second material nucleates at polar nanorod ends which have higher reactivity. (images taken from ref 35)

1.5 DISSERTATION OVERVIEW

Chapter 2 represents an example of scale-up synthesis of silicon nanowires using an Au-seeded SFLS growth mechanism. Silicon precursor decomposition mechanism in solution is crucial for nanowire synthesis and is discussed in depth. The influence of various solvents on the conversion of Si precursors for silicon nanowire growth is investigated. Optical photographs and the weight of collected Si nanowires from Au-seeded Si nanowire synthesis in different solvents are compared.

Silicon and germanium nanowire seeded by different metal nanoparticles instead of Au in supercritical fluid are discussed in Chapter 3. The morphology, yield, crystallinity of silicon and germanium nanowires using eight different metal

nanoparticle are compared by high resolution scanning electron microscopy (HRSEM) and high resolution transmission electron microscopy (HRTEM). Catalytic properties of metal nanoparticles related to silicon precursor decomposition chemistry are also discussed. The nanowire reaction temperatures were well below the eutectic temperatures of eight different metals with Si and Ge. A new nanowire growth methanism involveing nanowire nucleation from a solid alloy – called supercritical fluid-solid-solid (SFSS) mechanism- is proposed in Chatper 4. Evidence supporting solid alloy seeding is presented, including a comprehensive comparison of Au and Ni seeding germanium nanowires.

Silica nanotubes were synthesed using copper sulfide nanoparticles in a supercritical fluid, which is discussed in Chapter 5. The morphology and composition of the silica nanotubes are characterized by HRTEM and electron energy loss spectroscopy (EELS). The effect of oxygen on Cu- and Au- seeded nanotube synthesis is compared.

In Chapter 6, the role of organic surfactants on the formation of GeTe/Te heterostructures is presented, along with the effect of reaction parameters such as surfactant concentration and surfactant types on hybrid nanostructure synthesis are investigated.

1.6 REFERENCES

(1) J. D. Holmes, K. P. Johnston, R. C. Doty, B. A. Korgel, Science 2000, 287, 1471-1473.

(2) B. A. Korgel, Science 2004, 303, 1308-1309.

(3) For a recent review, see M. Law, J. Goldberger, P. Yang, Annu. Rev. Mater. Res. 2004, 34, 83.

(4) Y. Cui, C. M. Lieber, Science 2001, 291, 851-853.

(5) M. C. McAlpine, R. S. Friedman, S. Jin, K. H. Lin, W. U. Wang, C. M. Lieber, Nano Lett. 2003, 3, 1531-1535.

(6) Goldberger, J.; Fan, R.; Yang, P. *Accounts of Chemical Research* **2006,** *39*, 239-248.

(7) Xiong, Y.; Mayers, B. T.; Xia, Y. *Chem. Commun.* **2005**, 5013-5022.

(8) Fan, R.; Karnik, R.; Yue, M.; Li, D.; Majumdar, A.; Yang, P. *Nano Letters* **2005,** *5*, 1633-1637

(9) Daiguji, H.; Yang, P.; Szeri, A. J.; Majumdar, A. *Nano Letters* **2004,** *4*, 2315-2321.

(10) Gur, I.; Fromer, N. A.; Geier, M. L.; Alivisatos, A. P. *Science* **2005,** *310*, 462-465.

(11) Liu, J. S.; Tanaka, T.; Sivula, K.; Alivisatos, A. P.; Frechet, J. M. J. *Journal of the American Chemical Society* **2004,** *126*, 6550-6551.

(12) Huynh, W. U.; Dittmer, J. J.; Alivisatos, A. P. *Science* **2002,** *295*, 2425-2427.

(13) Wagner, R. S.; Ellis, W. C. *Appl. Phys. Lett.* **1964**, *4*, 89

(14) Binary Alloy Phase Diagram, 2nd ed,; ASM Internation: Materials Park OH. 1990; Vo.1.

(15) Morales, A. M. and Lieber, C. M., S*cience* **1998**, *279*, 208-211.

(16) T. J. Trentler, K. M. Hickman, S. C. Goel, A. M. Viano, P. C. Gibbons, W. E. Buhro, Science 1995, 270, 1791.

(17) D. Fanfair, B. A. Korgel, Cryst. Growth & Des. 2005, 5, 1971-1976.

(18) H.-Y. Tuan, D. C. Lee, T. Hanrath, B. A. Korgel, Nano Lett. 2005, 5, 681.

(19) H.-Y. Tuan, D. C. Lee, T. Hanrath, B. A. Korgel, Chem. Mater. 2005, 17, 5705.

(20) Hanrath, T.; Korgel, B. A. *Adv. Mater.* **2003**, *15*, 437-440.

(21) Lee, D. C.; Mikulec, F. V.; Korgel, B. A. *J. Am. Chem. Soc.* **2004,** *126*, 4951-4957.

(22) Lee, D. C.; Hanrath, T.; Korgel, B. A. *Angew. Chem. Int. Ed.* **2005,** *44*, 3573-3577.

(23) Tuan, H.-Y.; Lee, D. C.; Korgel, B. A. *Angew. Chem, Int. Ed.* **2006,** *45*, 5184-5187.

(24) Davidson, F. M., III; Schricker, A. D.; Wiacek, R. J.; Korgel, B. A. *Adv. Mater.* **2004,** *16*, 646-649.

(25) Davidson, F. M., III; Wiacek, R.; Korgel, B. A. *Chem. Mater.* **2005,** *17*, 230-233.

(26) Cui, Y.; Lauhon, L. J.; Gudiksen, M. S.; Wang, J. F.; Lieber, C. M. *Applied Physics Letters* **2001,** *78*, 2214-2216.

(27) Savage, P. E.; Goplan, S.; Mizan, T. I.; Martino, C. J.; Brock, E. E. *AIChE Journal* **1995**, *41*, 1723-1778.

(28) Dixon, D. J.; Johnston, K. P. In *Encyclopedia of Separation*; Ruthven, D. M., Ed.; John Wiley: New York, 1997, pp 1544-1569.

(29) Ziegler, K. J.; Doty, R. C.; Johnston, K. P.; Korgel, B. A. *J. Am. Chem. Soc.* **2001**, *123*, 7797-7803.

(30) Korgel, B. A.; Hanrath, T.; Davidson, F. M. in *Encyclopedia of Chemical Processing* **1**(1) (ed Lee, S. K. B.) 3191-3203 (Marcel Dekker, 2006).

(31) For a recent review, see P. S. Shah, T. Hanrath, K. P. Johnston, B. A. Korgel, J. Phys. Chem. B 2004, 108, 9574-9587.

(32) Holmes, J. D.; Lyons, D. M.; Ziegler, K. J. *Chem. Eur. J.* **2003**, *9*, 2144-2156.

(33) Murray, C. B.; Norris, D. J.; Bawendi, M. G. *Journal of the American Chemical Society* **1993,** *115*, 8706-8715.

(34) Yin, Y.; Alivisatos, A. P. *Nature* **2005,** *437*, 664-670.

(35) Jun, Y. W.; Choi, J. S.; Cheon, J. *Angewandte Chemie-International Edition* **2006,** *45*, 3414-3439.

(36) Cozzoli, P. D.; Pellegrino, T.; Manna, L. *Chemical Society Reviews* **2006,** *35*, 1195-1208.

Chapter 2: High Yield Si Nanowire Synthesis in Supercritical Benzene

2.1 INTRODUCTION

Semiconductor nanowires are an exciting class of nanomaterials due to their size-dependent electrical and optical properties, mechanical flexibility and solution dispersibility. Silicon (Si) nanowires are particular interesting because of the importance of Si in the semiconductor industry. Silicon nanowires might be used to fabricate Si nanowire field effect transistors and highly sensitive sensors of bio-, chem- and drug- species.[1-5]

Various approaches, including chemical vapor deposition, oxide assisted, laser ablation and supercritical fluid methods have been developed to synthesize silicon nanowires.[6-12] Among these methods, colloidal metal nanoparticle-seeded silicon nanowire approach via a vapor-liquid-solid (VLS) growth mechanism is an effect way in solution to produce high quality silicon nanowires.[7] Solution-liquid-solid (SLS) growth has also been developed to synthesize II-Vl and III-V nanowires in solution. Our lab has developed a supercritical fluid-liquid-solid (SFLS) approach to synthesize group IV Si and Ge nanowires.[8-12]

One advantage of solution growth of nanowires is a much higher throughput of nanowires is possible compared to gas-phase approaches. In our lab, one-gram germanium (Ge) nanowires were recently synthesized in one batch using a 250 ml parr reactor, demonstrating that large-scale synthesis is possible.[13] However, we

found the scale up of the synthesis of silicon nanowires to be much more challenging. The yield of previous silicon nanowire synthesis we found in supercritical hexane was about only 1%, and the results we found to be very sensitive to reaction conditions such as temperature and reactant chemistry.

Chapter 2 demonstrates high yield (up to 63%) silicon nanowire synthesis in supercritical benzene. The soulvents were found to significantly influence the phenylsilane decomposition in solution. A proposed decomposition mechanism of monophenylsilane for silicon nanowire growth is also presented. Finally, various organics including phenyl- and alkyl- types are used as reaction solvents to understamd how the solvent affects the yield of Au-seeded SFLS-grown Si nanowires.

2.2 SUPERCRITICAL FLUID CONTINUOUS FLOW REACTION

2.2.1 Si Nanowire Synthesis

Supercritical fluid nanowire reactions were carried out in a 10 ml titanium grade 2 reactor. The supercritical fluid continuous flow reaction of Au-seeded silicon is shown in Figure 2.1 The inlet and outlet of the 10 ml Ti reactor cell were both connected to a high-pressure (1/16” i.d.) tubing via a LM-6 HIP (High Pressure Equipment Co.) reducer. The inlet 1/16” stainless steel tubing was collected to a six-way valve (valco) with a 10 ml injection loop. The outlet of the 10 ml cell was collected to a micro control-metering valve (HF4-V, HIP) to precisely control the

reactants outlet rate from the reactor. The reactor cell was covered with heating tape and insulation and the temperature is maintained to within ±1 ˚C by a temperature controller (Omega). A high pressure liquid chromatography (HPLC) pump was used to pressurize the reactor system and the pressure is monitored with a digital pressure gauge (Sensotech). Prior to the reaction, a clean Si deposition wafer was placed into the reactor to collect produced Si nanowires.

A typical precursor solution was prepared in a nitrogen-filled glove box. Monophenylsilane (MPS) was added to anhydrous hexane, toluene, or benzene prepared at a 125 mM concentration and calculated amount of dodecanthiol-coated Au nanoparticle solution (1 mg/ml) was added to the precursor solution to reach Au:Si ratio at 1:1000.

In a typical continuous flow nanowire reaction, the reactor was heated to desired temperature and pressured to 3.4 MPa and the outlet end was closed. The precursor solution was then brought out from the glove box and was injected into the 10ml injection loop. The precursor solution was injected at a 0.5 ml/min injection rate. When the pressure reached 6.9 MPa, the micro-control metering valve was slightly manually opened and adjusted to equilibrate the system pressure to 6.2 MPa. When the collected solution is approximately 10 ml, the micro-control metering valve was closed and the injection flow and heater was turn off. Fresh air was used to cool the reactor cell until it reached room temperature. The reactor was carefully opened because of the remaining pressure inside the reactor. The deposited

Si substrate was removed and cleaned. The Ti reactor was immersed in chroform and sonicated for 10 min for collection of nanowires deposited on the wall. All collected nanowires were then stored under nitrogen for further characterization and nanowire device fabrication.

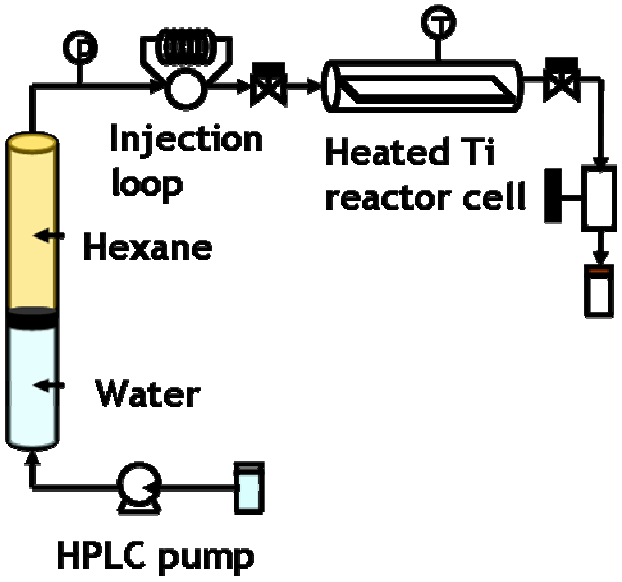

Figure 2.1: Schematic of the high pressure reactor system used for nanowire synthesis in a supercritical fluid.

2.2.2 Si nanowire Characterization

Nanowires were imaged by HRSEM on the deposition substrate without further purification using a LEO 1530 field-emission SEM at 1 – 3kV accelerating voltage with working distances ranging between 2 – 5 mm. For HRTEM and STEM imaging, nanowires were either drop-cast from chloroform dispersions or dry

transferred by scratching the deposition substrate onto 200-mesh lacey carbon-coated copper or nickel grids (Electron Microscope Sciences). Images were acquired using 200 kV accelerating voltage on a JEOL 2010F equipped with an Oxford INCA ED spectrometer.

2.3 HISTORY OF SILICON NANOWIRE SYNTHESIS IN ORGANIC SOLVENT

In 2000, Holmes et al. described silicon nanowire synthesis in supercritical hexane using organic monolayer-coated Au nanoparticles as crystallization seeds.[1] However, the synthesized silicon nanowires were coated with a thick carbonaceous layer and the yield of silicon nanowires was very low. In 2003, Lu et al. tethered Au nanoparticles on a silicon substrate to reduce the agglomeration of liquid alloy seed droplets during the nanowire growth and confined Si nanowire growth on the substrate.[14] Compared to the floating Au nanoparticles in solution, this method can efficiently control nanowire diameter; however, this method can not yield large amount of silicon nanowires, conflicting with the goal of large-scale nanomaterial synthesis in solution phase. In 2005, Lee et al. identified monophenylsilane (MPS) a promising reactant for producing silicon nanowires.[15]

MPS undergoes a bimolecular disproportionation reaction to create silane and diphenylsilane. Silane decomposes to silicon at themperatures above 350 ˚C. Utilizing MPS as a silicon precursor, the quantity of silicon nanowires in one-batch was increased to 1-2 mg. However, the yield of silicon nanowires is only 1%, showing that "*few ratio*" of MPS was converted to silane in the reaction. A

continuous flow reactor with very concentrated precursor solution resulted in primary amorphous particles and other byproducts.

2.4 MONOPHENYLSILANE DISPROPORTIONATION

Monophenylsilane was a promising precursor for crystal silicon nanowire growth in supercritical fluid as demonstrated by Lee et al. Levy et al. studied the stability and thermal decomposition of aryl-silanes in the late 1960s.[16-17] They concluded that monophenylsilane decomposition followed a bimolecular disproportionation reaction in the temperatures between 350 ˚C to 500 ˚C. The overall decomposition kinetics of the aryl-type silanes can be represented as a set of similar reaction pattern:

$$2Ph_{4-n}SiH_n \rightarrow Ph_{5-n}SiH_{n-1} + Ph_{3-n}SiH_{n+1} \qquad (2.1)$$

In their discussion, they proposed that a major pathway to produce sillane was from the decomposition of a four-center activated complex, which was formed by the combination of two MPS moleculses (Figure 2.2). In the complex, the molecular rearrangement of a phenyl group and a hydrogen atom occurs due to the high mobility of the phenyl group, leading and diphenylsilane as reaction products. Lee et al. demonstrated silicon atoms from the MPS disproportionation reaction are sufficient for producing high quality Si nanowire in supercritical fluid.

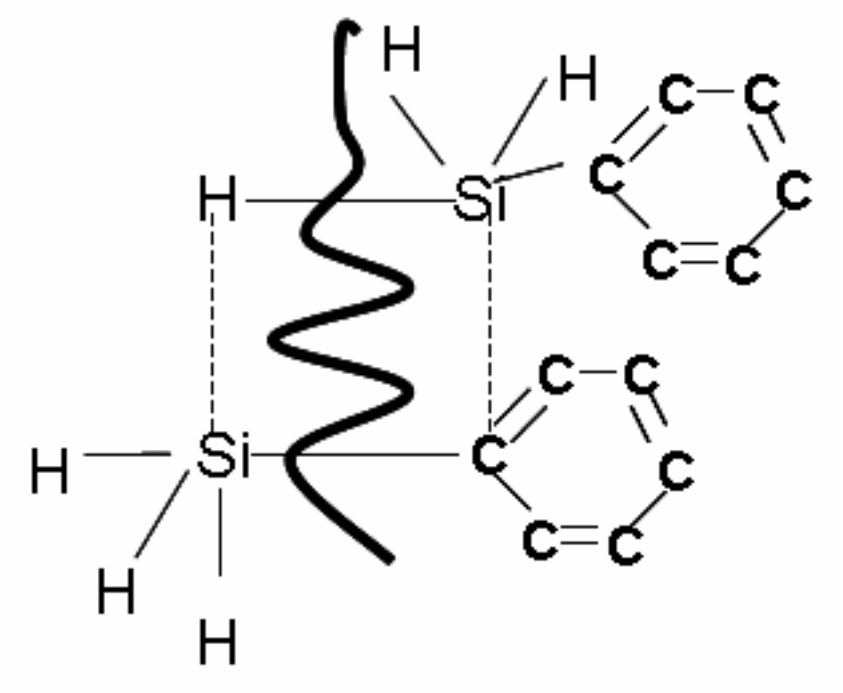

Figure 2.2: Formation of four center activated complex and the molecular phenyl bond rearrangement.

2.5 ORGANIC SOLVENT SELECTION

The conversion of MPS to silicon nanowires in supercritical hexane is only about 1%. The role of the solvents was investigated. Three different organic solvents were studies: (1) benzene, (2) toluene and (3) hexane.

2.6 RESULTS AND DISCUSSION

Figure 2.3 shows the photographs of Si nanowires collected on a silicon wafter placed in the reactor carried out in hexane, toluene and benzene. The largest quantity werer produced in benzene as shown in Fgure 2.3a. The reaction in toluene

gave fewer Si nanowires and reaction in hexane gave relatively few silicon nanowire products.

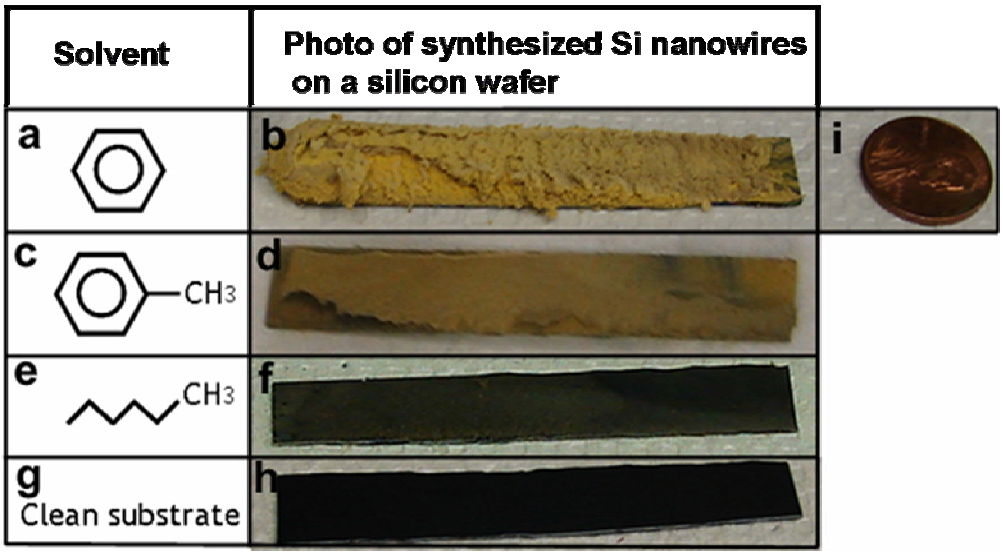

Figure 2.3: Au-seeded silicon nanowires via SFLS using (a) hexane, (c) toluene and (e) hexane and the corresponding synthesis results (b-f)

XRD of the Si nanowire product is shown in Figure 2.4 and matches with diamond cubic Si. The peak intensity ratios in the XRD pattern for the (111):(220):(311) reflections is 1:55:30 - similar to the peak ratios expected with randomly oriented crystalline powder Si with the intensity ratio of 100:56.9:36.1. This is probably because the nanowires are randomly-oriented on the substrate.

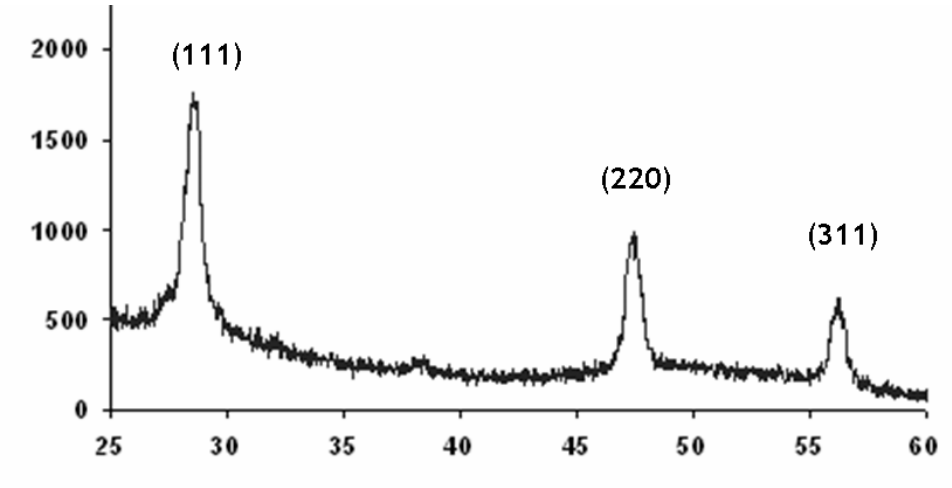

Figure 2.4: XRD pattern of Si nanowire sample.

As described in equation 2.1, the maxium conversion of monophenylsilane to silane by disproportionation is 75%. Figure 2.5 shows product weight obtained from reactions in different organic solvents. The reaction in benzene gives 46.8 mg of silicon nanowires with a 63% yield. The yield was only 38.4% in toluene and the XRD data from nanowires showed some broad (111) diffraction peaks corresponding to amorphous Si produced as a byproduc. In hexane, only 1% of the MPS was converted to Si nanowires.

solvent	injected Si (mg)	Output silicon nanowires (mg)	Yield(%)
Benzene	74.3	46.8	63
Toluene		28.6	38.4
Hexane		~1	1.4

Figure 2.5: Silicon nanowire weight and yield of reactions carried out in different solvents.

Figure 2.6 shows photographs of the nanowire product collected from a reaction in supercritical benzene. The color is dark yellow corresponding to the color of nano-size silicon. The production of Si nanowires is about 2.3 mg/min! This is a very fast Si nanowire production rate, which can not be met by CVD and provides an example of high yield high production silicon nanowire synthesis in solution.

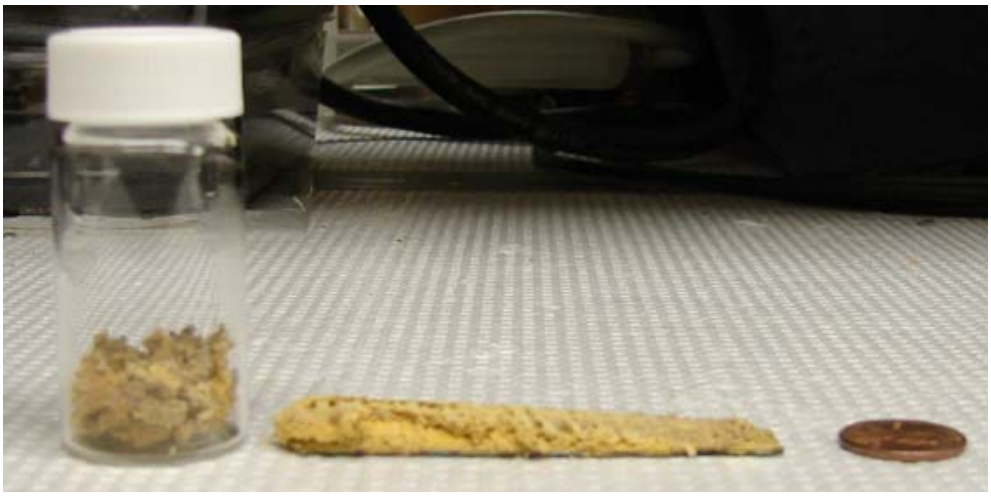

Figure 2.6: Photograph of Si nanowires produced in a single reaction in supercritical benzene.

Figure 2.7 shows a SEM image of as-synthesized Si nanowires in supercritical benzene. Higher magnification images show Si nanowires over 20 μm long with a average diameter of 20 nm (Figure 2.7b). The Si nanowires were crystalline with few extended defects (Figure 2.8). <111> is the predominant growth direction by observed over 100 Si nanowires.

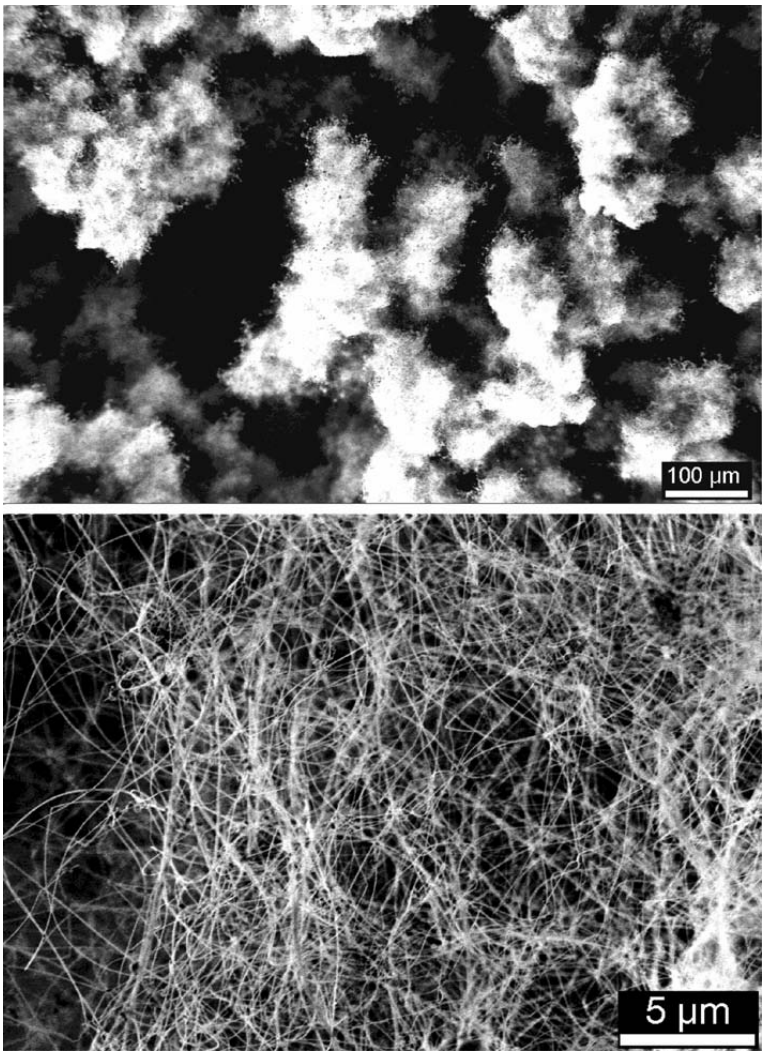

Figure 2.7: HRSEM images of silicon nanowires obtained from monophenysilane in the presence of Au nanoparticles in supercritical benzene with a Au/Si molar ratio of 1:1000.

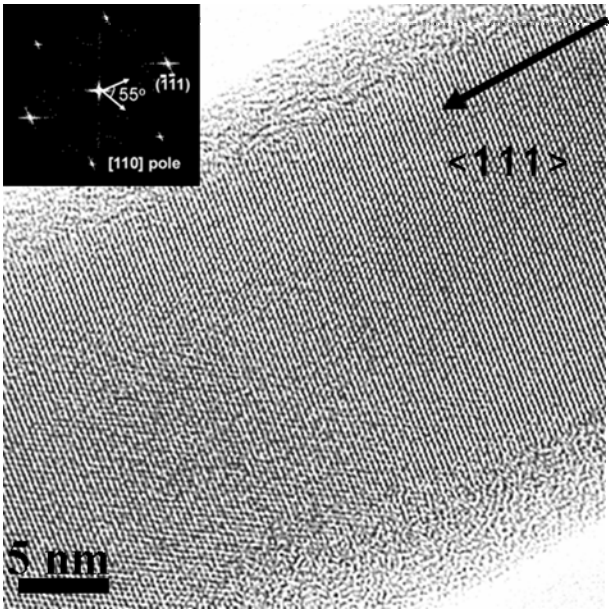

Figure 2.8: High-resolution TEM (HRTEM) images of a Si nanoiwre produced by Au-SFLS process in supercritical benzene.

2.7 CONCLUSIONS

46.8 mg Au-seeded silicon nanowires (with 63% yield) were synthesized in supercritical benzene which is over 50 times more than the quantity obtained from previous results in supercritical hexane. Aromatic solvents such as bezene and toluene significantly increase silicon nanowire production cpmared to aliphatic solvents, apparently helps “to stabilizing” the activated complex and enhancing MPS disproportionation.

2.8 REFERENCES

(1) J. D. Holmes, K. P. Johnston, R. C. Doty, B. A. Korgel, Science 2000, 287, 1471-1473.

(2) B. A. Korgel, Science 2004, 303, 1308-1309.

(3) For a recent review, see M. Law, J. Goldberger, P. Yang, Annu. Rev. Mater. Res. 2004, 34, 83.

(4) Y. Cui, C. M. Lieber, Science 2001, 291, 851-853.

(5) M. C. McAlpine, R. S. Friedman, S. Jin, K. H. Lin, W. U. Wang, C. M. Lieber, Nano Lett. 2003, 3, 1531-1535.

(6) Wang, N.; Zhang, Y. F.; Tang, Y. H.; Lee, C. S.; Lee, S. T. *Applied Physics Letters* **1998,** *73*, 3902-3904.

(7) Morales, A. M. and Lieber, C. M., S*cience* **1998**, *279*, 208-211.

(8) T. J. Trentler, K. M. Hickman, S. C. Goel, A. M. Viano, P. C. Gibbons, W. E. Buhro, Science 1995, 270, 1791.

(9) D. Fanfair, B. A. Korgel, Cryst. Growth & Des. 2005, 5, 1971-1976.

(10) H.-Y. Tuan, D. C. Lee, T. Hanrath, B. A. Korgel, Nano Lett. 2005, 5, 681.

(11) H.-Y. Tuan, D. C. Lee, T. Hanrath, B. A. Korgel, Chem. Mater. 2005, 17, 5705.

(12) Hanrath, T.; Korgel, B. A. *Adv. Mater.* **2003**, *15*, 437-440.

(13) Schricker, A. D.; Joshi, S. V.; Hanrath, T.; Banerjee, S. K.; Korgel, B. A. *Journal of Physical Chemistry B* **2006,** *110*, 6816-6823.

(14) Lu, X. M.; Hanrath, T.; Johnston, K. P.; Korgel, B. A. *Nano Letters* **2003,** *3*, 93-99.

(15) Lee, D. C.; Hanrath, T.; Korgel, B. A. *Angew. Chem. Int. Ed.* **2005,** *44*, 3573-3577.

(16) Levy A, Coutant R.W., Maeryman E.L., Trent D.E., Aerospace Research laboratories, 65-64 1965 April

(17) Coutant RW, Levy A., A Aerospace Research laboratories, 69-215 Oct 1965

Chapter 3: Nanocrystal-Mediated Crystallization of Silicon and Germanium Nanowires in Supercritical Fluid: The Role of Catalysis and Solid-Phase Seeding*

3.1 INTRODUCTION

The size-dependent properties, large surface-area-to-volume ratios, dispersibility in solvents, and mechanical flexibility of semiconductor nanowires make them an exciting class of materials.[1-3] Silicon (Si) nanowires in particular can be both n and p-doped, interface well with an insulating oxide and conducting metal silicide and these nanowires might be applied in Si CMOS (complementary metal oxide semiconductor) circuits or with organics on flexible plastic substrates.[4,5] Germanium is similar to Si in many respects, but with a higher carrier mobility. Gold-seeded vapor-liquid-solid (VLS) growth is a common route to Si and Ge nanowire synthesis at low growth temperatures (~360^{o}C).[1,3,6-8] Unfortunately, Au traps electrons and holes in both Si and Ge and poses a serious contamination problem for nanowire integration with Si CMOS. Surprisingly few Au alternatives have been investigated for nanowire seeding. Si nanowires have been seeded by CVD with Ti particles[9] and Ga droplets[10], and in organic solvents, Si and Ge nanowires were synthesized using Ni nanocrystals.[11,12] Au alternatives have been explored more extensively for other semiconductors: Sn for ZnO wires, [13] various

* Portions of this chapter have been previously published as Hsing-Yu Tuan; Doh C. Lee;Tobias Hanrath; and Brian A. Korgel; Nano Letter., 2005, 5, 681-684

and

metal films for vapor-grown tin oxide nanowires,[14] and low melting metals such as In and Bi for solution synthesis of Group II-VI[15,16], III-V[17-19] and Ge nanowires.[20]

In chapter 3, various nanocrystals – Co, Ni, CuS, Mn, Ir, $MnPt_3$, Fe_2O_3, and FePt are explored as seeds for Si and Ge nanowire synthesis. Si and Ge nanowires were seeded by metal nanoparticles via solid-phase diffusion and we called this nanowire approach supercritical-solid-solid (SFSS) growth mechanism. The detail of SFSS mechanism will be discussed in Chapter 4. Finally, the investigation of catalytic properties of Ni and Co for Si precursor decomposition is represented.

3.2 EXPERIMENTAL

3.2.1 Different Metal Nanoparticles Preparation

Figure 3.1 shows TEM images of colloidal Co (Figure 3.1a), Ni (Figure 3.1b), CuS (Figure 3.1c), Mn (Figure 3.1d), Ir (Figure 3.1e), $MnPt_3$ (Figure 3.1f), Fe_2O_3 (Figure 3.1g), and FePt (Figure 3.1h) nanocrystals used to seed Si and Ge nanowires; their size distributions had standard deviations less than 20% about mean diameters ranging between 4.2 and 10.2 nm.

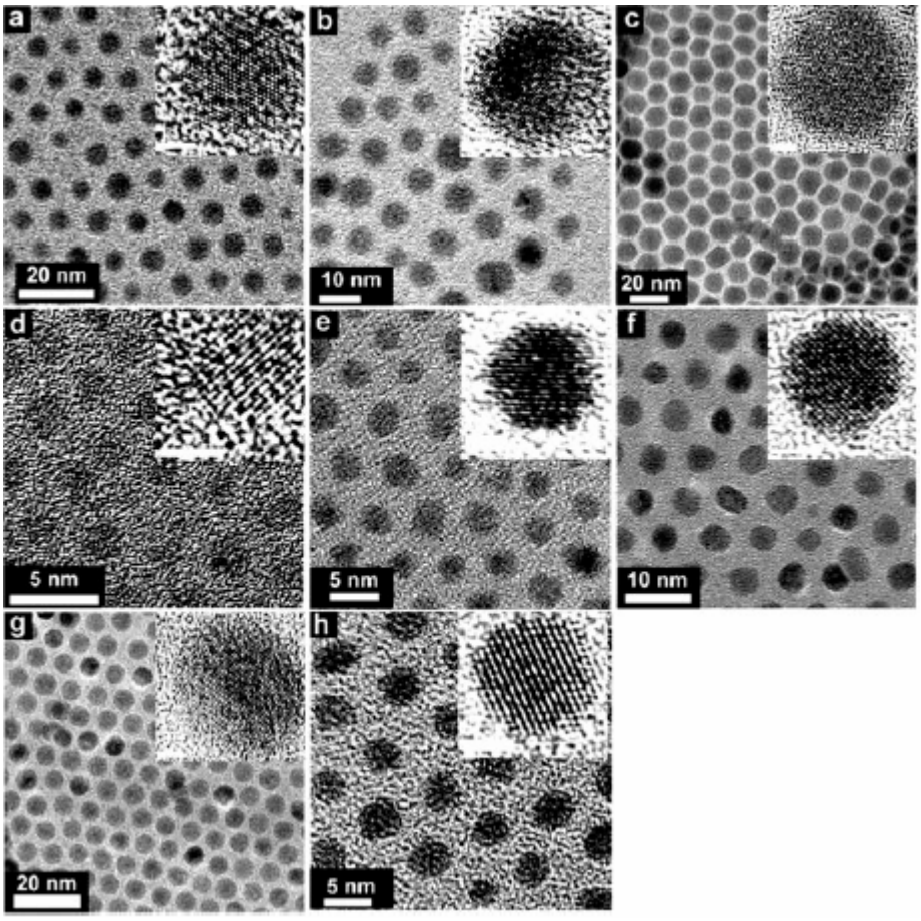

Figure 3.1: TEM images of metal nanocrystals studied as Si and Ge nanowire seeds: (a) Co, (b) Ni, (c) CuS (d) Mn, (e) Ir, (f) MnPt3, (g) Fe2O3 and (h) FePt. Inset scale bars are 2 nm.

Nanocrystals were prepared by arrested precipitation in hot-solvent media as described in the literature.[21-26] The representative Ni nanoparticle synthesis was described below.

The synthesis of Ni nanocrystals was carried out employing high-temperature (250°C) reduction of metal salts in the presence of capping ligands. 1 mmol of $Ni(CH_3COO)\cdot 4H_2O$ was mixed with 0.5 mmol of oleic acid, 2 mmol of

trioctylamine and 0.25 mmol of trioctylphosphine in 10mL of diphenylether in a three-neck flask. The mixture was agitated at room temperature while flushing with nitrogen for ~20 min. The temperature of the reacting solution was detected using K-type thermocouple (Omega) connected to temperature controller (Omega). The solution was heated to 200°C, and 0.5 mmol of trioctylphosphine was injected. Then the green solution turned into a dark-green color. While the mixture was heated to 250°C, 0.5 g of 1,2-hexadecanediol dissolved in 2.5 mL of diphenylether was prepared in a separate flask, and the mixture was heated to 80°C under nitrogen atmosphere and then was injected into the main reaction vessel that had reached 250°C. The temperature immediately dropped to ~220°C, and was raised back to 250°C where the mixture was being agitated isothermally for 20 min.

Upon completion of the reaction, the heating element was removed and the solution was cooled to room temperature while being stirred. The solution was then collected and centrifuged at 8000 rpm for 10 min, and a small amount of the poorly capped particles was precipitated out and discarded. The supernatant was mixed with 20 mL of ethanol and the Ni nanocrystals capped with organic stabilizer were flocculated and easily collected after centrifugation at 8000 rpm for 10 min. The precipitate was carefully collected after an additional rinse with ethanol. Purified nanocrystals were readily dissolved in hexane. In order to ease the preparation of the stock solution for nanowire growth and to prevent surfactant of

nanocrystals from falling off, the nanocrystal solution was dried and quantitatively measured amount of the crystals was brought into nitrogen glove-box.

3.2.2 Semi-Batch Nanowire Synthesis

The experimental setup of silicon and germanium nanowires by different nanoparticles is similar to the one used in Chapter 2 but with semi-batch type reaction as shown in Figure 3.2. Nanowires were synthesized in semi-batch 10 mL Ti grade-2 reactor connected to a high-pressure liquid chromatography (HPLC) pump for pressure control (500-1000 psi) and reactant injection (0.5 ml/min). One side of valve of the reactor was connected with 6-way valve (Valco) equipped with a smaller 500µl loop made of 1/16in o.d 0.03 in. id stainless steel high-pressure tubing and the other side is a close end. The reactor was pressurized to 3.4 MPa with toluene and then heated to the reaction temperature. 500 µL of 150 mM MPS in toluene with Si:nanocrystal mole ratios of 50:1 (Co), 100:1 (Ni), 150:1 (CuS), 50:1 (Mn), 50:1 (Ir), 50:1 ($MnPt_3$), 50:1 (Fe_2O_3), and 50:1 (FePt), were injected from a 6-way valve injection loop (Valco) at 0.4 mL/min. For Ge nanowires, 500 µL of 80 mM DPG in toluene were injected with Ge:nanocrystal mole ratios of 100:1 (Co), 100:1 (Ni), 100:1 (CuS), 50:1 (Mn), 20:1 (Ir), 100:1 ($MnPt_3$), 200:1 (Fe_2O_3), and 200:1 (FePt). The reaction pressure was increased to 10.3 MPa with additional toluene. After 10 min, the reactor was immersed in ice-water and cooled to room temperature. The reactor was opened carefully since the remaining high

pressure inside the reaction. The deposition substrate was removed and cleaned and then was stored under nitrogen.

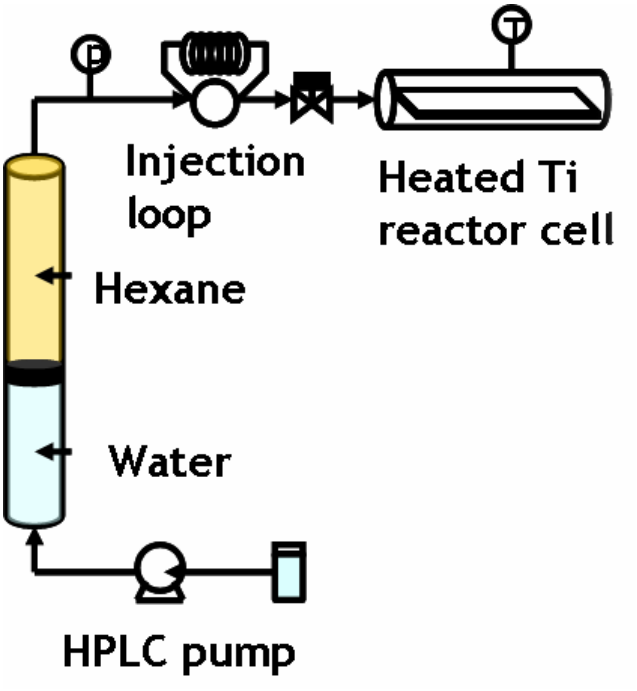

Figure 3.2: A semi-batch supercritical fluid experimental setup for silicon and germanium nanowire synthesis using different metal nanoparticles in supercritical fluid.

3.2.3 Silicon Precursor Solutions

In addition to aryl- substitute silicon precursors, alkyl- and Si- substitute silicon precursors are selected as candidates for probing the catalytic properties of Ni and Co nanoparticles. Selected Si precursors are:

1) monophenylsilane (MPS, Gelest)

2) octylsilane (OS, Gelest)

3) Trisilane (TS, Aldrich)

The molecular structures of the selected silicon precursors are shown in Figure 3.3. Silicon precursors are always stored in a nitrogen-filled glove box to prevent oxidation.

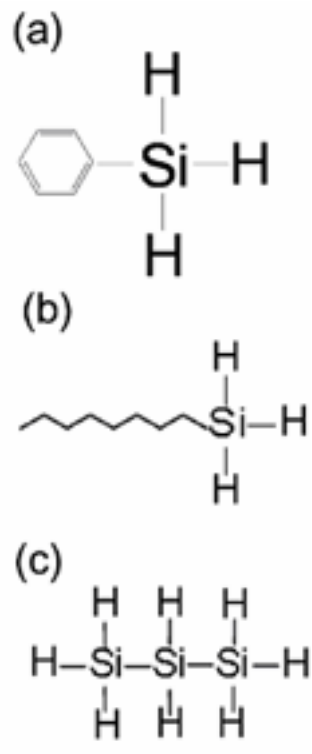

Figure 3.3: Molecular structures of selected organosilane Si precursors for investigation of catalytic properties of metal nanoparticle.

3.3 RESULTS AND DISCUSSION

3.3.1 Effect of Metal nanoparticles on Si and Ge Nanowire Growth

Figure 3.4 shows the reaction products. All of the nanocrystals seeded Si and Ge nanowires from monophenylsilane (MPS) and diphenylgermane (DPG), but *with varying success* (summarized in Table 3.1). In general, straight nanowires are crystalline with few extended defects; whereas, curly wires are usually amorphous or polycrystalline. Co nanocrystals gave the highest yield of straight, long (>10 μm) Si and Ge nanowires (Figure 3.4). Ni nanocrystals also produced crystalline Si and Ge nanowires with good yield. CuS nanocrystals produced straight crystalline Si nanowires with good yield but slightly shorter lengths (3-10 μm) and Fe_2O_3 nanocrystals produced high quality Ge nanowires with relatively high yield.

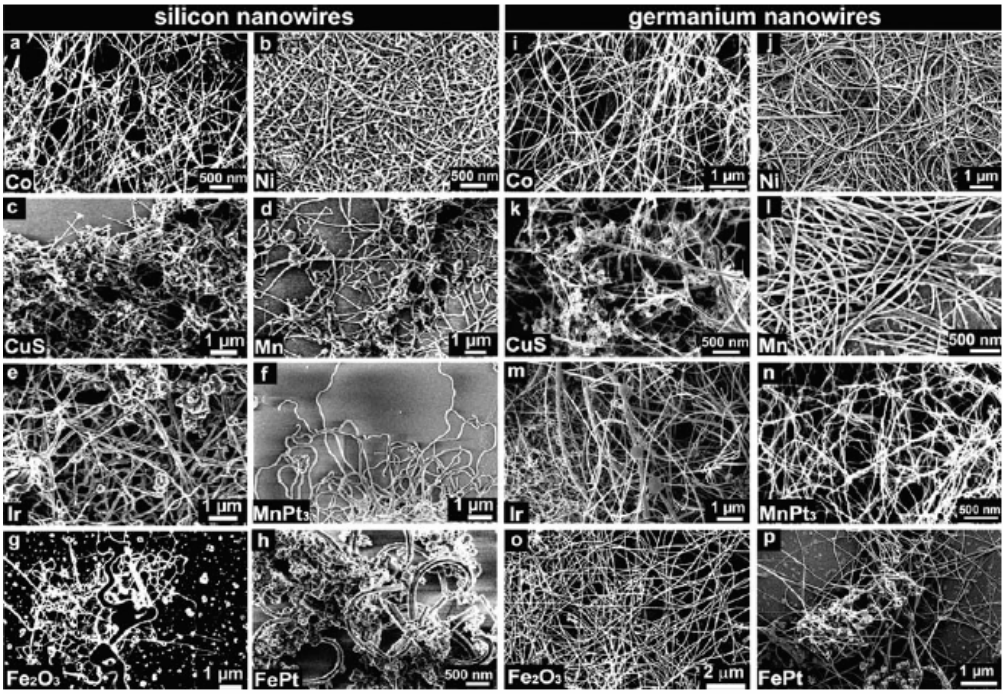

Figure 3.4: SEM images of (a-h) Si and (i-p) Ge nanowires synthesized in supercritical toluene from MPS (150 mM, 500°C, 10.3 MPa) and DPG (80 mM, 460°C, 10.3 MPa), respectively.

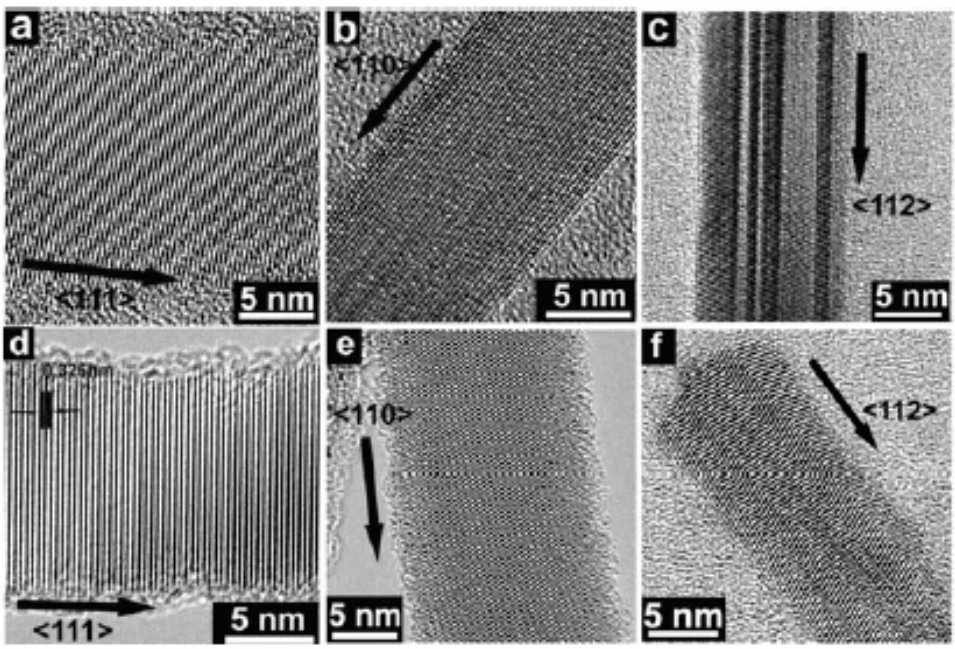

Figure 3.5: HRTEM images of Si (a-c) and Ge (d-f) nanowires seeded by (a-c) Co, (d-e) Fe2O3 and (f) CuS showing <110>, <111> and <112> growth directions. Co, Fe2O3 and CuS seeding gave Si and Ge nanowires with equal proportions of <111> and <110> oriented nanowires, with ~5% of the sample containing <112> oriented nanowires, usually with longitudinal {111} twins, as in (c). The 0.326 nm lattice spacing agrees with the (111) d-spacing for bulk Ge (0.327nm).

Si and Ge nanowires were grown by decomposing silanes or germanes in high temperature (450~500^{o}C), high pressure (10.3 MPa)—*e.g.* supercritical—toluene.[27,28] Under these reaction conditions, Au nanocrystals seed nanowires via the "supercritical fluid-liquid-solid" (SFLS) mechanism in which nanowires evolve from a liquid Au:Si (or Au:Ge) eutectic. In combination with Si and Ge, many of the seed materials studied here do not form *liquid* eutectics until reaching temperatures well above 500^{o}C, and are not expected to work for "VLS"-like

growth. However, they form solid alloys below 500^{o}C, perhaps making *solid-phase* nanowire seeding possible.

All of the nanocrystals produced nanowires at temperatures significantly below their bulk eutectic temperatures (summarized in Table 3.1). The small size of the seed nanocrystals reduces the eutectic temperature; however, a drop of nearly 350^{o}C is unlikely.[12] These nanocrystals most likely promote nanowire crystallization from *solid*-phase seeds. Solid-phase metal-seeded nanowire growth has also been proposed in other systems: Si (Ti,[9], Ni[11]), Ge (Fe,[29] Ni[12]), GaAs (Au),[30] InAs (Au),[31] and ZnSe (Au,[32] Fe[33]) nanowires. Solid-phase seeding is a viable growth mechanism, provided that the seed particles are small enough for rapid saturation by solid-state diffusion and there is a high solid solubility of semiconductor in the metal. Co, Ni, Fe and Cu all form alloys with Si and Ge at the growth temperatures and EDS analysis of the seed particles found at the tips of many nanowires revealed silicide and germanides (Figures 3.6 and 3.7). In the particles located at the tips of nanowires seeded with CuS and Fe_2O_3 nanocrystals, S and O was not observed in significant quantities, indicating that wires probably crystallize from copper silicide and iron germanide phases. Perhaps CuS and Fe_2O_3 are first reduced to Cu and Fe metal in the reaction mixture, followed by nanowire growth. Particles found at the tips of FePt seeded nanowires exhibited all three elements—Fe, Pt and Ge—indicating that nanowire growth probably originates from a ternary Fe:Pt:Ge phase.

Si and Ge nanowires seeded with Ni, Co, Fe_2O_3 and CuS exhibited two predominant growth directions—<111> and <110>—in nearly equal proportions (Figure 3.5) ~5% of the nanowires also had <112>-oriented growth. This is different than Au-seeded Si and Ge nanowires in organic solvents, which have exhibited preferential growth in either the <111> (Si) or <110> (Ge) directions, with only a small proportion of <110> (or <111>) and <112> orientations.[28,34] Perhaps the difference in nanowire growth direction relates to the solid-phase nanowire seeding process. However, it is interesting to note that regardless of the metal used to seed the nanowires (i.e., Au or Ni, Co, etc.), <112>-oriented nanowires always tend to have longitudinal {111} twins, as in the wires in Figures 3.5 c and 3.5 f.

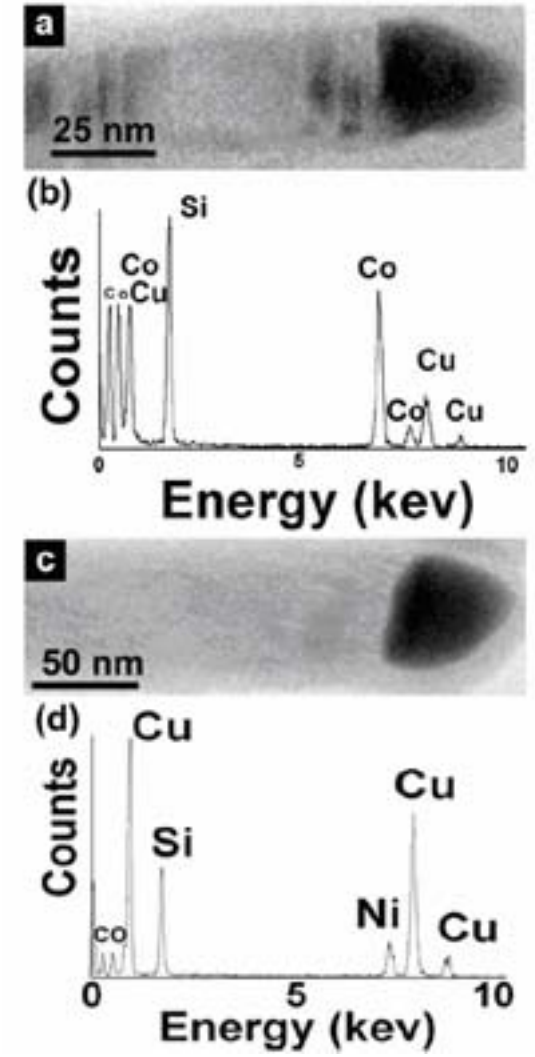

Figure 3.6: TEM images of particles located at the tips of Si nanowires seeded with (a) Co and(c) CuS nanocrystals. Energy dispersive X-ray spectra (EDS) taken at the particle tips shows thecomposition to be (b) Co-Si and (d) Cu-Si alloys. In (b), the Cu signal is from the copper TEM grid and the Ni signal in (d) is from the nickel TEM grid. Note that in (d), no S signal was detected in the tip.

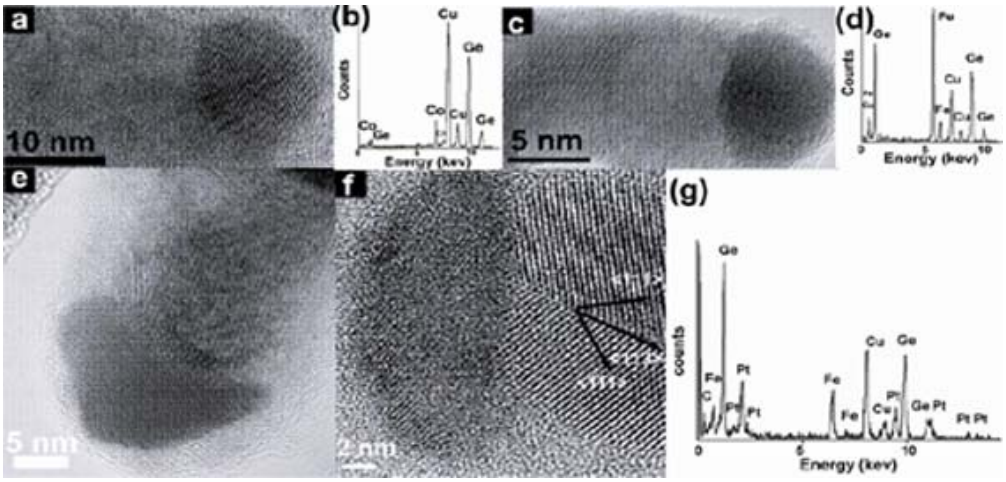

Figure 3.7: TEM images of particles observed at the tips of Ge nanowires seeded with (a) Co, (c) Fe_2O_3, and (e,f) FePt nanocrystals. The associated EDS data (b,d,g) was obtained by focusing the electron beam on the tip to reveal its composition. The Cu signal is from the TEM grid. Note the nanowire in (f), which shows the appearance of an interesting <113>-oriented twin at 29° withrespect to <111> growth axis.

Nanowire	Seed	Nanocrystal diameter [nm]	Reaction temp. [°C][a]	Eutectic temp. [°C][h]	Product description
Si	Co	9.7	500[b]	1200	Long straight wires
Si	Ni	5.6	460	964	Long straight wires
Si	CuS	11.7	500	802[d]	Good yield, shorter wires
Si	Mn	4.7	500	1040	Crystalline wires, low yield
Si	Ir	4.2	500	1470	Amorphous particles & curly wires
Si	$MnPt_3$	5.1	500	N/A	Low yield, mostly curly wires
Si	Fe_2O_3	10.2	500	1200[e]	Amorphous particles & few wires
Si	FePt	4.3	500	N/A	Amorphous particles
Ge	Co	9.7	460[c]	817	Long straight wires
Ge	Ni	5.6	460	762	Long straight wires
Ge	CuS	11.7	460	644[f]	Short curly wires
Ge	Mn	4.7	460	720	Crystalline wires, low yield
Ge	Ir	4.2	460	N/A	Wires & amorphous particles
Ge	$MnPt_3$	5.1	460	N/A	Straight wires with rough surfaces
Ge	Fe_2O_3	10.2	460	838[g]	Long straight wires
Ge	FePt	4.3	460	N/A	Wires & amorphous particles

Table 3.1: Summary of seed nanocrystal composition and selected properties and reaction conditions.

[a] The optimal synthesis temperature for Si nanowires was approximately 408C higher than for Genanowires in all cases, indicating slower Si nanowire growth kinetics. [b] The optimum reactiontemperature for cobalt-seeded Si nanowires from MPS was approximately 50 8C higher than the optimalsynthesis temperature (450 8C) using Au seeds. [c] The optimum reaction temperature for cobalt-seededGe nanowires from DPG is approximately 80 8C higher than the optimal synthesis temperature (380 8C)using Au seeds. [d] Value based on Cu:Si phase diagram, because S appears to outgas from the seedparticles. [e] Value based on Fe:Si phase diagram, because iron silicide appears to be the seedcomposition. [f] Value based on Cu:Ge phase diagram, because Sappears to outgas from the seedparticles. [g] Value based on Fe:Ge phase diagram, because iron germanocide appears to be the seedcomposition. [h] Ref 35

3.3.2 Catalytic Heterogeneous Decomposition of Silicon Precursors by Metal Nanoparticles

3.3.2.1 The Role of Au Nanoparticles in Si Precursor Decomposition

In VLS growth, the metal seed dissolves the semiconductor and recrystallizes it as a nanowire and has a *passive* role in the precursor decomposition chemistry.[3,6,28] Au does not *catalyze* reactant *decomposition*, but simply helps drive crystallization (perhaps one could call Au a "crystallization catalyst," but not a catalyst for reactant decomposition). Au-seeded CVD nanowire growth typically uses very reactive precursors, such as silane, and there is generally no need to use catalytic seed metals to promote reactant decomposition. However, sidewall deposition can occur with reactive precursors and lead to substantial diameter tapering over the length of the wire.[36,37] Catalytic seeds might be able to lower the growth temperature and help prevent sidewall deposition. We have found it impossible to thermally decompose these precursors to *crystalline* Si in organic solvents, even in the presence of Au nanocrystals (see Figs 3.8a and 3.9a), due to the thermal stability of the Si-C and Si-Si bonds in alkylsilanes and trisilane. The Si-C bond in octylsilane is very stable and does not undergo thermolysis at temperatures lower than ~500^{o}C. Furthermore, the alkyl moiety in octylsilane is not kinetically labile like the phenyl group in arylsilanes and cannot disproportionate to yield silane. In trisilane, hydrogen atoms dissociate easily from the molecule but the Si-Si bonds do not cleave at temperatures accessible in organic solvents. Thermal

decomposition of trisilane in toluene at 460^{o}C yields very reactive Si trimers that homogeneously nucleate into amorphous Si colloids[38] and do not produce nanowires by Au-seeded SFLS. Apparently, the Si-Si bonds must be "cracked" in order to form nanowires. These Si reactants require a catalytic seed to promote nanowire formation.

3.3.2.2 The Role of Ni Nanoparticles in Si Precursor Decomposition

In contrast to Au, the transition metals Ni, Co and Fe, are well-known catalysts for molecular decomposition reactions. For carbon nanotube growth, Fe, Co and Ni are used as *catalyst*s that *enhance reactant decomposition* at the seed surface, while also promoting "crystallization" of the nanostructure—in this case, graphitization and tube growth.[39-41] We have also found that in addition to promoting Si crystallization, the Ni nanocrystals catalyze the decomposition of silane precursors, such as alkylsilanes and trisilane, that do not yield crystalline nanowires in the Au nanocrystal-seeded SFLS process due to their poor reactivity. Figures 3.8 and 3.9 show Si nanowires synthesized from octylsilane and trisilane using Ni nanocrystals. Ni nanocrystals promote Si nanowire growth with relatively high yield from both octylsilane and trisilane.

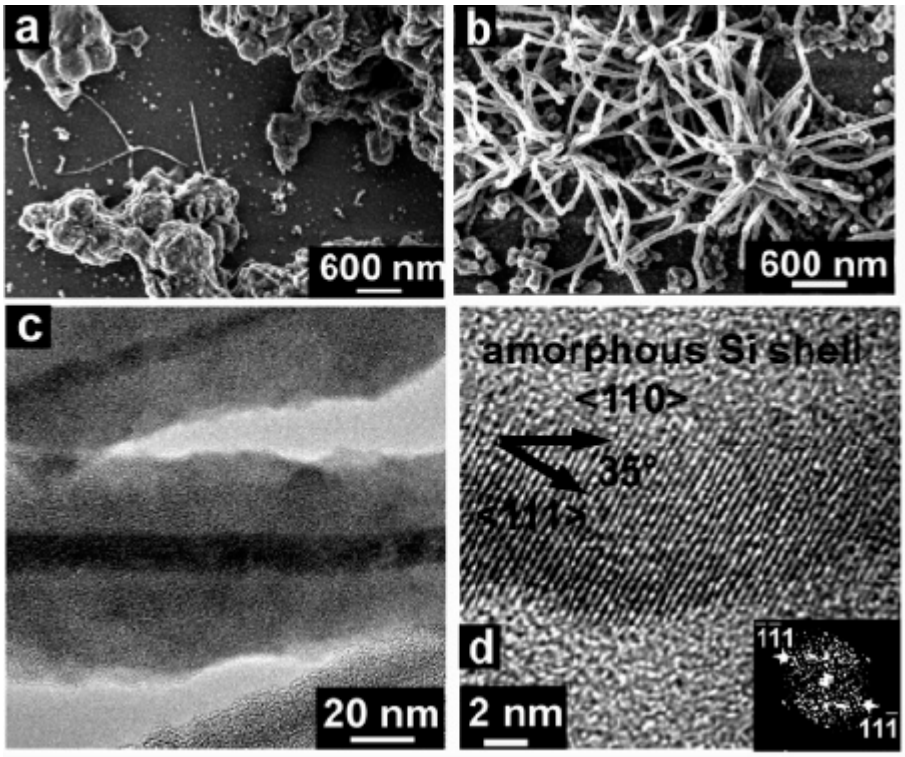

Figure 3.8: Si synthesized with octylsilane in toluene at 17.9 MPa and 460°C: SEM images of product obtained using (a) Au and (b) Ni nanocrystals ([Si]/[Ni]=100) and (c,d) TEM images of the Si nanowires synthesized by Ni-seeded SFSS from octylsilane. In (c) and (d), note the characteristic amorphous shell that coats the crystalline core that results from sidewall deposition of octylsilane.

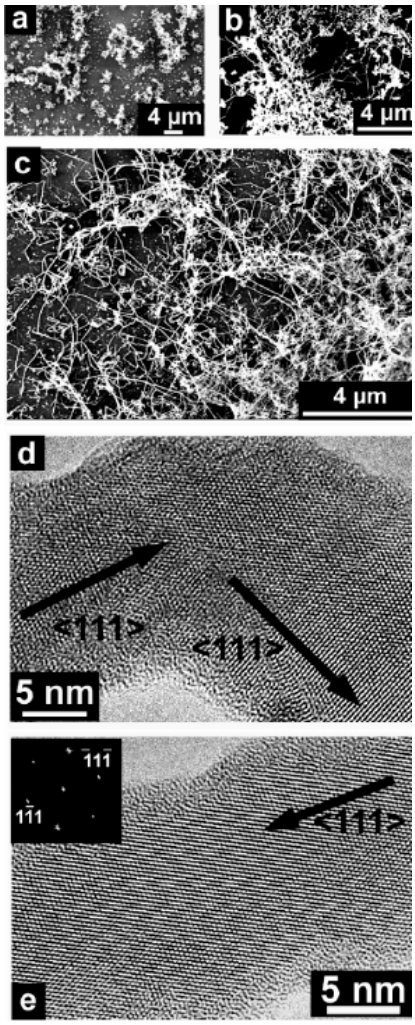

Figure 3.9: Si produced from trisilane in hexane at 14.3 MPa and 450°C: SEM images of product obtained using (a) Au nanocrystals ([Si]/[Au]=5), (b) Ni nanocrystals ([Si]/[Ni]=10), and (c) Ni nanocrystals ([Si]/[Ni]=5). (d,e) TEM images of of nanowires obtained from trisilane in the presence of Ni nanocrystals. In contrast to nanowires grown from MPS and octylsilane, the nanowires shown here have grown in the <111> direction. Even in the case of the kinked wire in (D), the growth direction remains <111>.

Although the Si nanowires formed using octylsilane and trisilane are crystalline and relatively long, the quality of the wires is still not as high as those

obtained with MPS. In contrast to MPS, both octylsilane and trisilane gave significant amounts of amorphous sidewall deposition. The more significant sidewall deposition from trisilane is certainly expected, as it undergoes rapid dehydrogenation to a very reactive "bare" Si trimer that will "stick" to anything it sees in solution.[38] Sidewall growth could be eliminated to some extent by using higher [Ni]/[Si], with the best Si nanowires obtained from trisilane by using nearly two orders of magnitude larger [Ni]/[Si] than in the case of MPS (5 vs 100). One drawback with using very high [Ni]/[Si] is that the Si supply to the metal seeds can become starved, which leads to crystallographic defects[42]. Sidewall-deposited Si from octylsilane is amorphous, but in contrast to trisilane, most likely contains significant carbon contamination. Octylsilane dehydrogenation may happen quite rapidly at 460^{o}C, however, the Si-C bond is thermally very stable and at these temperatures in supercritical toluene, and octylsilane tends to dimerize and form thermally stable oligomers. For example, most of the particulates in Figure 3.8a are large precipitates of aggregated oligomers and amorphous mixtures of carbon and silicon. Therefore, in order to produce crystalline Si nanowires from octylsilane, the Ni nanocrystals must first catalyze its decomposition to make crystalline nanowires.

3.3.2.3 The Role of Co Nanoparticles in Si Precursor Decomposition

Figure 3.10 shows TEM and SEM images of Si nanowires seeded by Co nanocrystals in supercritical toluene from MPS, octylsilane and trisilane—all three

reactants gave nanowires. Co nanocrystals enhance octylsilane decomposition enough to promote nanowire formation; however, the nanowire quality is only marginal as the nanowires are coated with an amorphous layer with significant carbon content (Figure 3.10i, 3:1 C:Si by EDS in shell). Co nanocrystals were found to promote Si nanowire formation using trisilane at temperatures as low as 350 ˚C, although the majority product at this low temperature was amorphous Si colloids (Figure 3.10d). Co enhances heterogeneous trisilane decomposition relative to homogeneous particle formation. Si nanowires produced with trisilane at 400°C had very little sidewall deposition and few particulates; slightly higher temperature (450^{o}C) gave significant sidewall deposition (Figure 3.10h).

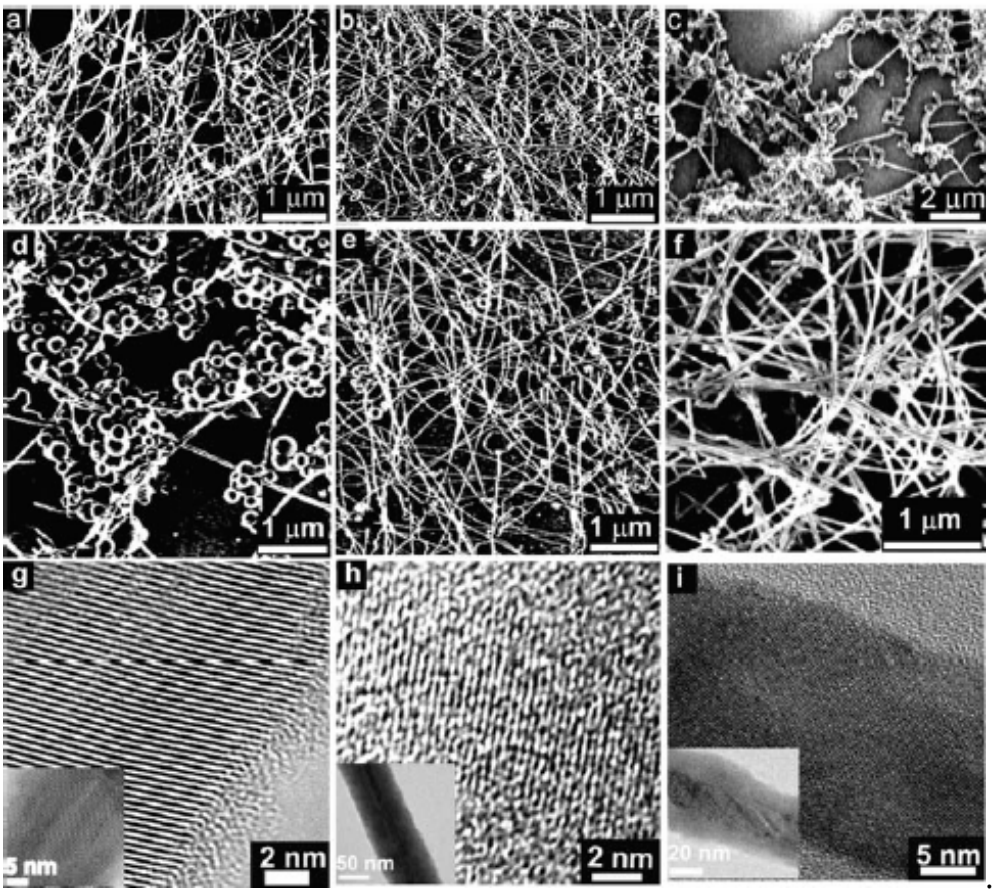

Figure 3.10: Co nanocrystal-seeded Si nanowires. HRSEM images of Si nanowires synthesized in supercritical toluene (10.3 MPa) from (a) MPS (500°C), (b) trisilane (400°C), and (c) octylsilane (500°C). HRSEM images of Si nanowires synthesized in supercritical toluene (10.3 MPa) from trisilane at (d) 350°C, (e) 400°C, and (f) 450°C. (g-i) TEM images of Si nanowires synthesized in supercritical toluene (10.3 MPa) with (d) trisilane (400°C), (e) trisilane (450°C) and (f) octylsilane (500°C). The nanowires in (h) and (i) are coated with an amorphous shell, as shown more clearly in the low resolution TEM images in the insets in (e) and (f). The shell material in (h) is amorphous Si and in (i) it is amorphous 3:1 C:Si (by EDS).

Figure 3.11 provides an overview of the Ni and Co-seeded SFSS synthetic mechanism. Octylsilane and trisilane require heterogeneous catalytic decomposition on the Ni and Co surface to form nanowires; whereas, MPS can undergo homogeneous disproportionation to silane, which can then give rise to nanowire growth. Nanowires produced by SFLS and SFSS from MPS are of relatively high quality with little sidewall growth because of the low precursor reactivity, which results in Si formation isolated to the metal seed particle surface. This study highlights the importance of the precursor decomposition kinetics on the quality of nanowires grown by the "VLS" approach. The growth temperature must by high enough to sustain precursor decomposition and nanowire crystallization, but not so high that sidewall growth occurs to an appreciable extent. In CVD VLS, the precursor reactivity can be decreased and balanced by feeding in additives, such as H_2 in the case of Au-seeded Ge nanowire growth from GeH_4.[9] In solution, additional species can be added to the reactor, however, much less is known about the decomposition kinetics of organosilanes (and organometallics in general) in high pressure solvents, and finding the appropriate nanowire growth conditions is still a challenge. Nonetheless, we have demonstrated in this study that reaction conditions can be optimized to produce nanowires in solution with equal or better quality than those synthesized by gas-phase methods, with the potential for scale-up and high throughput synthesis.

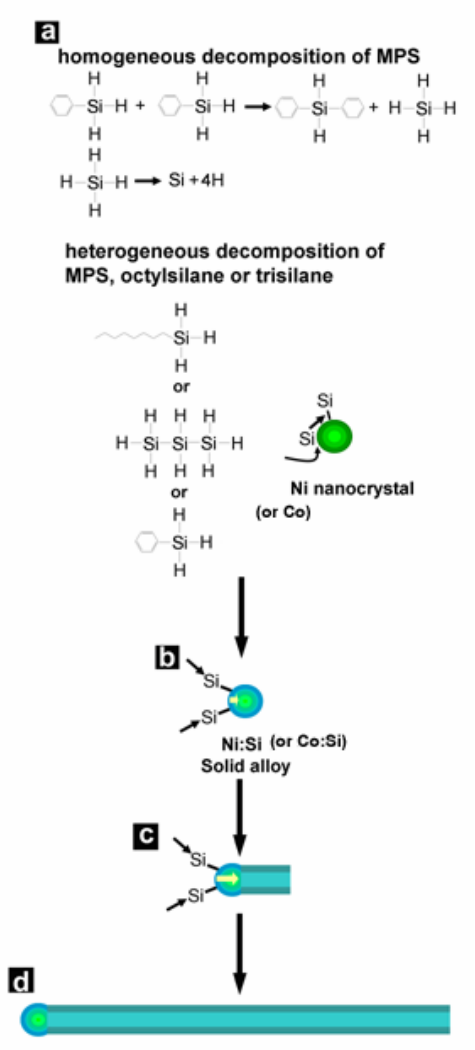

Figure 3.11: Si nanowire growth via SFSS. (a) Homogeneous MPS decomposition occurring by disproportionation versus heterogeneous MPS, octylsilane, and trisilane decomposition catalyzed by the Ni and Co surface. (b) Si atoms diffuse into the Ni and Co nanocrystal until reaching saturation. (c) Silicon nanowire nucleates and crystallizes from the Ni:Si or Co:Si alloy interface, growing to produce the high aspect ratio nanowire illustrated in (d).

3.4. CONCLUSIONS

Of the nanocrystals studied, Co gave the highest yield and quality of both Si and Ge nanowires, rivaling Au-seeded reactions. All growth temperatures were well below the bulk eutectic temperatures, indicating solid-phase seeding. Solid-phase seeding can probably occur for any semiconductor with a high solubility in the seed metal; however, the growth temperature must be sufficiently high for fast saturation by solid state diffusion, which can occur relatively fast in nanometer-diameter seed particles. Ni and Co also were also found to *catalyze* silane decomposition to promote Si nanowire growth from octylsilane and trisilane. In gas-phase reactions, the use of catalytic transition metal seeds might enable lower temperature reactions for less sidewall deposition and better diameter control. As more seed materials are studied, the solid-phase growth mechanism may become as prevalent as liquid-eutectic seeding, and the use of catalytic seed particles might serve as a general approach for improved diameter control, as it has for carbon nanotube growth.

3.5 REFERENCES

(1) J. D. Holmes, K. P. Johnston, R. C. Doty, B. A. Korgel, Science 2000, 287, 1471-1473.

(2) B. A. Korgel, Science 2004, 303, 1308-1309.

(3) For a recent review, see M. Law, J. Goldberger, P. Yang, Annu. Rev. Mater. Res. 2004, 34, 83.

(4) Y. Cui, C. M. Lieber, Science 2001, 291, 851-853.

(5) M. C. McAlpine, R. S. Friedman, S. Jin, K. H. Lin, W. U. Wang, C. M. Lieber, Nano Lett. 2003, 3, 1531-1535.

(6) R. S. Wagner, W. C. Ellis, Appl. Phys. Lett. 1964, 4, 89.

(7) J. T. Hu, T. W. Odom, C. M. Lieber, Acct. Chem. Res. 1999, 32, 435-445.

(8) T. Hanrath, B. A. Korgel, Adv. Mater. 2003, 15, 437-440.

(9) D. W. Wang, H. J. Dai, Angew. Chem. Intl. Ed. 2002, 41, 4783-4786.

(10) T. I. Kamins, R. S. Williams, D. P. Basile, T. Hesjedal, J. S. Harris, J. Appl. Phys. 2001, 89, 1008.

(11) M. K. Sunkara, S. Sharma, R. Miranda, G. Lian, E. C. Dickey, Appl, Phys. Lett. 2001, 79, 1546.

(12) H.-Y. Tuan, D. C. Lee, T. Hanrath, B. A. Korgel, Nano Lett. 2005, 5, 681.

(13) H.-Y. Tuan, D. C. Lee, T. Hanrath, B. A. Korgel, Chem. Mater. 2005, 17, 5705.

(14) Y. Ding, P. X. Gao, Z. L. Wang, J. Am. Chem. Soc. 2004, 126, 2066.

(15) P. Nguyen, H. T. Ng, M. Meyyappan, Adv. Mater. 2005, 17, 1773.

(16) H. Yu, J. B. Li, R. A. Loomis, P. C. Gibbons, L. W. Wang, W. E. Buhro, J. Am. Chem. Soc. 2003, 125, 16168-16169.

(17) J. W. Grebinski, K. L. Hull, J. Zhang, T. H. Kosel, M. Kuno, Chem. Mater. 2004, 16, 5260.

(18) T. J. Trentler, K. M. Hickman, S. C. Goel, A. M. Viano, P. C. Gibbons, W. E. Buhro, Science 1995, 270, 1791.

(19) S. P. Ahrenkiel, O. I. Micic, A. Miedaner, C. J. Curtis, J. M. Nedeljkovic, A. J. Nozik, Nano Lett. 2003, 3, 833.

(20) D. D. Fanfair, B. A. Korgel, Cryst. Growth & Des. 2005, 5, 1971-1976.

(21) V. F. Puntes, D. Zanchet, C. K. Erdonmez, A. P. Alivisatos, J. Am. Chem. Soc. 2002, 124, 12874.

(22) C. B. Murray, S. Sun, H. Doyle, T. Betley, MRS Bull. 2001, 26, 985.

(23) A. Ghezelbash, B. A. Korgel, Langmuir 2005, 21, 9451.

(24) C. A. Stowell, B. A. Korgel, Nano Lett. 2005, 5, 1203.

(25) T. Hyeon, S. S. Lee, J. Park, Y. Chung, H. B. Na, J. Am. Chem. Soc. 2001, 123, 12798.

(26) S. Sun, C. B. Murray, D. Weller, L. Folks, A. Moser, Science 2000, 287, 1989.

(27) For a recent review, see P. S. Shah, T. Hanrath, K. P. Johnston, B. A. Korgel, J. Phys. Chem. B 2004, 108, 9574-9587.

(28) D. C. Lee, T. Hanrath, B. A. Korgel, Angew. Chem. Int. Ed. 2005, 44, 3573.

(29) S. Mathur, H. Shen, V. Sivakov, U. Werner, Chem. Mater. 2004, 16, 2449.

(30) A. I. Persson, M. W. Larsson, S. Stenstroem, B. J. Ohlsson, L. Samuelson, L. R. Wallenberg, Nature Mater. 2004, 3, 677.

(31) K. A. Dick, K. Deppert, T. Mrtensson, B. Mandl, L. Samuelson, W. Seifert, Nano Lett. 2005, 5, 761.

(32) Y. Ohno, T. Shirahama, S. Takeda, A. Ishizumi, Y. Kanemitsu, Appl. Phys. Lett. 2005, 87, 043105.

(33) A. Colli, S. Hofmann, A. C. Ferrari, C. Ducati, F. Martelli, S. Rubini, S. Cabrini, A. Franciosi, J. Robertson, Appl. Phys. Lett. 2005, 86, 153103.

(34) T. Hanrath, B. A. Korgel, *Small* **2005**, *1*, 717-721

(35) Binary Alloy Phase Diagram, 2nd ed,; ASM Internation: Materials Park OH. 1990; Vo.1.

(36) H. Adhikari, A. F. Marshall, C. E. D. Chidsey, P. C. McIntyre, *Nano Lett.* **2006**, *6*, 318-232.

(37) E. Tutuc, S. Guha, J. O. Chu, *Appl. Phys. Lett.* **2006**, *88*, 043113.

(38) Pell, L. E.; Schricker, A. D.; Mikulec, F. V.; Korgel, B. A., Langmuir 2004, 20, 6546-6548.

(39) H. J. Dai, J. Kong, C. W. Zhou, N. Franklin, T. Tombler, A. Cassell, S. S. Fan, M. Chapline, *J. Phys. Chem. B* **1999**, *103*, 11246-11255.

(40) D. C. Lee, F. V. Mikulec, B. A. Korgel, *J. Am. Chem. Soc.* **2004**, *126*, 4951-4957.

(41) D. C. Lee, B. A. Korgel, *Mol. Simul.* **2005**, *31*, 637.

(42) Lu, X.; Hanrath, T.; Johnston, K. P.; Korgel, B. A., *Nano Lett.* **2003,** 3, 93-99

Chapter 4: Germanium Nanowire Synthesis: An Example of Solid- Phase Seeded Growth with Nickel Nanocrystals [1]

4.1 INTRODUCTION

Colloidal routes to nanomaterials synthesis can provide high quality nanocrystals and nanowires of metals and semiconductors that can be dispersed in solvents and deposited onto substrates or incorporated into polymer composites for electronic and optical applications.[1] However, the Group IV semiconductors silicon (Si) and germanium (Ge) have been extremely challenging to synthesize in solution, with only marginal success for Si and Ge nanocrystals due to the difficulties associated with the precursor chemistry and the significant energy barrier to crystallization.[2-10] In 2000[11], we demonstrated a high yield crystalline Si nanowire synthesis in a high pressure high temperature organic solvent using diphenylsilane as a Si precursor with Au nanocrystals to seed and promote Si crystallization and later extended this approach to Ge[12], GaAs[13], and GaP[14] nanowires. Extension of the vapor-liquid-solid (VLS) mechanism from the gas phase to organic solvents requires synthetic temperatures exceeding the Au:Si and Au:Ge eutectic temperature (both at ~360^{o}C), which can be achieved in solvents pressurized above their critical points—we have called this synthetic approach "supercritical fluid-liquid-solid" (SFLS) growth.[15, 16]

---

[1] Portions of this chapter have been previously published as Hsing-Yu Tuan; Doh C. Lee;Tobias Hanrath; and Brian A. Korgel; *Chem. Mater.*, 2005, 17, 5705-5711

Since Au forms a deep trap in Si (and Ge), Au-seeded nanowires are relatively undesirable for electronic applications combining with Si CMOS (complementary-metal-oxide-semiconductor) technology and other metals would be preferable as seeds. The challenge facing SFLS nanowire growth is that the *liquid* metal:semiconductor eutectic temperatures of alternative metals considered more compatible with Si CMOS, such as Fe, Ni, Ti, and Co, form eutectics with Si and Ge at very high temperatures[17]—well above the decomposition temperatures of most organic solvents (for example, 650^{o}C for toluene).[18] However, Si and Ge have very high *solid* solubility in these metals, and metal silicides commonly form by solid-solid diffusion at annealing temperatures ranging from 400^{o}C to 650^{o}C, depending on the material[19, 20]—in the range accessible for supercritical organic solvents!

In a recent *Letter*, we reported that Ni nanocrystals will promote Si nanowire synthesis at temperatures as low as 450^{o}C, which is more than 350^{o}C below the lowest temperature Ni-Si eutectic and concluded that Ni nanocrystal-seeded Si nanowire growth can occur by a *solid-phase* seeding mechanism from the metal particle.[21] Here we provide further evidence supporting that the solid-phase seeding mechanism occurs under certain growth conditions, showing that Ni nanocrystals promote the formation of high quality crystalline Ge nanowires in organic solvents at growth temperatures approximately 350^{o}C below the lowest Ni:Ge eutectic temperature. These results are consistent with other recent VLS

nanowire growth studies in the gas phase:[22, 23] for example, Kamins, et. al., demonstrated Si nanowire synthesis from $TiSi_2$ seeds,[22] and Samuelson and coworkers have proposed solid phase seeding of GaAs nanowires from Au nanocrystals under certain conditions.

In this chapter, five proofs are presented to support supercritical fluid-solid-solid (SFSS) nanowire growth mechanism: (1) calculations of the expected diameter-dependent melting point depression showing that the Ni nanocrystals in the size-range used for the Ge nanowire synthesis should be in the solid phase; (2) evidence that the quality of the nanowires depends sensitively on the $NiGe_x$ seed particle diameter, which contrasts the case for Au-seeded Ge nanowire synthesis; (3) measurements of the nanowire diameter distribution, revealing that it is shifted to smaller diameters relative to the Au-seeded synthesis due to much slower growth of larger diameter nanowires; (4) measurements of the the nanowire growth rate, which relates inversely to the nanowire diameter; and (5) estimates of the solid-state diffusion rate that show that nanowire growth could proceed by either core or surface-enhanced diffusion.

4.2 EXPERIMENTAL

Ge nanowires were synthesized in a semibatch 1 mL titanium grade-2 high pressure reactor, heated in a brass block as described in detail by Hanrath and Korgel.[12] An oxidized Si wafer (4 x 30mm) was placed in the reactor to help collect the nanowires. The reactor was filled with toluene and sealed, then attached to a

high pressure liquid chromatography (HPLC) pump which was used to pressurize and precursor injection. The reactor was flushed with anhydrous toluene 3mins with flow rate 1.5 ml/min. The reactor was first pressurized with more anhydrous oxygen-free toluene to a pressure of 3.4 MPa. Then 350 µL of toluene was injected from a 6-way valve injection loop containing 80mM DPG and Ni nanocrystals at a Ge:Ni mole ratio of 100:1, at a flow rate 0.25 ml/min into the toluene-filled reactor at reaction temperatures ranging from 410°C to 460°C. The reactor was further pressurized to a final reaction pressure of 27.8MPa. The reaction was kept at temperature for 10 minutes. The reactor was then removed from the heating block and allowed to cool to room temperature. The reaction product appears as a dark orange-brown product. The nanowires are stored under nitrogen until use.

4.3 RESULTS

Figure 4.1a shows an SEM image of Ge nanowires obtained by decomposing DPG in the presence of Ni nanocrystals in toluene at 460°C and 23.4MPa. The nanowires are crystalline Ge with diamond cubic structure, and extensive TEM imaging, such as the images in Figure 4.2, shows that the nanowires exhibit few extended defects. The average nanowire length is greater than 10 µm and the diameters ranged from 5 to 30 nm in diameter, with most nanowires in the 5 to 15 nm diameter range.

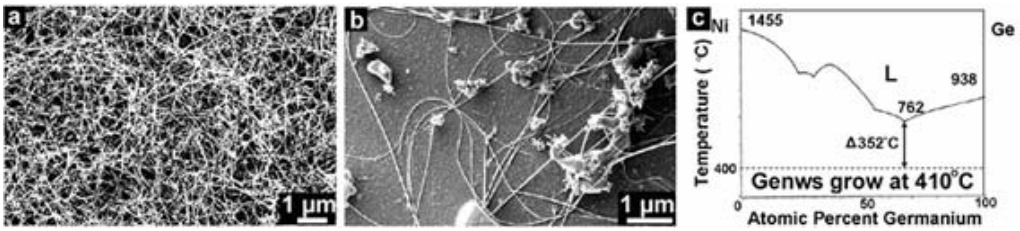

Figure 4.1: SEM images of Ni nanocrystal-seeded Ge nanowires obtained using 80 mM DPG fed into toluene at (a) 460°C and (b) 410ºC at 23.4MPa. (c) The pseudo Ni-Ge phase diagram shows the Ge nanowire synthesis temperature ("Genws"; dashed line) at 352ºC below the lowest eutectic temperature.

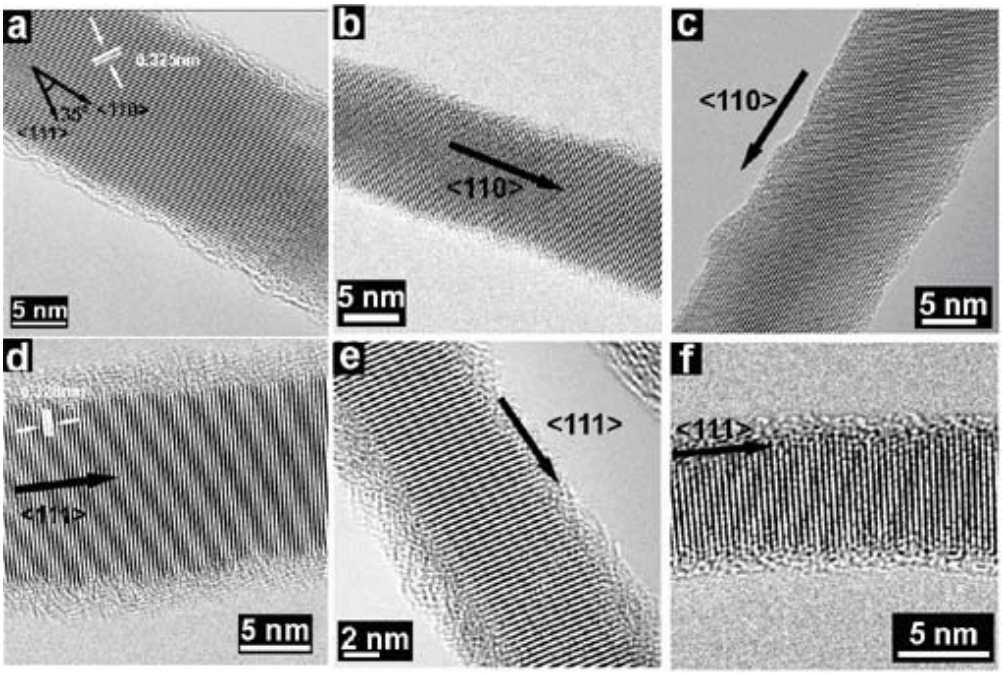

Figure 4.2: TEM images of Ni nanocrystal-seeded Ge nanowires revealing both (a-c) <110> and (d-f) <111> growth directions that are independent of diameter.

Nanowires could be produced at reaction temperatures as low as 410°C (Figure 4.1b), although the product yields drop off rapidly as the reaction

temperature decreases. These reaction temperatures are several hundreds of degrees below the lowest Ni-Ge eutectic temperature, as seen from the phase diagram in Figure 4.1c.[17] The Ni:Ge mole ratio required for the highest quality Ge nanowires (1:100) is about an order of magnitude higher than what is needed for Au-seeded SFLS growth of Ge nanowires (1:1000) at the same DPG reaction concentration. The optimum reaction temperature is also ~80^{o}C higher for Ni seeding compared to Au seeding.[12] This seems to indicate slower growth kinetics from the solid Ni:Ge seeds than the liquid Au:Ge seeds; however, the difference in optimum synthesis temperature could simply relate to the differences in Ni:Ge and Au:Ge phase compositions and temperatures.

Most nanowire growth direction was found to be either <110> or <111> in approximately equal proportions with minor part (less than 5%) of <112> growth direction. The TEM images in Figure 4.2(a-c) show <110>-oriented Ge nanowires with 15.8 nm, 10 nm and 13.7 nm diameters. Figure 4.2 (d-f) show Ge nanowires <111>-oriented nanowires with 12.6 nm, 6.5nm and 5.9nm diameters. The observed 0.325 nm (Figure 4.2a) and 0.328 nm (Figure 4.2d) lattice spacings in the TEM images agree well with the (111) d-spacing for bulk Ge (0.327 nm). Figure 4.3 shows a histogram of the nanowire growth direction as a function of diameter range, between 5-10 nm, 11-15 nm, or greater than 15 nm, obtained from HRTEM images of 80 nanowires. There is a slightly higher occurrence of <111>-oriented nanowires in the small size range and slightly more <110>-oriented wires with

diameters greater than 15 nm; however, the difference in occurrence is marginal and not statistically significant for the larger wires. These results sharply contrast SFLS-grown Ge nanowires from Au nanocrystal seeds, which exhibit <110> growth directions with >90% occurrence, regardless of diameter.[25]

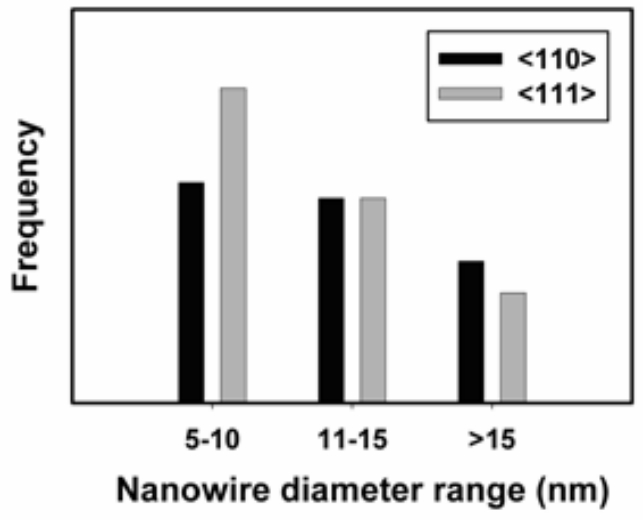

Figure 4.3: Histogram showing the relative occurrence of <110> and <111>-oriented Ge nanowires as a function of diameter.

Ni:Ge alloy nanocrystals can be found by TEM at the tip of most nanowires, as shown in the example in Figure 4.4. Nanobeam EDS (Figures 4.4(b,c)) from the nanowire core shows only Ge and from the tip particle shows a mixture of Ni and Ge. EDS measurements of more than thirty $NiGe_x$ particles found at the tips of nanowires gave $NiGe_x$ alloy compositions ranging between $1.5 < x < 2.8$. In cases where the lattice planes were observed in the nanocrystal at the nanowire tip (the tip needs to be oriented with the proper zone axis), the lattice spacings matched those of orthorhombic $NiGe_2$. It is worth noting that there was no apparent correlation

between growth direction and Ni:Ge composition in the seed particle. In all cases where lattice structure could be observed, as in Figures 4.5(a,b) for example showing crystalline $NiGe_2$ particles at the tips of two Ge nanowires with different growth direction, the crystal structure (FFT pattern) and lattice spacings matched those of orthorhombic $NiGe_2$.[26]

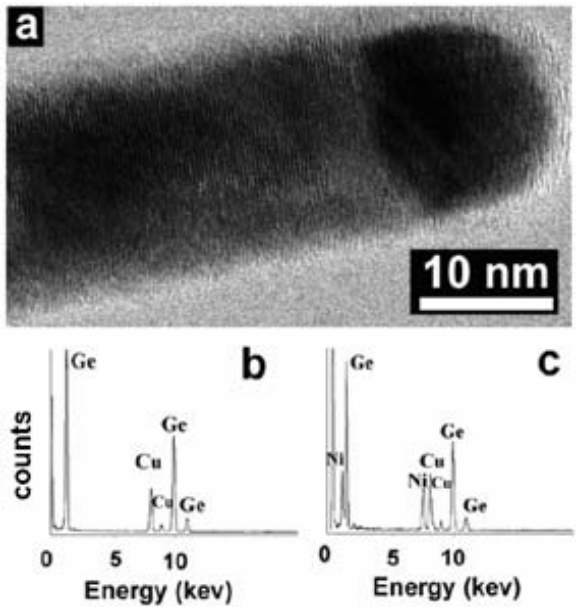

Figure 4.4: (a) TEM image of a Ni:Ge alloy seed particle at the end of a 14.5 nm Ge nanowire. Nanometer-scale EDS reveals (b) only Ge in the core of the wire and (c) Ge and Ni in the particle at the nanowire tip. The Cu signal is from the copper TEM grid.

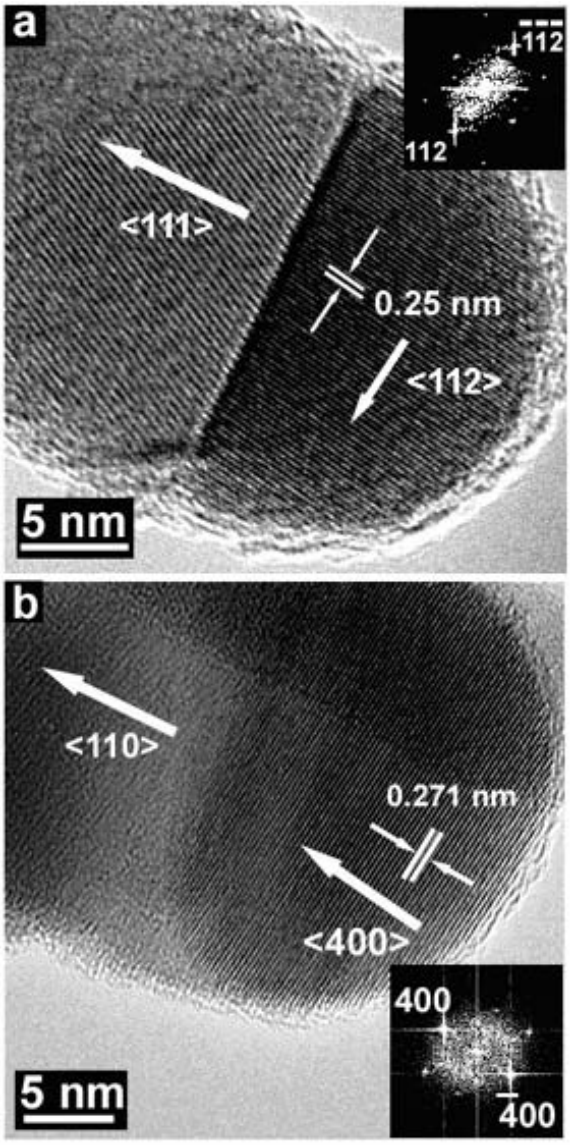

Figure 4.5: HRTEM of two $NiGe_2$ seeds at the ends of (a) <111> and (b) <110> oriented Ge nanowires. (Insets) Fast Fourier transform (FFTs) of the HRTEM images. The FFTs index to orthorhombic $NiGe_2$ and the visible lattice spacings of (a) 0.25 nm and (b) 0.271 nm also match the NiGe2 (112) and (400) d-spacings, respectively.

4.4 DISCUSSION

4.4.1 Melting Point Depression of Ni Nanocrystals

One concern about concluding that Ge nanowires grow from a solid Ni-Ge seed is that the melting temperature of nanocrystals smaller than ~20 nm in diameter can drop significantly as a result of the Kelvin effect, leading to a depressed eutectic temperature that could enable SFLS growth. For example, Dai and coworkers grew Ge nanowires from Au nanocrystal seeds at ~280°C, apparently as a result of size-dependent depression in the Au-Ge eutectic temperature[27], and Hanrath and Korgel observed Au-seeded SFLS Ge nanowire synthesis at temperatures slightly below the bulk Au-Ge eutectic temperature at 361°C.[12] The melting point depression for Au and Ag nanocrystals is well-known and has been measured.[28] But the melting point of Ni nanocrystals has not been measured, so the expected size dependence of the melting temperature was calculated using the modified Pawlow theory (see below equation): [28]

$$\left(1-\frac{T_m}{T_o}\right)-\frac{2}{L\rho_s r_c}\left[\gamma_s-\gamma_l\left(\frac{\rho_s}{\rho_l}\right)^{2/3}\right]-\frac{2T_o}{\rho_s L r_c}\left[\gamma_s(\eta_s-2\alpha_s)-\gamma_l(\eta_l-2\alpha_l)\left(\frac{\rho_s}{\rho_l}\right)^{2/3}\right]\left(1-\frac{T_m}{T_o}\right)=0 \qquad (1)$$

using the parameters listed in Table 4.1. The calculated melting temperature depression for Au[28] and Ni are shown in Figure 4.6. Only at very small sizes—less than ~2.0 nm diameter—do finite size effects begin to deviate from this classical approximation of the surface energy.[28]

Note: r is the radius of Au or Ni cluster.

parameter	symbol (units)	solid phase	liquid phase
density[a]	ρ (kg/m^3)	8908	8700
surface tension[b]	γ (J/m^2)	2.28	1.78
	$\partial\gamma/\partial T$[b]	-5.5×10^{-4}	-1.2×10^{-3}
linear expansion coefficient[b]	α (K^{-1})	1.75×10^{-5}	5.26×10^{-5}
latent heat[a]	L (J/kg)	2×10^5	
melting temperature[a]	T_o (K)	1728	
η[a]	$(1/\gamma)(\partial\gamma/\partial T)$	2.41×10^{-4}	6.74×10^{-4}

[a] Ref 29. [b] Ref 30.

Table 4.1: Parameters Used to Calculate the Diameter Dependence of the Melting Temperature of Ni Using Eq 1.

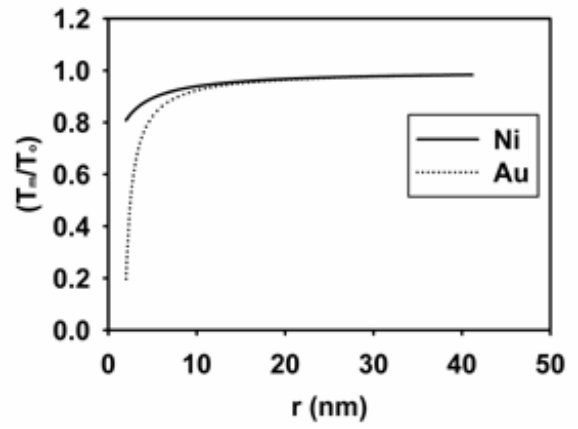

Figure 4.6: Size-dependent melting temperatures (T_m) of Ni and Au nanocrystals normalized by the bulk melting temperature (T_o) calculated using the modified Pawlow theory (Eqn 1).Note : The Au parameters were taken from Ref. 28.

The melting point depression for Ni nanocrystals is not nearly as severe as for Au. For 2 nm diameter particles, the melting point is depressed by ~80% for Au, but only ~20% for Ni. The ~5 nm diameter Ni nanocrystals are only expected to have a melting point depression of about 10%. If the Ni-Ge eutectic were depressed by a factor of 10%, it would drop by about 100^{o}C, which is still over 200^{o}C higher than the nanowire growth temperature. Furthermore, given that many of the nanowires are larger than 10 nm in diameter, and there would be even less of a melting point depression. It is highly unlikely that Ni-seeded Ge nanowires grow from a liquid alloyed seed droplet at 410~460^{o}C.

4.4.2 The $NiGe_x$ Seed Particle Shape

The shape of the $NiGe_x$ particles at the tips of the wires depended strongly on the nanowire diameter. $NiGe_x$ particles at the ends of small diameter Ge nanowires (<15 nm) were hemispherical (i.e., lens-shaped) with diameters corresponding close to the starting Ni nanocrystal size (Figures 4.7(a,b). In contrast, particles at the tips of large diameter nanowires (>25nm) were irregularly shaped, consistent with aggregated nanocrystals that had only partially coalesced. For example, the $NiGe_x$ particle in Figure 4.7d at the tip of a 32nm diameter nanowire has an irregular cubic faceted shape and the $NiGe_x$ particle in Figure 4.7f at the end of a very large 67 nm diameter nanowire (which incidentally is very rare) has a very irregular shape, also characteristic of aggregated partially coalesced nanocrystals. Nanobeam EDS showed that both the smaller diameter regularly-

shaped, and the larger diameter irregularly-shaped, $NiGe_x$ particles at the tips of the nanowires had a Ni:Ge ratio in the range of 1.5 to 2.8. Because the seed particle remains a solid during nanowire growth, the coalescence rate is very slow. The $NiGe_x$ seed particle morphology contrasts the Au-Ge seed particles observed at the tips of Ge nanowires in the SFLS growth process. The SFLS process can also yield very large diameter nanowires under certain growth conditions; for example, a batch process starting with 2 nm diameter Au nanocrystals can produce Ge nanowires ranging from 10 to 100 nm in diameter. The Au particles at the tips of the wires, however, are all spherical, like those shown in Figrue 4.7(f). The Au-Ge particles at the tips of the wires are much more prone to aggregation and coalescence than the $NiGe_x$ particles because they are in the liquid phase.

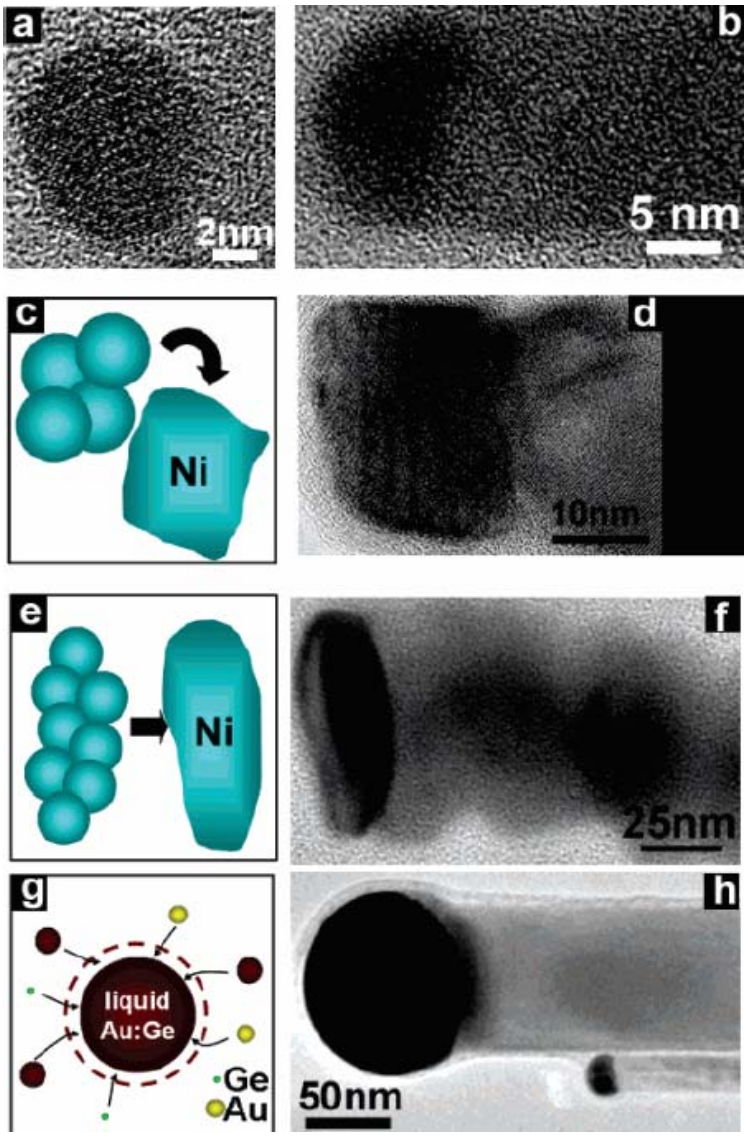

Figure 4.7: (a) TEM image of a Ni nanocrystal. (b,d,f) TEM images showinig the $NiGe_x$ seed particles at the tips of Ge nanowires with increasing diameters: 15 nm, 32 nm, 67 nm. (h) TEM image of Au seeds at the ends of 22 nm and 98 nm diameter Ge nanowires grown by SFLS. (c,e,g) Illustrations of seed particle aggregation that occurs during nanowire growth.

4.4.3. Diameter Distribution of SFSS-grown Ge Nanowires

Figure 4.8 compares the Ge nanowire diameter distributions obtained using Ni and Au nanocrystals as seeds under the same reaction conditions. The Ni-seeded wires have a narrower size distribution and are much smaller than the Au-seeded nanowires. The Ni-seeded wires have an average diameter of 14.5 nm and more than 80% of Ge nanowires were smaller than 20nm. The Au-seeded nanowires on the other hand are polydisperse and larger, with an average diameter of 54.8 nm. Seed particle aggregation must occur in both reactions, however, the Au nanocrystals aggregate to a much higher extent than the Ni nanocrystals. Au particles form liquid Au-Ge droplets during nanowire growth that are highly susceptible to aggregation with other Au seed particles (note that this seed aggregation process must occur at the very early stages of growth since the diameters do not increase noticeably along the length of the nanowires); whereas, Ni nanocrystals form a solid Ni-Ge alloy that is much less susceptible to aggregation.

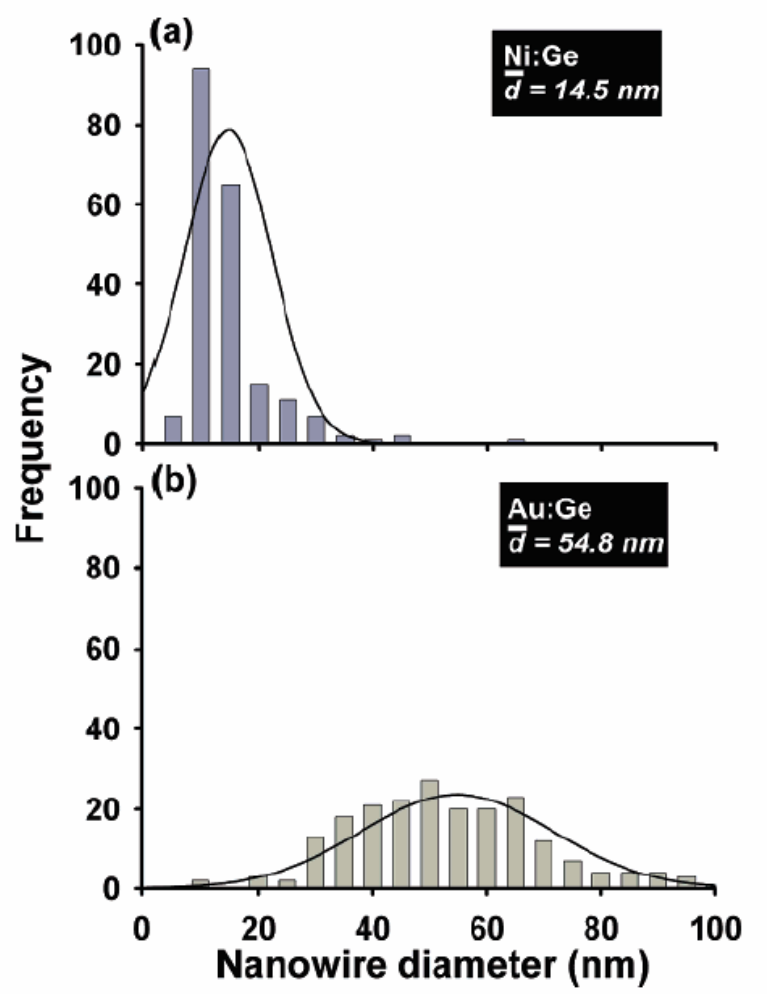

Figure 4.8: Diameter distributions of Ge nanowires synthesized in toluene at 460°C, 23.4MPa, and a Ge:metal mole ratio of 100:1 using (a) 5.6 nm diameter Ni nanocrystals and (b) 2 nm diameter Au nanocrystals as seeds.

Another reason that the Ni-seeded Ge nanowire size distribution is centered in the small size range relates to the apparent relationship between the growth rate and the diameter. Larger diameter Ge nanowires exhibit large concentrations of extended defects and poor morphology, as shown in Figure 4.9, consistent with slow

growth. Narrow diameter Ni-seeded Ge nanowires (<15 nm) are straight and crystalline and are much longer than the larger diameter nanowires. Larger diameter Au-seeded Ge nanowires, on the other hand, were observed to be as large as 100 nm in diameter with straight morphologies and very few extended defects (Figure 4.9d). Ge diffusion through the nanocrystal seed is relatively fast in liquid Au-Ge, regardless of the diameter; whereas, the solid-state diffusion rates become limiting as the Ni-Ge seed particles become larger than ~15 nm in diameter.

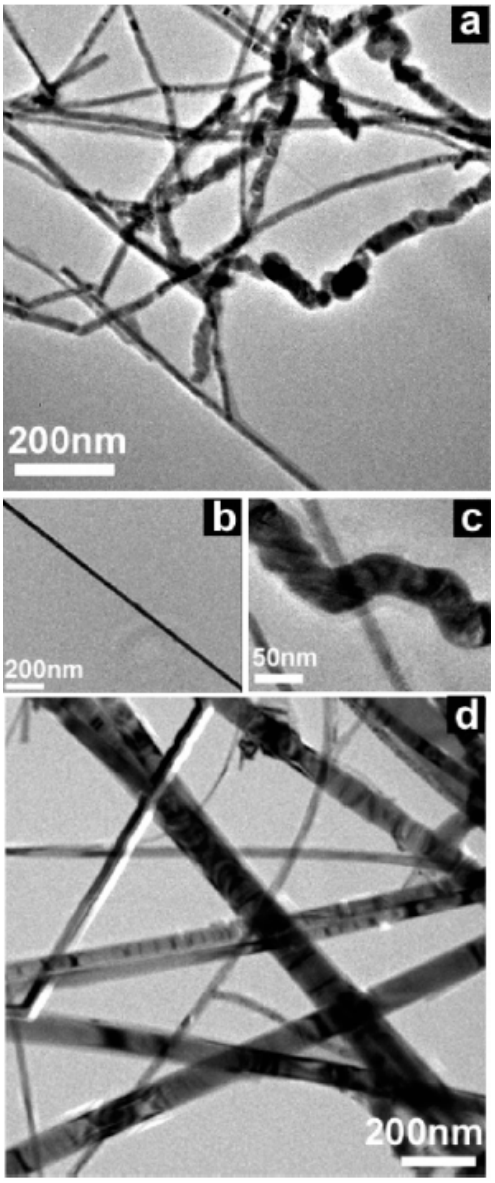

Figure 4.9: TEM images of Ge nanowires seeded by (a-c) Ni and (d) Au nanocrystals.

4.4.4 DIFFUSION-LIMITED GROWTH

Several investigators have predicted for *VLS* nanowire growth that the growth rate should decrease as the diameter decreases as a result of the Kelvin effect, which lowers the supersaturation in smaller diameter nanocrystals[31, 32]. The growth rates of the Ni-seeded Ge nanowires, however, appear to be limited by semiconductor diffusion through the metal seed particle with the opposite size dependence of faster growth for smaller diameter wires. From the observed nanowire growth rates, one can estimate a lower limit for the solid-phase diffusion coefficient of Ge in Ni needed for solid-phase seeding of the wires. Based on the observed lengths *L*, obtained from the reactor (consider 10μm with 10 min reaction time), the linear growth rate (dL/dt) must be at least 1 μm/min (0.017 m/sec). The Ge flux supplied to the tip of the solid nanowire surface, $Flux\big|_{surface}$, by diffusion through the seed metal tip to maintain this growth rate is

$$Flux\big|_{surface} = \rho_{Ge}\frac{dL}{dt}$$

The mass transfer rate at the solid nanowire surface interfaced with the metal particle can be expressed as:[33]

$$Flux\big|_{surface} = k_m \Delta C_{Ge,alloy}$$

where k_m is the mass transfer coefficient (cm/sec) and $\Delta C_{Ge,alloy}$ is the concentration gradient of Ge in the alloyed metal tip from the solvent/metal interface to the metal/semiconductor interface. If nanowire crystallization kinetics

are assumed to be much faster than the rate of Ge diffusion through the metal seed particle, then the concentration at the metal/semiconductor interface will be zero. If we assume the highest possible concentration gradient and take the Ge concentration at the metal/solvent interface as the concentration of pure Ge so that $\Delta C_{Ge,alloy} \approx C_{Ge,pure} = \rho_{Ge}$, then we see that $k_m \geq (dL/dt)$ in order to sustain nanowire growth. For simplicity, we can estimate k_m for transport to the center of a sphere, which gives $k_m = D/R_{sphere}$. Although the metal seed particle is not exactly spherical, this assumption provides an order of magnitude estimate for the rate of diffusion of Ge from the metal/solvent interface to the metal/nanowire interface. Taking the smallest diameter nanowires observed, $R_{sphere} = 2.5\,\text{nm}$, and Ge in Ni diffusivity ($D_{Ge \rightarrow Ni}$) of $D \geq 4.25 \times 10^{-13}\,\text{cm}^2/\text{sec}$ is needed to maintain wire growth. This is about six to orders of magnitude *faster* than the measured bulk diffusivity of Ge in Ni at 460°C ($D_{Ge \rightarrow Ni} = 1.79*10^{-19}$ cm^2/s).[34] This appears to indicate that the solid-state seeding mechanism is physically unrealistic; however, the bulk diffusivity of Ni in Ge is *extremely fast*, with $D_{Ni \rightarrow Ge} = 4.6*10^{-7}$ cm^2/s.[35] As DPG decomposes, Ge adsorbs to the surface of the Ni seed particles, and then Ni can counterdiffuse *into* the Ge to promote nanowire growth as illustrated in Figure 4.10 (e-h). Another possibility is a surface-enhanced diffusion process, as shown in Figure 4.10 (b-d), in which adsorbed Ge diffuses around surface of the solid Ni nanocrystal to incorporate in the nanowire. This type of

surface diffusion growth mechanism appears to occur for Fe nanocrystal-seed multiwall carbon nanotube growth from supercritical toluene[18, 36], and is a possibility.

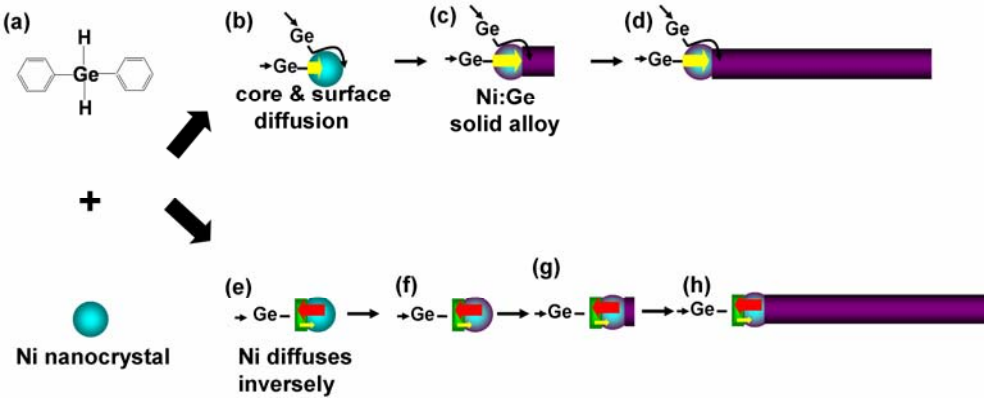

Figure 4.10: Schematic of two possible SFSS growth mechanisms: (b-d) surface-enhanced solid state diffusion process; (e-h) solid-state volume counter-diffusion process.

4.5 CONCLUSIONS

Ni nanocrystals are effective seeds for growing Ge nanowires at temperatures well below the lowest eutectic temperature on the Ni-Ge phase diagram. Substantial evidence indicates that the nanowires are growing via a solid-phase seeding process. Model calculations showed that a size-dependent melting temperature depression would not be sufficient to induce melting of the $NiGe_x$ seed particles, there appears to be a significant decrease in growth rate with increasing nanowire diameter, and the diffusion rates of Ni into Ge are orders of magnitude faster than required for nanowire growth. In fact, the strong size dependence of the

nanowire growth rates appears to *focus* the diameter distribution at smaller sizes and prevent significant accumulation of larger diameter nanowires. This kind of "size-focusing" does not appear to happen in VLS-type growth from liquid alloy seed particles, where the diameter distributions must be controlled through careful processing parameter changes[16], representing an advantage of the SFSS process over SFLS. Solid-phase metal nanocrystal seeding of semiconductor nanowires provides a complementary growth mechanism to liquid-phase seeding. Both processes are driven by thermodynamic equilibrium between a metal:semiconductor alloy phase and the pure crystalline semiconductor. Solid-phase seeding, however, can become kinetically limited—especially at lower temperature—by relatively slow semiconductor diffusion through the seed particle to the nanowire interface, especially for larger diameter nanowires. The fact that it should be possible to grow semiconductor nanowires using alternative metals with very high liquid metal:semiconductor eutectics at significantly lower temperature greatly increases the number of metals available and range of potential operating conditions for "VLS"-type nanowire synthesis, which is important for future integration of nanowires in devices.

4.6 REFERENCES

(1) Law, M.; Goldberger, J.; Yang, P. *Annu. Rev. Mater. Res.* **2004,** *34*, 83-122.

(2) Heath, J. R.; LeGoues, F. K. *Chem. Phys. Lett.* **1993,** *208*, 263-268.

(3) Zou, J.; Baldwin, R. K.; Pettigrew, K. A.; Kauzlarich, S. M. *Nano Lett.* **2004,** *4*, 1181-1186.

(4) Taylor, B. R.; Fox, G. A.; Hope-Weeks, L. J.; Maxwell, R. S.; Kauzlarich, S. M.; Lee, H. W. H. *Mater. Sci. Eng. B* **2002,** *B96*, 90-93.

(5) Wilcoxon, J. P.; Samara, G. A.; Provencio, P. N. *Phys. Rev. B* **1999,** *60*, 2704-2714.

(6) Wilcoxon, J. P.; Provencio, P. P.; Samara, G. A. *Phys. Rev. B* **2001,** *64*, 035417/1-035417/9.

(7) Holmes, J. D.; Ziegler, K. J.; Doty, R. C.; Pell, L. E.; Johnston, K. P.; Korgel, B. A. *J. Am. Chem. Soc.* **2001,** *123*, 3743-3748.

(8) Lu, X.; Ziegler, K. J.; Ghezelbash, A.; Johnston, K. P.; Korgel, B. A. *Nano Lett.* **2004,** *4*, 969-974.

(9) Gerion, D.; Zaitseva, N.; Saw, C.; Casula, M. F.; Fakra, S.; Van Buuren, T.; Galli, G. *Nano Lett.* **2004,** *4*, 597-602.

(10) Wang, W.; Huang, J.; Ren, Z. *Langmuir* **2005,** *21*, 751-754.

(11) Holmes, J. D.; Johnston, K. P.; Doty, R. C.; Korgel, B. A. *Science* **2000,** *287*, 1471-1473.

(12) Hanrath, T.; Korgel, B. A. *J. Am. Chem. Soc.* **2002,** *124*, 1424-1429.

(13) Davidson, F. M., III; Schricker, A. D.; Wiacek, R. J.; Korgel, B. A. *Adv. Mater.* **2004,** *16*, 646-649.

(14) Davidson, F. M., III; Wiacek, R.; Korgel, B. A. *Chem. Mater.* **2005,** *17*, 230-233.

(15) Hanrath, T.; Korgel, B. A. *Adv. Mater.* **2003,** *15*, 437-440.

(16) Shah, P. S.; Hanrath, T.; Johnston, K. P.; Korgel, B. A. *J. Phys. Chem. B* **2004,** *108*, 9574-9587.

(17) Thaddeus B. M.; Hiroaki O., S. P. R., Linda K. *Binary Alloy Phase Diagram*, , 2nd ed,; ASM Internation: Materials Park OH. 1990; Vo.1.

(18) Lee, D. C.; Mikulec, F. V.; Korgel, B. A. *J. Am. Chem. Soc.* **2004,** *126*, 4951-4957.

(19) Hsieh, Y. F.; Chen, L. J.; Marshall, E. D.; Lau, S. S. *Thin Solid Films* **1988,** *162*, 287-294.

(20) Tuan, H.-Y.; Lee, D. C.; Hanrath, T.; Korgel, B. A. *Nano Lett.* **2005,** *5*, 681-684.

(22) Kamins, T. I.; Williams, R. S.; Basile, D. P.; Hesjedal, T.; Harris, J. S. *J. Appl. Phys.* **2001,** *89*, 1008-1016.

(23) Persson, A. I.; Larsson, M. W.; Stenstroem, S.; Ohlsson, B. J.; Samuelson, L.; Wallenberg, L. R. *Nature Mater.* **2004,** *3*, 677-681.

(24) Murray, C. B.; Sun, S.; Doyle, H.; Betley, T. *MRS Bull.* **2001,** *26*, 985-991.

(25) Hanrath, T.; Korgel, B. A. *Small* **2005,** *1*, 717-721.

(26) Takizawa, H.; Uheda, K.; Endo, T. *Journal of Alloys and Compounds* **2000,** *305*, 306-310.

(27) Wang, D.; Dai, H. *Angew. Chem. Int. Ed.* **2002,** *41*, 4783-4786.

(28) Castro, T.; Reifenberger, R.; Choi, E.; Andres, R. P. *Phys. Rev. B* **1990,** *42*, 8548-8556.

(29) *CRC Handbook of Chemistry and Physics 85th*, edited by David R. Lide, 2004).

(30) Murr, E. L. *Interfacial Phenomena in Metals and Alloys*, Addison-Wesley, Reading, 1975.

(31) Wu, Y.; Fan, R.; Yang, P. *Nano Lett.* **2002,** *2*, 83-86.

(32) Givargizov, E. I. *J. Crystal Growth* **1975,** *31*, 20-30.

(33) Bird, R. B.; Stewart, W. E.; Lightfoot., E. N., Wiley, 2002.

(34) Mantl, S.; Rothman, S. J.; Nowicki, L. J.; Lerner, J. L. *J. Phys. F: Metal Phys.* **1983,** *13*, 1441-8.

(35) Goldsmid, H. J. *Diffusion in Semiconductors* **1963**, Inspec, London.

(36) Lee, D. C.; Korgel, B. A. *Mol. Simul. in press*.

Chapter 5: Silicon nanowires and silica nanotbues seeded by copper sulfide nanocrystals

5.1 INTRODUCTION

Semiconductor nanowires[1] can be made using chemical routes, such as vapor-liquid-solid (VLS),[2,3] solution-liquid-solid (SLS)[4,5] and supercritical fluid-liquid-solid (SFLS)[6-8] methods and they are being explored as active components in new chemical sensors,[9] photovoltaics,[10] electronics,[11,12] medical diagnostics[13] and optoelectronic[14] devices. Nanotubes[15] are also being explored for these kinds of applications, but their hollow cores make them additionally suitable for use as nanosize containers,[16-18] reaction compartments,[19-22] or nanofluidic pipes to transfer or separate fluids and molecules[15,23,24] in lab-on-a-chip applications. The most successful chemical approaches to making nanotubes involve templating, which can give high quality nanotubes but requires multiple reaction steps and tends to give relatively small amounts of material. More scalable, direct synthetic routes for nanotubes are desired.

Chemical routes to nanotubes of materials with sp^2 bonding, like carbon, have been thoroughly studied. sp^2-bonding leads to sheet-like crystal structure that thermodynamically favors hollow tube formation[25,26] and nanotubes of these "fullerene-like" materials spontaneously form at very high temperature (i.e., >1000^{o}C).[27-29] Nanotubes also form at significantly reduced temperature (<800^{o}C) when metal particles are used as catalytic seeds to speed reactant decomposition and

provide nucleation and growth sites for the tubes.[30-33] The three-dimensional bonding of materials like amorphous silica, however, provides no thermodynamic driving force for nanotube formation[34,35] and kinetic routes must be developed for nanotubes of this class of materials. Templating is the most common chemical approach. The pores of mesoporous substrates can be coated with a material and then the substrate dissolved to leave free-floating nanotubes.[36-41] Sacrificial wire-shaped materials, such as carbon nanotubes and nanofibers,[22,42-44] inorganic nanowires[45-48] or rod-shaped surfactant aggregates[50-58] have been used as nanotube templates.[59] And "reactive templating" has been explored, in which a nanowire is chemically converted to a hollow nanotube by a surface reaction, as in the conversion of ZnO nanowires to ZnS nanotubes,[60,61] Se nanowires into CdSe nanotubes[62] and Ag nanowires into Au nanotubes.[63,64] Templating, however, requires multiple synthetic steps—template generation, materials deposition, and template dissolution—and often provides relatively low yields. Direct synthetic routes are more desirable from a manufacturing standpoint, but it is not clear at the moment how to rationally design such systems.

There is indeed precedent in the literature for direct synthesis of nanotubes of materials with 3D bonding. For example, TiO_2 nanotube "forests" have been produced by direct electrochemical anodization of Ti substrates.[65,66] Amorphous InP nanotubes,[67,68] GaN nanotubes,[69] crystalline AlN nanotubes,[70,71] and Sb_2S_3 nanotubes[72] have been obtained from high temperature vaporization (>1000^{o}C) and

condensation processes; and Se,[73] TiO_2,[74,75] ZnO[76] and perovskite[77] nanotubes have formed under hydrothermal and sonochemical conditions. In these systems, impurities appear to serve as nanotube nucleation and growth sites (i.e., Si for SiO_2; In for InP) for the nanotubes; for example, In,[78] Ge,[79] CdSe,[80] and In_2S_3,[81] have promoted amorphous SiO_2 nanotube formation in vapor-phase reactions; a Ni catalyst layer generated GaN nanotubes;[82] Ga metal has induced GaP nanotube formation;[83] Au particles have seeded amorphous Si nanotubes;[84] and CeO_2 particles have promoted TiO_2 nanotube growth under hydrothermal conditions.[85] This evidence shows that a chemical approach to nanotubes (of materials with 3D crystal structure) analogous to "VLS" nanowire growth should be possible. Here, we report such a synthesis, of amorphous SiO_2 nanotubes seeded by CuS nanocrystals in supercritical toluene at 500°C and 10.3 MPa using monophenylsilane (MPS) as a reactant in the presence of trace water and oxygen as oxidizing agents.

In Chapter 5, copper sulfide (CuS) nanocrystals are found to induce the growth of silicon (Si) nanowires or silica (SiO_2) nanotubes in supercritical toluene at 500°C at 10.3 MPa using monophenylsilane (MPS) as a reactant. Crystalline Si nanowires form under inert reaction conditions; whereas, amorphous SiO_2 nanotubes form when small amounts of water and oxygen are present. A portion of the SiO_2 nanotubes (~5%) were found to be helically coiled. The CuS seed particles convert to Cu metal during nanowire and nanotube growth, and since the growth temperature is several hundred degrees below the Cu:Si eutectic of 800°C,

both nanowires and nanotubes appear to be growing from solid-phase seed particles. Gold (Au) nanocrystals were found to yield predominantly SiO_2 nanofibers as opposed to tubes under similar reaction conditions, with no coiled nanotubes or nanofibers. The silica/metal interface morphology was examined and found to differ significantly for Au and Cu, which perhaps explains the difference in silica morphology produced by these two metals.

5.2 EXPERIMENTAL

5.2.1 Reaction Chemicals

Anhydrous toluene (99.8%), anhydrous hexane, monophenylsilane (MPS, 97%) were purchased from Sigma-Aldrich, stored under nitrogen and used as received. 5 nm diameter dodecanethiol-coated gold nanocrystals were synthesized as described by Saunders, et al.[86] Oleylamine and octenoic acid stabilized CuS nanocrystals (12 nm diameter) were synthesized as described by Ghezelbash and Korgel.[87]

5.2.2 REACTOR SETUP AND PROCEDURE

Crystalline Si nanowires and amorphous SiO_2 nanotubes were synthesized in a 10 mL Ti grade-2 tubular high-pressure reactor as described in Refs. 88 and 89. The reactor is connected to a high-pressure liquid chromatography (HPLC) pump that regulates the reactor pressure and provides a convenient way to inject reactants into the reactor. The reactor is encased in an insulated brass block and the reactor temperature is monitored by a thermocouple. The reactor pressure is adjusted by a

micro-control valve attached to the exit port on the reactor. In a nitrogen-filled glove box (O_2 < 0.2 ppm), a small clean and dried Si wafer is placed in the reactor, which helps to collect the nanowires and nanotubes produced in the reaction. The reactor is sealed in the glove box and then connected externally to the HPLC pump and placed in the heated brass block. After the reactor reaches the desired temperature (typically ~500 ^{o}C), anhydrous and oxygen-free toluene is added to the reactor until reaching a pressure of 3.4 MPa.

5.2.3 Silicon Nanowire Synthesis

CuS nanocrystal-seeded Si nanowires were made using a reactant solution of 500 µL anhydrous deoxygenated toluene with 150 mM MPS and CuS nanocrystals (150:1 Si:CuS mole ratio) prepared in a nitrogen-filled glove box. For Au nanocrystal seeding, the reactant solution was 500 µL anhydrous deoxygenated toluene with 350 mM MPS and a 1000:1 Si:Au mole ratio. Once the reactor was pre-heated as described above, the reactant solution was loaded into a 1 mL syringe, taken out of the glove box and injected into a six-way HPLC injection loop (Valco). The reactant mixture was pumped into the reactor at a flow rate of 0.4 mL min^{-1} until reaching a final pressure of 10.3 MPa. After 10 min, the reactor was submerged in an ice-water bath for 2 min and then cooled to room temperature by flowing air over it. Most of the nanowire product is collected as a powder on the Si collection wafer in the reactor and on the reactor walls.

5.2.4 Silica Nanotube Synthesis

Silica nanotubes were produced following the same procedure used to make nanowires, except that trace water and oxygen are present in the reactant solution. 450μL of the oxygen-free anhydrous toluene reactant solution (150 mM MPS and 150:1 Si:CuS mole ratio; or 350 mM MPS and 1000:1 Si:Au mole ratio) was removed from the glove box by syringe and 50 μL of "benchtop" toluene was added. The benchtop toluene is saturated with water (0.001 vol%) and oxygen (~1.0 mM) and serves as the source of these reactants.

5.2.5 Materials Characterization

Reaction products were characterized by high-resolution scanning electron microscopy (HRSEM), transmission and scanning transmission electron microscopy (TEM and STEM), X-ray energy dispersive spectroscopy (EDS), X-ray diffraction (XRD), and electron energy loss spectroscopy (EELS). HRSEM images were obtained on a LEO 1530 field-emission SEM with 1-3 kV accelerating voltage with working distances ranging between 2 to 5 mm, typically by looking at the deposition substrate with the collected product. HRTEM, STEM, EDS, and EELS were performed on a field-emission JEOL 2010F TEM equipped with a Gatan parallel-EELS GIFF spectrometer and an Oxford INCA EDS. For TEM and STEM imaging, the nanowires and nanotubes were transferred by scratching the material off the deposition substrate onto a 200-mesh lacey carbon-coated nickel grid (Electron

Microscope Sciences). TEM images were obtained at 200 kV accelerating voltage. EELS, line scan EDS, and EDS-mapping were performed with the microscope in STEM mode at 200 kV accelerating voltage. EELS spectra were obtained by focusing the electron beam to a 0.7nm diameter spot and then acquiring spectra as a function of probe position on the nanowire or nanotube. XRD was performed using a Phillips vertical scanning diffractometer using 12 deg/min scan rate with 0.02 degrees increment in the continuous locked coupled mode. XRD measurements were performed on nanowires and nanotubes evaporated onto a quartz substrate from concentrated dispersions in chloroform.

5.3 RESULTS AND DISCUSSION

5.3.1 Silicon Nanowire Synthesis with CuS Nanocrystals

Crystalline Si nanowires form when MPS is thermally decomposed in anhydrous, oxygen-free supercritical toluene at 500 °C and 10.3 MPa in the presence of CuS nanocrystals. Figure 5.1 shows an SEM image of Si nanowires produced in such a reaction, along with high resolution TEM and XRD data confirming that they are crystalline diamond cubic Si. The reaction yield is comparable to Au nanocrystal-seeded Si nanowire reactions, but the CuS-seeded nanowires are slightly shorter, with an average length of 7.4 μm and diameters ranging between 5 and 20 nm (as observed by SEM from over 100 wires) (For details about Au nanocrystal-seeded Si nanowires, see Refs. 88 and 89).

Nanowires were observed with three different growth directions, <111>, <110> and <112>, and Figures 5.1b-d show examples of nanowires with each growth direction. Of 104 nanowires examined by high resolution TEM, ~75% of the nanowires had grown in the <111> direction, ~20% in the <110> direction and ~5% in the <112> direction. All of the nanowires observed with <112> growth direction also had lamellar {111} twins extending down their length, as seen in Figure 5.1c. This kind of {111} twinning down Si nanowires with <112> growth direction has also been observed in SFLS-grown Si nanowires seeded with Au nanocrystals.[88,90,91]

Nanobeam EDS (Figure 5.1f) reveals both Cu and Si in the seed particle. It is difficult to quantify the Cu:Si ratio by nanobeam EDS because of background scattering from the Si nanowire, but both Cu and Si are clearly present in the seed particle. Note that S is absent and therefore does not appear to be involved in nanowire seeding. Sulfur was observed at the tip of a few nanowires, but this was rare, and in these cases the nanowires tended to have large diameters and many crystallographic defects (See Section 5.3.6 for details). It is interesting to note that Kohno and Takeda observed Si nanowire formation form a Si wafer coated with a CuS powder heated to 1230^{o}C.[92] Although their reaction temperatures are many hundreds of degrees higher than ours and the nanowire growth mechanism is slightly different (the wafer is the source of Si for the nanowires), it is interesting to note that they also found that sulfur diffused out of the seed particles in their reactions as well, and the nanowires were seeded by copper. VLS (and SFLS)

nanowire growth requires the formation of a liquid eutectic between the seed metal and the semiconductor at the growth temperature. With the loss of S from the CuS nanocrystals, for VLS growth to occur, the reaction temperature should be above the Cu:Si eutectic; however, our nanowire growth temperature is well below the lowest temperature Cu:Si eutectic at 800°C.[93] However, Si has a high solid solubility in Cu, which makes solid-phase nanowire seeding possible, as we have observed with Ni and Co metal seed particles for Si and Ge nnaowires.[94-96] As long as the seed particle is small enough for solid-state diffusion to keep up with the rate of nanowire crystallization (which is the case for the 10~20 nm diameter seeds used here),[95] nanowires can grow from a solid-phase seed by supercritical fluid-solid-solid (SFSS) growth.

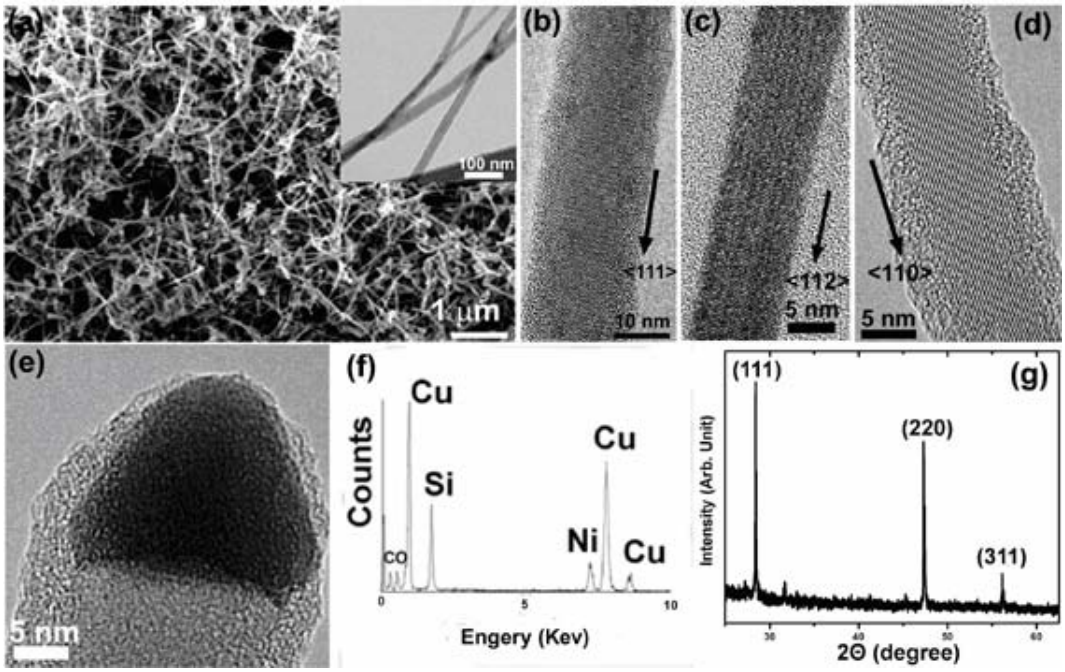

Figure 5.1: Si nanowires synthesized in supercritical toluene at 10.3 MPa and 500° C using MPS as a reactant in the presence of CuS nanocrystals. (a) HRSEM image of Si nanowires. Inset: low-resolution TEM of three Si wires. (b-d) TEM images of Si nanowires with three different growth directions: <111>, <112>, and <110>. <111> is the predominant growth direction. (e) TEM image of a Cu-Si alloy particle at the end of a 19.3 nm diameter Si nanowire. (f) Nanobeam EDS data obtained from the metal seed at the tip of the nanowire, revealing the presence of Cu and Si. (The Ni signal originates from the Ni TEM grid.) (g) XRD peaks from the reaction product matches diamond cubic Si (PDF #27-1402).

5.3.2 Silica Nanotube Synthesis

MPS decomposition in supercritical toluene at 500oC and 10.3 MPa in the presence of CuS nanocrystals gave amorphous silica (SiO2) nanotubes instead of Si

nanowires when trace water and oxygen was added to the reaction mixture, Figure 5.2 shows silica nanotubes produced from such a reaction. A small number of crystalline Si nanowires were also observed, most likely because the water and oxygen concentrations in the reactions were too low to completely oxidize the products (See Section 5.3.7 for details). Overall, the SiO_2 nanotubes are shorter and not as straight as crystalline Si nanowires synthesized under inert conditions. EDS (Fig. 5.2h) and EELS (Fig. 5.3) both confirmed the nanotube composition to be SiO_2. The Si and O concentration profiles in EDS line scans mirror one another, with both the Si and O signals attenuated when the beam is positioned in the center of the nanotube. In EELS line scans (Figure 5.3), the absorption edge of the Si nanowire matches the Si L2,3 energy for monocrystalline Si at ~100 eV (Figures 5.3a-b) and the lineshape change and energy shift of the Si L2,3 absorption edge to ~105 eV is consistent with SiO_2.[97]

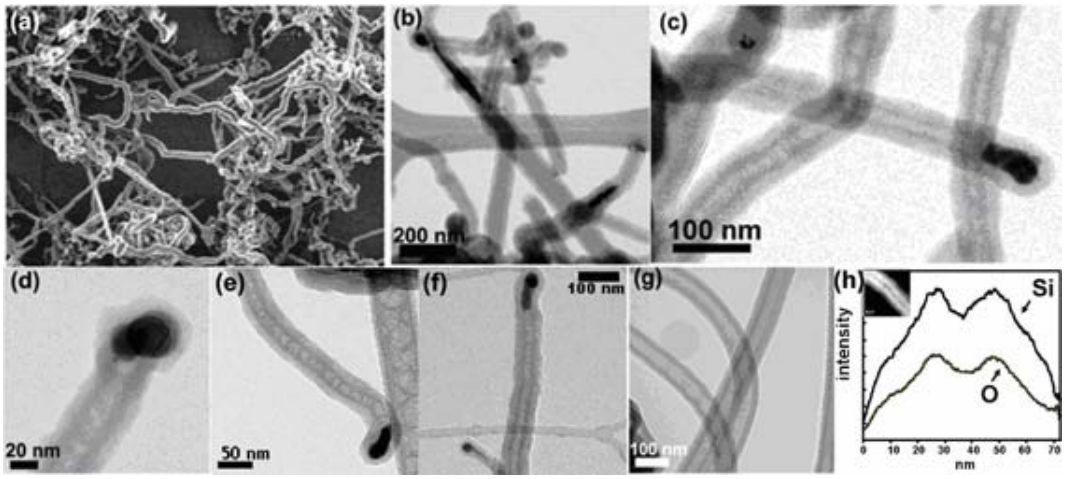

Figure 5.2: Silica nanotubes produced from MPS in supercritical toluene at 10.3 MPa at 500°C with trace water and oxygen in the presence of CuS nanocrystals. (a) HRSEM image of a field of silica nanotubes. (b-g) TEM images of silica nanotubes. The dark particles in the images are Cu. Note that the nanotubes in (e) and (f) have a bamboo morphology. (h) EDS linescans across the silica nanotube in the inset. Both oxygen and silicon are present and their concentration profiles mirror each other.

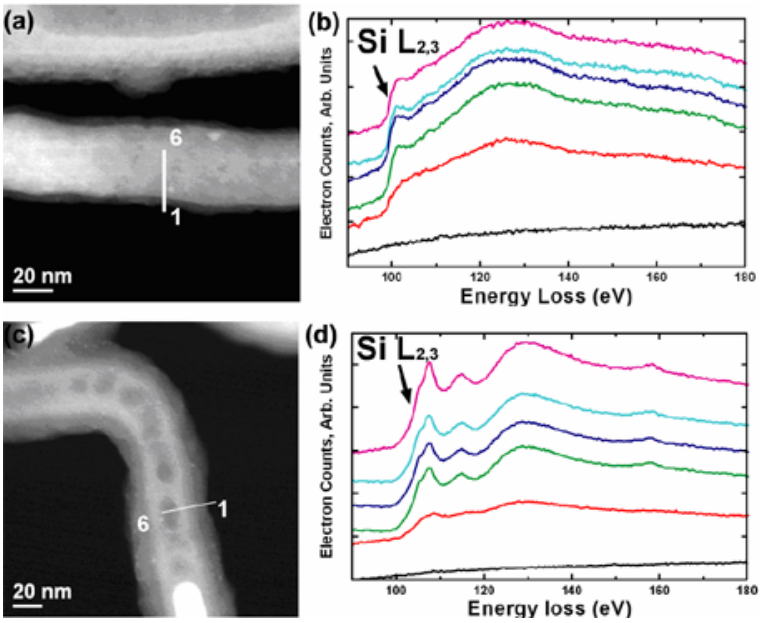

Figure 5.3: (a,c) STEM images and (b,d) EELS line scans of an (a,b) Si nanowire synthesized in supercritical toluene at 500°C, 10.3 MPa and CuS nanocrystals under inert conditions with MPS and (c,d) an SiO_2 nanotube made under similar reaction conditions in the presence of water and oxygen.

5.3.3 Silica Nanotubes and Nanofibers Seeded with Au Nanocrystals

When Au nanocrystals were used as seeds in the MPS decomposition reactions in toluene at 500oC at 10.3 MPa with trace water and oxygen in the reactant mixture, a combination of SiO_2 nanofibers and nanotubes (Figure 5.4) formed, although the majority of the product was solid amorphous SiO2 nanofibers with only one nanotube for every 20 nanofibers observed. Both the nanowires and nanotubes were amorphous (by TEM) and EDS confirmed that they were SiO_2.

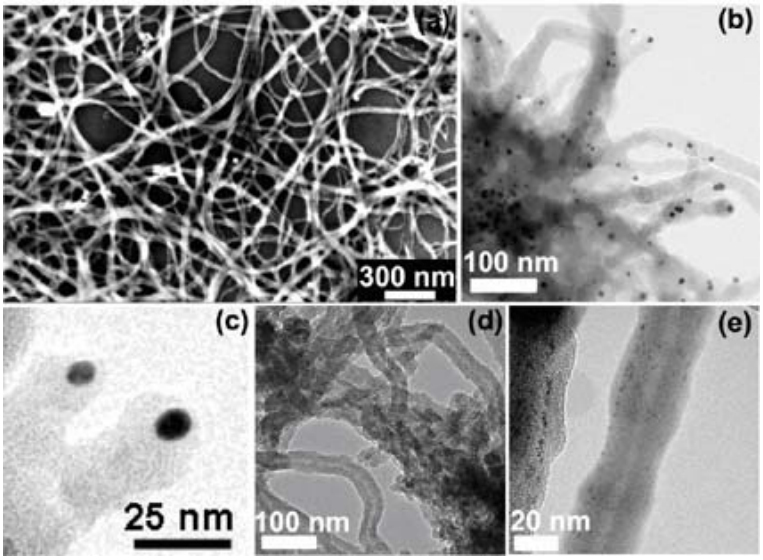

Figure 5.4: Silica nanotubes and nanofibers formed in the presence of Au nanocrystals by decomposing 350 mM MPS in toluene at 10.3 MPa at 500°C with Si:Au=1000:1 and trace water and oxygen: (a) HRSEM of a field of silica nanofiber; (b-c) TEM images of silica nanofibers with Au nanoparticle at their ends; (d) TEM of a region with a mix of silica nanofibers and nanotubes and (e) a single silica nanotube seeded with Au. Nanotubes made up approximately 5% of the sample.

5.3.4 Helical Silica Nanotubes Seeded by CuS Nanocrystals

Approximately 5% of the CuS nanocrystal-seeded SiO_2 nanotubes were observed to be helically coiled, like those in Figure 5.5. Nanotubes were observed to have both right-handed and left-handed helicities, and in some cases, the helicity changed down the length of an individual nanotube, as shown in Figures 5.4k-m. In some cases, the coiling stopped along the nanotube's length. Helical growth has been observed in other chemically-grown nanotubes and nanofibers, including Au-seeded silica fibers,[98] metal particle-catalyzed carbon nanotubes,[99] Co-seeded silica

fibers,[100] Fe particle-seed BN fibers,[101] and NiB particle-seeded SiC fibers.[102] Amelinckx et al.[99] proposed that the observed helical growth of multiwall carbon nanotubes seeded by metal particles resulted from a variation in the linear growth rate around the circumference of the nanotube at the metal/tube interface that creates a lateral stress that gives rise to coiling. McIlroy and coworkers[98,101,102] proposed that such a variation in growth rate at the metal seed interface can result from a circumferential difference in contact angle, which they call "contact angle anisotropy," between the metal seed and the nanotube or nanowire. Coiled silica nanotubes were not observed in the Au-seeded reactions, which probably relates to different wettability or interfacial contact between silica and Au and Cu, as discussed below.

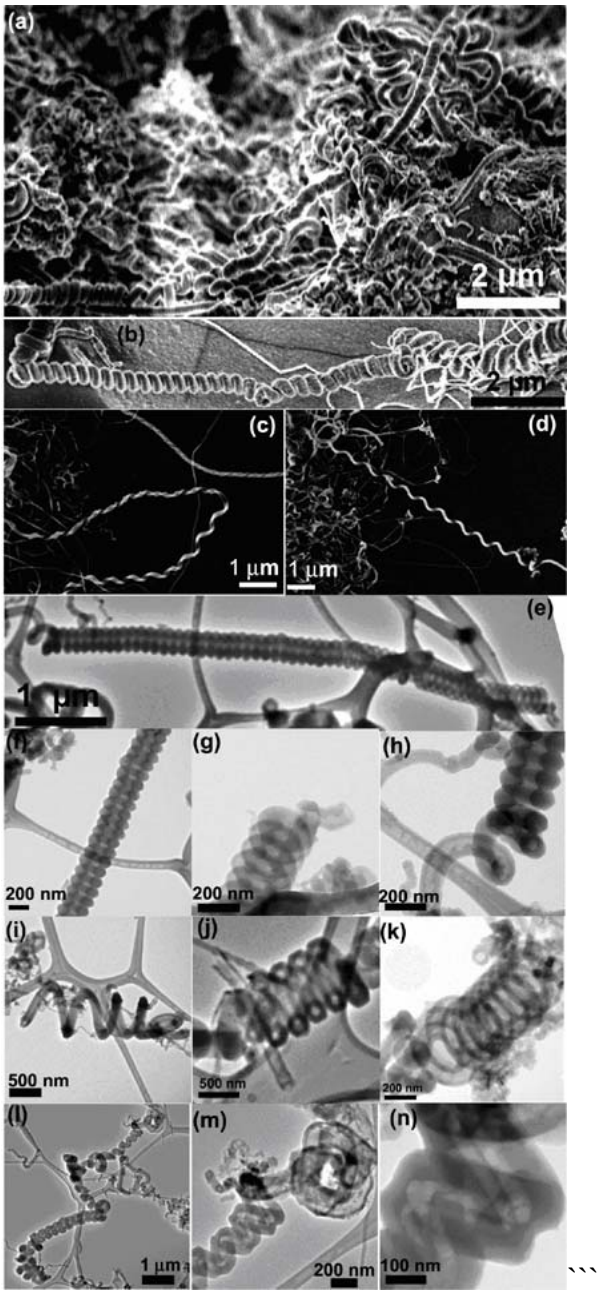

Figure 5.5: Helical silica nanotubes seeded by CuS nanocrystals in toluene at 10.3 MPa and 500°C with 150 mM MPS and trace water and oxygen.

5.3.5 Silica/Metal Interface Morphology

To try to understand why CuS nanocrystals yield predominantly SiO_2 nanotubes, while Au nanocrystals yield predominantly solid SiO_2 nanofibers (and no coiled structures), reactions were carried out with excess nanocrystals (50:1 nanocrystal:Si mole ratio) and the interfacial structure between the seed metal and the silica produced in the reaction was studied. Only aggregates of silica (or Si under inert conditions) embedded with Cu and Au particles, as shown in Figure 5.6, were produced at these excessive seed concentrations. There is not a significant difference between Cu/Si and Au/SiO_2 interface morphologies—the metal particles are approximately spherical and embedded uniformly in the aggregate—but the Cu/SiO_2 morphology is qualitatively different. In the SiO_2, the Cu particles have a tear-drop shape surrounded only partially by silica. We observed a similar "elongated" metal seed particle morphology at the tips of multiwall carbon nanotubes synthesized in supercritical toluene at 625°C,[32,33] and was recently reported to be important in *in situ* growth studies by TEM of metal particle-seeded multiwall carbon nanotubes.[103] Another significant difference between Cu and Au—that may ultimately relate to the difference in silica/metal interface morphology—is that Cu generates Si nanowires by solid-phase seeding, whereas Au forms a liquid eutectic with Si. It is unclear whether an Si nanowire forms that is subsequently oxidized in the presence of oxygen and water, or if Si oxidizes on the surface of the seed particle and then attaches to the end of the fiber or tube. In the case of Fe particle-seeded growth of multiwall carbon nanotubes, we found that

solid carbon fibers formed if C dissolved into the seed particle, while nanotubes formed when graphitic carbon appeared to associate only with the nanoparticle surface.[32,104] Cu seed particles are more likely than Au to permit surface oxidation of adsorbed Si. Cu and Au are chemically very different, as Cu can be both oxidized and reduced rather easily and could serve as an oxygen sink for oxidizing silicon at the particle surface, while gold is relatively inert to oxidation and reduction less likely to a substantial role in Si oxidation. It is possible that the observed difference in Au/ SiO_2 and Cu/SiO_2 interface morphology relates to the difference oxidation/reduction chemistry that occurs at the metal surface. More experiments are required to fully explore these ideas, but the metal/silica interface morphology is most like important to the formation of nanotubes.

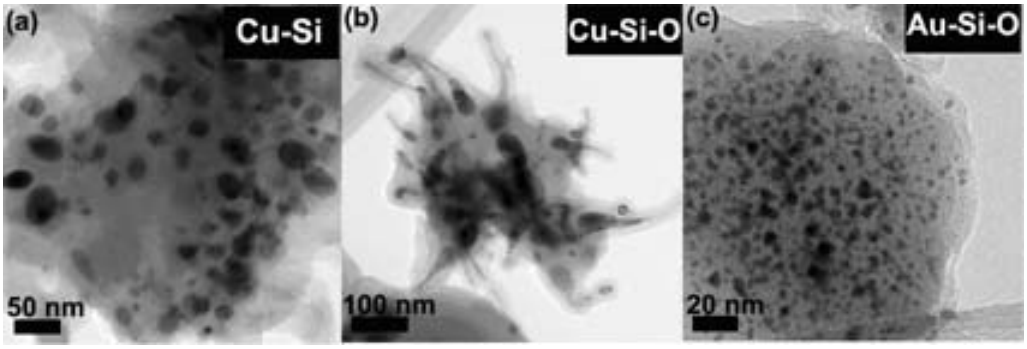

Figure 5.6: TEM images of (a) Cu nanoparticles embedded in Si formed by MPS decomposition in toluene at 500^{o}C and 10.3 MPa under inert reaction conditions (i.e., no oxygen and water); (b) Cu nanoparticles embedded in SiO_2 formed when trace oxygen and water were added to the reactions; and (c) Au nanoaprticles embedded in SiO_2 formed when trace oxygen and water were added to the reactions.

5.3.6 Sulfur Remaining in the CuS Seed Particle after Si Nanowire Growth

Figure 5.7 shows some representative TEM images of very large diameter crystalline Si nanowires obtained under inert reaction conditions. The tips of the wires had an amorphous aggregate with Cu, S and Si present. These nanowires appear to grow from aggregated seed particles, and perhaps the aggregation creates a diffusion barrier that prevents the complete loss of sulfur from the seed particle. Most of the nanowires observed with large amorphous Cu-Si-S seeds also had a large number of extended defects, as shown in Figure 5.8. Many of these defects are {111} twin planes. We also found some of the Si nanowires in which the metal seed particle at their tips ends up surrounded by amorphous silicon (Figure 5.9).

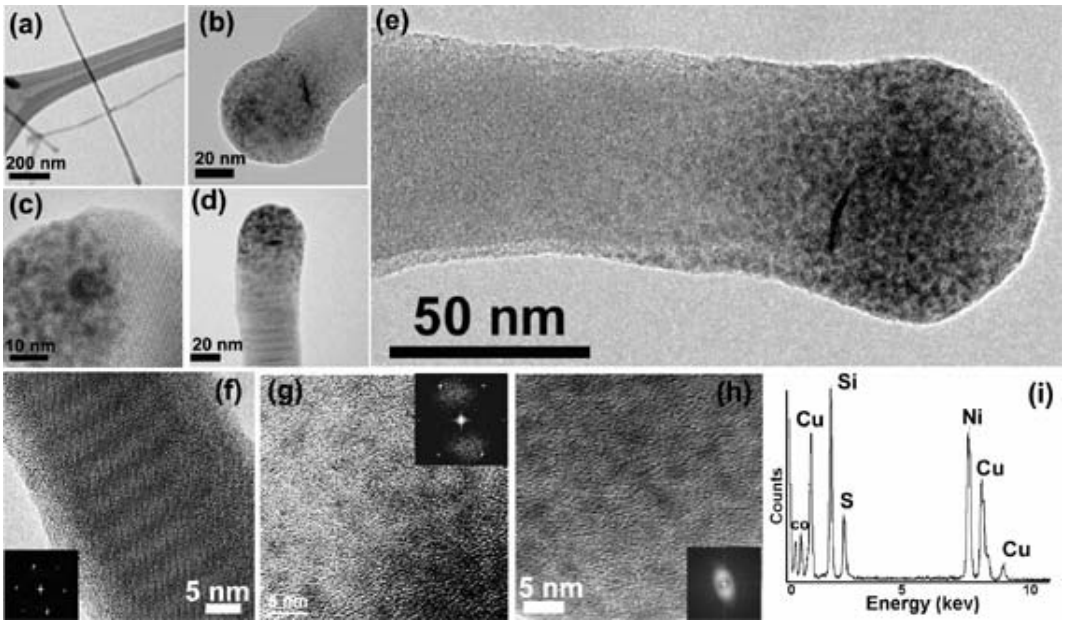

Figure 5.7: (a-e) TEM images of silicon nanowires with amorphous Cu-Si-S "seed" particles. The TEM images in (f-h) are higher magnification images obtained at different positions of the nanowire in (e). The image of the nanowire shown in (f) reveals that the nanowire is crystalline. The images in (g) and (h) show that the seed is an amorphous cluster of particles. (i) EDS on the tip confirms the presence of Si, Cu and S.

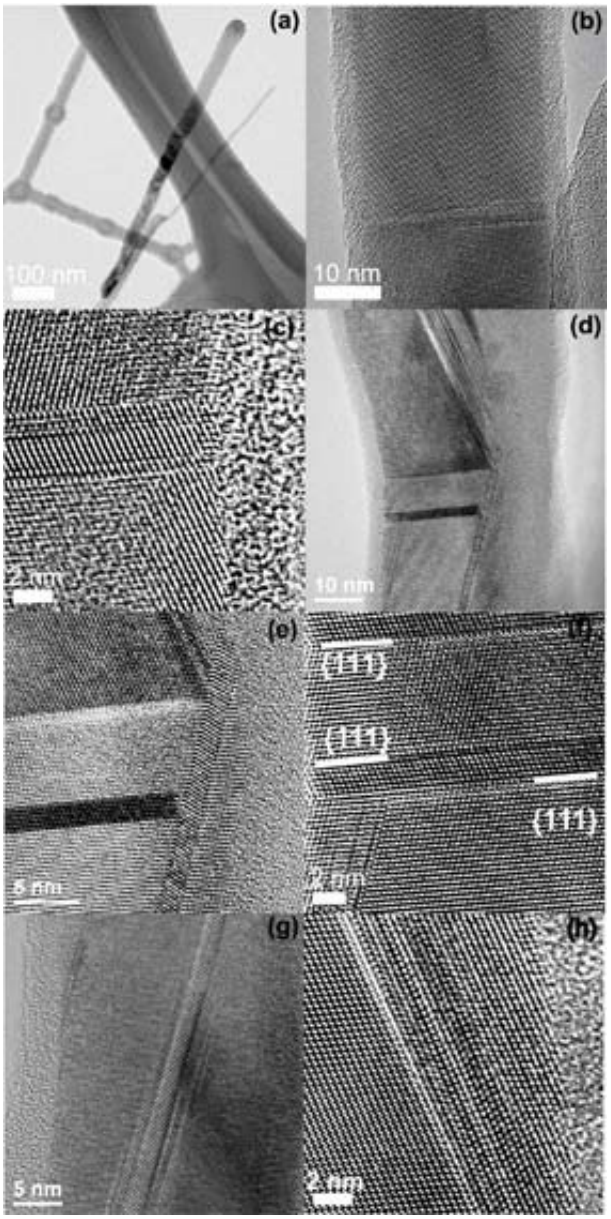

Figure 5.8: TEM images of an Si nanowire that was seeded by an amorphous Cu-Si-Si particle. Higher magnification images along the length of the nanowire (b-h) reveal many extended defects, including {111} twin planes.

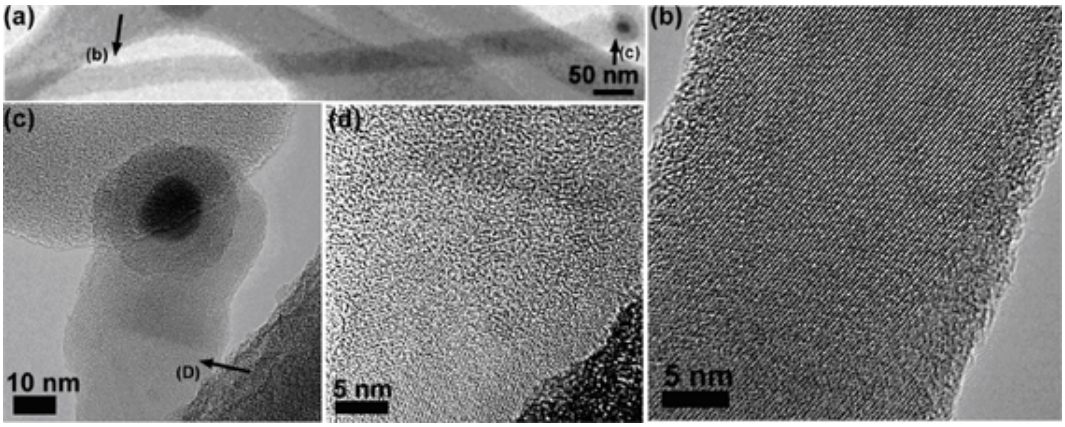

Figure 5.9: TEM images of a crystalline Si nanowire where the seed particle ends up surrounded by an amorphous coating that physically separates the seed form the nanowire.

5.3.7 A Small Proportion of Crystalline Si nanowires were Observed in the reactions with Trace Water and Oxygen

The MPS decomposition reactions carried out with trace water and oxygen that were found to yield predominantly SiO_2 nanotubes, were also found to produce a very small amount of crystalline Si nanowires. These nanowires, however, tended to have extremely large diameters, greater than 150 nm, and a rough morphology. Figure 5.10 shows an example of such an Si wire obtained from the reaction. The nanowire growth process is probably quite unstable, considering the final morphology of the wire.

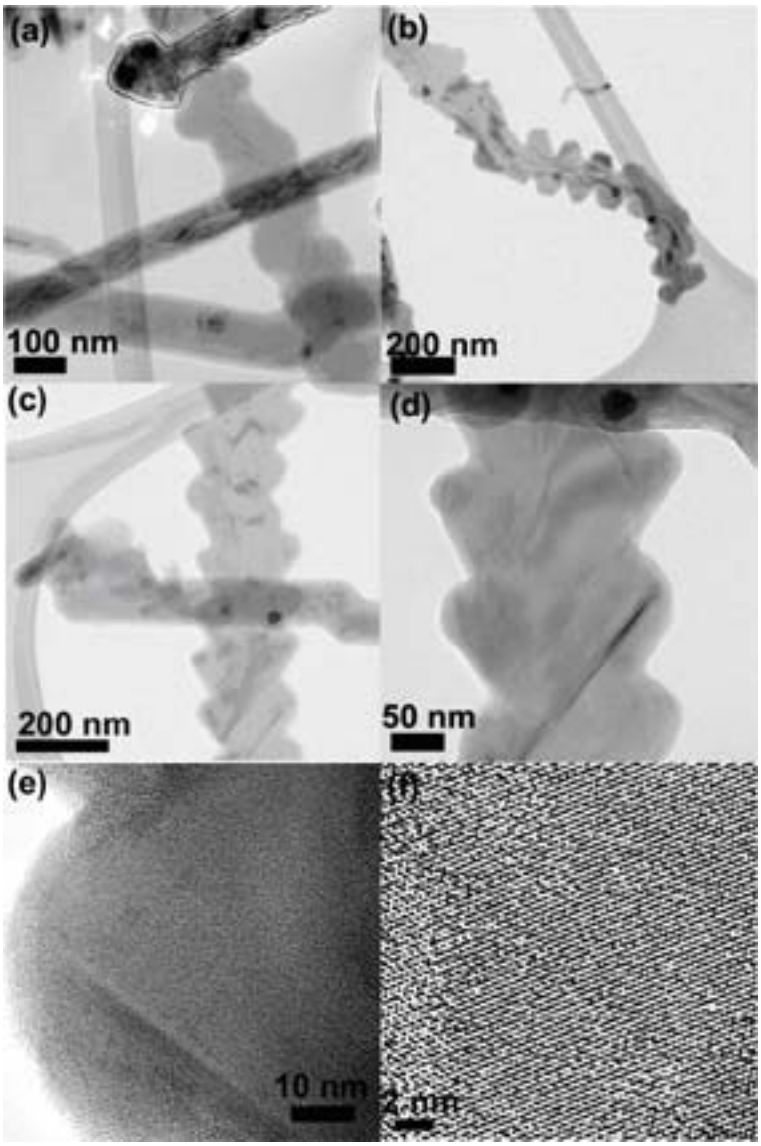

Figure 5.10: Very large diameter (>150 nm) crystalline Si nanowires with very rough surfaces were also found as a byproduct in the reactions carried out with trace oxygen in which silica nanotubes were the primary reaction product.

5.4 CONCLUSIONS

Crystalline high aspect-ratio Si nanowires form when MPS is thermally decomposed in anhydrous, oxygen-free supercritical toluene at 500^{o}C and 10.3 MPa in the presence of CuS nanocrystals. Sulfur is not found in the seed particles at the tips of the nanowires and apparently diffuses out of the seeds during the reactions; therefore, Cu metal appears to be the active component that seeds nanowire growth. The Si nanowires are grown several hundred degrees below the Cu:Si eutectic temperature and nanowire growth likely occurs by a solid-phase seeding process. When oxygen and water are present in the reactions, SiO_2 nanotubes form and some of these nanotubes (5% of total nanotube product) are helically coiled. When gold nanocrystals were used as seeds instead of CuS nanocrystals under the same reaction conditions with trace water and oxygen, solid silica nanofibers formed with only very few nanotubes. The difference in silica morphology produced by gold and CuS seeds appears to relate to qualitatively different metal/silica interface morphology for gold and copper. Cu seeds form the characteristic “tear-drop” shape that has been observed for metal seeds involved in the growth of multiwall carbon nanotubes. Au seed particles were not observed to take on this shape. Another important difference between Au and Cu is that Cu (unlike Au) can undergo both oxidation and reduction and perhaps oxidizes MPS to SiO_2 very effectively on the metal particle surface; whereas Au serves as a Si sink, leading to an Si nanowire that is then oxidized to SiO_2 as it evolves from the seed particle.

The most significant challenge facing the general design of metal seed particle-directed synthesis of nanotubes is overcoming the tendency of the seed particles to generate solid fibers, as opposed to hollow nanotubes. In "VLS" nanowire growth, crystallization occurs at the metal/semiconductor interface and the nanowire "precipitates" from the seed particle to produce a solid core. In contrast, nanotubes most likely form when "crystallization" occurs on the seed particle surface and the interfacial curvature of nanosize seeds initiates nanotube formation. For example, Chen, et al.[105] recently formed SiO_2 nanofibers under hydrothermal conditions using Fe seed particles and Zhang, et al.[106] demonstrated VLS-growth of SiO_2 nanofibers seeded with tin particles. McIlroy and coworkers[98] made helical silica nanofibers by VLS from Au seed particles. This study reported here shows that transition metal seed particles can also generate nanotubes under the right conditions and perhaps could provide a general route to the formation of a wide range of metal oxide nanotubes.

5.5 REFERENCES

(1) Korgel, B. A.; Hanrath, T.; Davidson, F. M. in *Encyclopedia of Chemical Processing* **1**(1) (ed Lee, S. K. B.) 3191-3203 (Marcel Dekker, 2006).

(2) Wagner, R. S.; Ellis, W. C. *Appl. Phys. Lett.* **1964**, *4*, 89.

(3) Hu, J. T.; Odom, T. W.; Lieber, C. M. *Acc. Chem. Res.* **1999**, *32*, 435-445.

(4) Trentler, T. J.; Hickman, K. M.; Goel, S. C.; Viano, A. M.; Gibbons, P. C.; Buhro, W. E. *Science* **1995,** *270*, 1791-1794.

(5) Wang, F. D.; Dong, A. G.; Sun, J. W.; Tang, R.; Yu, H.; Buhro, W. E. *Inorg. Chem.* **2006**, *45*, 7511-7521.

(6) Holmes, J. D.; Johnston, K. P.; Doty, R. C.; Korgel, B. A. *Science* **2000,** *287*, 1471-1473.

(7) Hanrath, T.; Korgel, B. A. *Adv. Mater.* **2003**, *15*, 437-440.

(8) Shah, P. S.; Hanrath, T.; Johnston, K. P.; Korgel, B. A. *J. Phys. Chem. B* **2004**, *108*, 9574-9587.

(9) Cui, Y.; Wei, Q.; Park, H.; Lieber, C. M. *Science* **2001,** *293*, 1289-1292.

(10) Law, M.; Greene, L. E.; Johnson, J. C.; Saykally, R.; Yang, P. D. *Nature Mater.* **2005**, *4*, 455-459.

(11) Cui, Y.; Lieber, C. M. *Science* **2001**, *291*, 851-853.

(12) Duan, X. F.; Niu, C. M.; Sahi, V.; Chen, J.; Parce, J. W.; Empedocles, S.; Goldman, J. L. *Nature* **2003**, *425*, 274-278.

(13) Patolsky, F.; Zheng, G. F.; Lieber, C. M. *Anal. Chem.* **2006**, *78*, 4260-4269.

(14) Huang, Y.; Duan, X. F.; Lieber, C. M. *Small* **2005**, *1*, 142-147.

(15) Goldberger, J.; Fan, R.; Yang, P. *Acc. Chem. Res.* **2006,** *39*, 239-248.

(16) Gasparac, R.; Kohli, P.; Mota, M. O.; Trofin, L.; Martin, C. R. *Nano Lett.* **2004**, *4*, 513-516.

(17) Jayaraman, K.; Okamoto, K.; Son, S. J.; Luckett, C.; Gopalani, A. H.; Lee, S. B.; English, D. S. *J. Am. Chem. Soc.* **2005**, *127*, 17385-17392.

(18) Rossi, M. P.; Ye, H. H.; Gogotsi, Y.; Babu, S.; Ndungu, P.; Bradley, J. C. *Nano Lett.* **2004**, *5*, 989-993.

(19) Halls, M. D.; Schlegel, H. B. *J. Phys. Chem. B* **2002**, *106*, 1921-1925.

(20) Khlobystov, A. N.; Britz, D. A.; Briggs, G. A. D. *Acc. Chem. Res.* **2005**, *38*, 901-909.

(21) Britz, D. A.; Khlobystov, A. N.; Porfyrakis, K.; Ardavan, A.; Briggs, G. A. D. *Chem. Commun.* **2005**, 37-39.

(22) Ogihara, H.; Takenaka, S.; Yamanaka, I.; Tanabe, E.; Genseki, A.; Otsuka, K. *Chem. Mater.* **2006**, *18*, 996-1000.

(23) Mitchell, D. T.; Lee, S. B.; Trofin, L.; Li, N. C.; Nevanen, T. K.; Soderlund, H.; Martin, C. R. *J. Am. Chem. Soc.* **2002**, *124*, 11864-11865.

(24) Lee, S. B.; Mitchell, D. T.; Trofin, L.; Nevanen, T. K.; Soderlund, H.; Martin, C. R. *Science* **2002**, *296*, 2198-2200.

(25) Rao, C. N. R.; Satishkumar, B. C.; Govindaraj, A.; Nath, M. *ChemPhysChem* **2001**, *2*, 78-105.

(26) Tenne, R. *Angew. Chem. Int. Ed.* **2003**, *42*, 5124-5132.

(27) Iijima, S. *Nature* **1991**, *354*, 56-58.

(28) Tenne, R.; Margulis, L.; Genut, M.; Hodes, G. *Nature* **1992**, *360*, 444-446.

(29) Chopra, N. G.; Luyken, R. J.; Cherrey, K.; Crespi, V. H.; Cohen, M. L.; Louie, S. G.; Zettl, A. *Science* **1995**, *269*, 966-967.

(30) Bethune, D. S.; Kiang, C. H.; de Vries, M. S.; Gorman, G.; Savoy, R.; Vazquez, J.; Beyers, R. *Nature* **1993**, *363*, 605-607.

(31) Lourie, O. R.; Jones, C. R.; Bartlett, B. M.; Gibbons, P. C.; Ruoff, R. S.; Buhro, W. E. *Chem. Mater.* **2000**, *12*, 1808-1810.

(32) Lee, D. C.; Mikulec, F. V.; Korgel, B. A. *J. Am. Chem. Soc.* **2004,** *126*, 4951-4957.

(33) Smith, D. K.; Lee, D. C.; Korgel, B. A. *Chem. Mater.* **2006**, *18*, 3356-3364.

(34) Patzke, G. R.; Krumeich, F.; Nesper, R. *Angew. Chem. Int. Ed.* **2002**, *41*, 2446-2461.

(35) Xiong, Y.; Mayers, B. T.; Xia, Y. *Chem. Commun.* **2005**, 5013-5022.

(36) Martin, C. R. *Science* **1994**, *266*, 1961-1966.

(37) Lakshmi, B. B.; Dorhout, P. K.; Martin, C. R. *Chem. Mater.* **1997**, *9*, 857-862.

(38) Hulteen, J. C.; Jirage, K. B.; Martin, C. R. *J. Am. Chem. Soc.***1998**, *120*, 6603-6604.

(39) Hoyer, P. *Langmuir* **1996**, *12*, 1411-1413.

(40) Zhang, M.; Bando, Y.; Wada, K.; Kurashima, K. *J. Mater. Sci. Lett.* **1999**, *18*, 1911-1913.

(41) Yen, H.-M.; Jou, S.; Chu, C.-J. *Mater. Sci. Eng. B* **2005**, *122*, 240-245.

(42) Ajayan, P. M.; Stephan, O.; Redlich, Ph.; Colliex, C. *Nature* **1995**, *375*, 564-567.

(43) Satishkumar, B. C.; Govindaraj, A.; Vogl, E. M.; Basumallick, L.; Rao, C. N. R. *J. Mater. Res.* **1997**, *12*, 604-606.

(44) Ogihara, H.; Sadakane, M.; Nodasaka, Y.; Ueda, W. *Chem. Mater.* **2006**, *18*, 4981-4983.

(45) Fan, R.; Wu, Y.; Li, D.; Yue, M.; Majumdar, A.; Yang, P. *J. Am. Chem. Soc.* **2003**, *125*, 5254-5255.

(46) Dong, Z. W.; Zhang, C. F.; Deng, H.; You, G. J.; Qian, S. X. *Mater. Chem. Phys.* **2006**, *99*, 160-163.

(46) Nemetschek, V. Th.; Hofmann, U. *Zeitschrift fur Naturforschung* **1953**, *8b*, 410-412.

(47) Mayya, K. S.; Gittins, D. I.; Dibaj, A. M.; Caruso, F. *Nano Lett.* **2001**, *1*, 727-730.

(48) Zygmunt, J.; Krumeich, F.; Nesper, R. *Adv. Mater.* **2003**, *15*, 1538-1541.

(49) Jung, J. H.; Lee, S.-H.; Yoo, J. S.; Yoshida, K.; Shimizu, T.; Shinkai, S. *Chem. Eur. J.* **2003**, *9*, 5307-5313.

(50) Jung, J. H.; Shinknai, S.; Shimizu, T. *Chem. Mater.* **2003**, *15*, 2141-2145.

(51) Jung, J. H.; Yoshida, K.; Shimizu, T. *Langmuir* **2002**, *18*, 8724-8727.

(52) Gopalakrishnan, G.; Segura, J.-M.; Stamou, D.; Gaillard, C.; Gjoni, M.; Hovius, R.; Schenk, K. J.; Stadelmann, P. A.; Vogel, H. *Angew. Chem. Int. Ed.* **2005**, *44*, 4957-4960.

(53) Rao, C. N. R.; Govindaraj, A.; Deepak, F. L.; Gunari, N. A.; Nath, M. *Appl. Phys. Lett.* **2001**, *78*, 1853-1855.

(54) Jang, J.; Yoon, H. *Adv. Mater.* **2004**, *16*, 799-802.

(55) Nakamura, H.; Matsui, Y. *J. Am. Chem. Soc.* **1995**, *117*, 2651-2652.

(56) Miyaji, F.; Davis, S. A.; Charmant, J. P. H.; Mann, S. *Chem. Mater.* **1999**, *11*, 3021-3024.

(57) Baral, S.; Schoen, P. *Chem. Mater.* **1993**, *5*, 145-147.

(58) Adachi, M.; Harada, T.; Harada, M. *Langmuir* **1999**, *15*, 7097-7100.

(59) Van Bommel, K. J. C.; Friggeri, A.; Shinkai, S. *Angew. Chem. Int. Ed.* **2003**, *42*, 980-999.

(60) Dloczik, L.; Engelhardt, R.; Ernst, K.; Fiechter, S.; Sieber, I.; Könenkamp, R. *Appl. Phys. Lett.* **2001**, *78*, 3687-3689.

(61) Zhang, H.; Yang, D.; Ma, X.; Que, D. *Nanotechnology* **2005**, *16*, 2721-2725.

(62) Jiang, X.; Mayers, B.; Herricks, T.; Xia, Y. *Adv. Mater.* **2003**, *15*, 1740-1743.

(63) Sun, Y.; Xia, Y. *Adv. Mater.* **2004**, *16*, 264-268.

(64) Sun, Y.; Wiley, B.; Li, Z.-Y.; Xia, Y. *J. Am. Chem. Soc.* **2004**, *126*, 9399-9406.

(65) Zwilling, V.; Aucouturier, M.; Darque-Ceretti, E. *Electrochim. Acta* **1999**, *44*, 921.

(66) Macak, J. M.; Tsuchiya, H.; Taveira, L.; Aldabergerova, S.; Schmuki, P. *Angew. Chem. Int. Ed.* **2005**, *44*, 7463-7465.

(67) Bakkers, E. P. A. M.; Verheigen, M. A. *J. Am. Chem. Soc.* **2003**, *125*, 3440-3441.

(68) Yin, L. W.; Bando, Y.; Golberg, D.; Li, M. S. *Appl. Phys. Lett.* **2004**, *85*, 3869-3871.

(69) Yin, L.-W.; Bando, Y.; Li, M.-S.; Golberg, D. *Small* **2005**, *1*, 1094-1099.

(70) Ma, Y. W.; Huo, K. F.; Wu, Q.; Lu, Y.N.; Hu, Y. M.; Hu, Z.; Chen, Y. *J. Mater. Chem.* **2006**, *16*, 2834-2838.

(71) Wu, Q.; Hu, Z.; Wang, X.; Lu, Y.; Chen, X.; Xu, H.; Chen, Y. *J. Am. Chem. Soc.* **2003**, *125*, 10176-10177.

(72) Yang, J.; Liu, Y.-C.; Lin, H.-M.; Chen, C.-C. *Adv. Mater.* **2004**, *16*, 713-716.

(73) Li, X.; Li, Y.; Li, S.; Zhou, W.; Chu, H.; Chen, W.; Li, I. L.; Tang, Z. *Crystal Growth & Design* **2005**, *5*, 911-916.

(74) Kasuga, T.; Hiramatsu, M.; Hoson, A.; Sekino, T.; Niihara, K. *Langmuir* **1998**, *14*, 3160-3163.

(75) Zhu, Y.; Li, H.; Koltypin, Y.; Hacohen, Y. R.; Gedanken, A. *Chem. Commun.* **2001**, 2616-2617.

(77) Mao, Y.; Banerjee, S.; Wong, S. S. *Chem. Commun.* **2003**, 408-409.

(78) Li, Y.; Bando, Y.; Golberg, D. *Adv. Mater.* **2004**, *16*, 37-40.

(79) Hu, J.-Q.; Meng, X.-M.; Jiang, Y.; Lee, C.-S.; Lee, S. T. *Adv. Mater.* **2003**, *15*, 70-73.

(80) Geng, B.; Meng, G.; Zhang, L.; Wang, G.; Peng, X. *Chem. Commun.* **2003**, 2572-2573.

(81) Liang, C.; Shimizu, Y.; Sasaki, T.; Umehara, H.; Koshizaki, N. *J. Mater. Chem.* **2004**, *14*, 248-252.

(82) Li, J. Y.; Chen, X. L.; Qiao, Z. Y.; Cao, Y. G.; Li, H. *J. Mater. Sci. Lett.* **2001**, *20*, 1987-1988.

(83) Wu, Q.; Hu, Z.; Liu, C.; Wang, X.; Chen, Y. *J. Phys. Chem. B* **2005**, *109*, 19719-19722.

(84) Li, C.; Liu, Z.; Gu, C.; Xu, X.; Yang, Y. *Adv. Mater.* **2006**, *18*, 228-234.

(85) Yue, L.; Gao, W.; Zhang, D.; Guo, X.; Ding, W.; Chen, Y. *J. Am. Chem. Soc.* **2006**, *128*, 11042-11043.

(86) Saunders, A. E.; Sigman, M. B., Jr.; Korgel, B. A. *J. Phys. Chem. B* **2004,** *108*, 193-199.

(87) Ghezelbash, A.; Korgel, B. A. *Langmuir* **2005,** *21*, 9451-9456.

(88) Lee, D. C.; Hanrath, T.; Korgel, B. A. *Angew. Chem. Int. Ed.* **2005,** *44*, 3573-3577.

(89) Tuan, H.-Y.; Lee, D. C.; Korgel, B. A. *Angew. Chem, Int. Ed.* **2006,** *45*, 5184-5187.

(90) Davidson, F. M.; Lee, D. C.; Fanfair, D. D.: Korgel, B. A. *J. Phys. Chem. C* **2007**, *111*, 2929-2935.

(91) Korgel, B. A.; Lee, D. C.; Hanrath, T.; Yacaman, M. J.; Thesen, A.; Matijevic, M.; Kiaas, R.; Kisielowski, C.; Diebold, A. C., *IEEE Transactions on Semiconductor Manufacturing* **2006**, *19*, 391-396.

(92) Kohno, H.; Takeda, S. *Jpn. J. Appl. Phys.* **2002**, *41*, 577-578.

(93) Thaddeus, B. M.; Hiroaki, O.; Subramanian, P. R.; Linda, K. *Binary Alloy Phase Diagram*, , 2nd ed,; ASM Internation: Materials Park OH. 1990; Vo.1.

(94) Tuan, H.-Y.; Lee, D. C.; Hanrath, T.; Korgel, B. A. *Nano Lett.* **2005,** *5*, 681-684.

(95) Tuan, H.-Y.; Lee, D. C.; Hanrath, T.; Korgel, B. A. *Chem. Mater.* **2005,** *17*, 5705-5711.

(96) Tuan, H.-Y.; Lee, D. C.; Korgel, B. A. *Angew. Chem. Int. Ed.* **2006,** *45*, 5184-5187.

(97) Colder, A.; Huisken, F.; Trave, E.; Ledoux, G.; Guillois, O.; Reynaud, C.; Hofmeister, H.; Pippel, E. *Nanotechnology*, **2004**, *15*, L1-L4.

(98) Wang, L.; Major, D.; Paga, P.; Zhang, D.; Norton, M. G.; McIlroy, D. N. *Nanotechnology* **2006**, *17*, S298-S303.

(99) Amelinckx, S.; Zhang, X. B.; Bernaerts, D.; Zhang, X. F.; Ivanov, V.; Nagy, J. B. *Science* **1994,** *265*, 635-639.

(100) Qu, Y.; Carter, J. D.; Guo, T. *J. Phys. Chem. B* **2006**, *110*, 8296-8301.

(101) McIlroy, D. N.; Zhang, D.; Kranov, Y.; Norton, M. G. *Appl. Phys. Lett.* **2001**, *79*, 1540-1542.

(102) Zhang, D.; Alkhateeb, A.; Han, H.; Mahmood, H.; McIlroy, D. M.; Norton, M. G. *Nano Lett.* **2003**, *3*, 983-987.

(103) Hofmann, S.; Sharma, R.; Ducati, C.; Du, G.; Mattevi, C.; Cepek, C.; Cantoro, M.; Pisana, S.; Parvez, A.; Cervantes-Sodi, F.; Ferrari, A. C.; Dunin-Borkowski, R.; Lizzit, S.; Petaccia, L.; Goldoni, A.; Robertson, J. *Nano Lett.* **2007**, *7*, 602-608.

(104) Lee, D. C.; Korgel, B. A. *Molecular Simulation* **2005**, *31*, 637-642.

(105) Chen, P.; Xie, S.; Ren, N.; Zhang, ,Y.; Dong, A.; Chen, Y.; Tang, Y. *J. Am. Chem. Soc.* **2006**, *128*, 1470-1471.

(106) Zhang, J.; Xu, B.; Yang, Y.; Jiang, F.; Li, J.; Wang, X.; Wang, S. *J. Non-Crystalline Solids* **2006**, *352*, 2859-2862.

Chapter 6: Synthesis of Bipyramidal Germanium Telluride (GeTe) Particles and GeTe/Te Heterostructures

6.1 INTRODUCTION

Nanomaterial heterostructures, that is, multiple materials are linked together into one nano-object, merge the properties of the individual materials and can be used in the next generation of devices with diverse functions. Various kinds of hierarchical heterostructures have been reported; for example, 1-D nanowire heterostructures including nanowire superlattice, core-shell coaxial nanocables, and bi-coaxial nanowires[1-27]; Zero-dimensional (OD) crystal heterostructures including core-shell nanoparticles, heterodimers and oligomers of nanoparticles; OD-1D nanocrystal-nanorod heterostructures.[28-30]

Strategies for synthesizing hybrid nanomaterials normally include one-step or sequential feeding different reactants in the reaction. Various kinds of heterostructures are formed depending on the interfacial energies between the two materials. For example, if two materials have limited miscibility or large interfacial energy, or only certain regions of the surface of starting material are accessible for the other materials, the two materials tend to undergo phase segregation and form heterodimers or oligomers of nanoparticle heterostructures.

In many cases of hybrid colloidal nanocrystal synthesis in solution phase, external organic surfactants play important roles as hybridation initiators via their interaction with reactants. Surfactants stabilize a certain surface by “selective

adhesion" and change the surface energy and reactivity of different planes, giving a change to allow a second material nucleate at the higher reactivity sites of the starting materials.[28-30] Moreover, many unexpected hybrid nanostructures were often observed in the organic ligand-medicated reactions. Organic surfactants own strong structural and compositional effect on colloidal nanocrystal synthesis.

Chapter 6 represents an example of GeTe/Te heterstructures synthesis by introducing various organic surfactants. Organic surfactants are found to direct the formation of this kind of heterostructures. The morphology and composition of GeTe/Te heterstructures, GeTe nanoparticles, and Te nanorods are characterized using TEM, SEM, EDS, and XRD. The effects of organic surfactant concentration and organic surfactant types on the GeTe-Te heterostructure synthesis are discussed.

6.2 EXPERIMENTAL

The experimental setup of germanium telluride (GeTe) nanomatrial synthesis is similar to the one used in Chapter 3 but with different reaction parameters. GeTe particles and GeTe-Te heterostructure were synthesized in a semi-batch 10 mL Ti grade-2 reactor connected to a high-pressure liquid chromatography (HPLC) pump for pressure control (500-1000 psi) and reactant injection (0.5 ml/min). One side of valve of the reactor was connected with 6-way valve (Valco) equipped with a smaller 500µl loop made of 1/16in o.d 0.03 in. id stainless steel high-pressure tubing and the other side is a close end. The reactor was pressurized to 3.4 MPa with hexane and then heated to the reaction temperature.

For GeTe nanoparticle reaction, 500 µL of 80 mM diphenylgermane (DPG) and Trioctylphosphine-tellurium (TOP-Te) in hexane were injected from a 6-way valve injection loop (Valco) at 0.5 mL/min. The reaction pressure was increased to 13.7 MPa with additional hexane. For GeTe-Te heterosructure reaction, organic surfactants including octanol, oleic acid, isoprene, and 1-hexadecanthiol were added into the precursor solution at various volume concentrations. After 5 min, the reactor was immersed in ice-water and cooled to room temperature. The reactor was opened carefully since the remaining high pressure inside the reaction. The deposition substrate was removed and cleaned and then was stored under nitrogen.

6.3 RESULTS AND DISCUSSION

6.3.1 Bipyramidal Germanium Telluride (GeTe) nanoparticle

Figure 1 shows the SEM images of GeTe bipyramidal nanoparticles by introducing DPG and Top-Te at 460 ˚C in supercritical hexane. As shown in Figure 6.1a, bipyramidal particles tend to aggregate together but separate particle can be found (Figure 6.1b).The diameters of bipyramidal GeTe particles range from 300-1µm by observing over 100 particles. Nanometer-scale energy-dispersive X-ray energy spectral (EDS) shows the atomic ratio of the GeTe particles with Ge:Te ratio of 1:1. The crystal structure of these GeTe particles is rhombohedral. The

bipyramidal facet structure of GeTe evolves from its rhombohedral crystal structure. The bipyrimidal GeTe particles are octaheral (figure 6.1d) as shown in figure 6.1c.

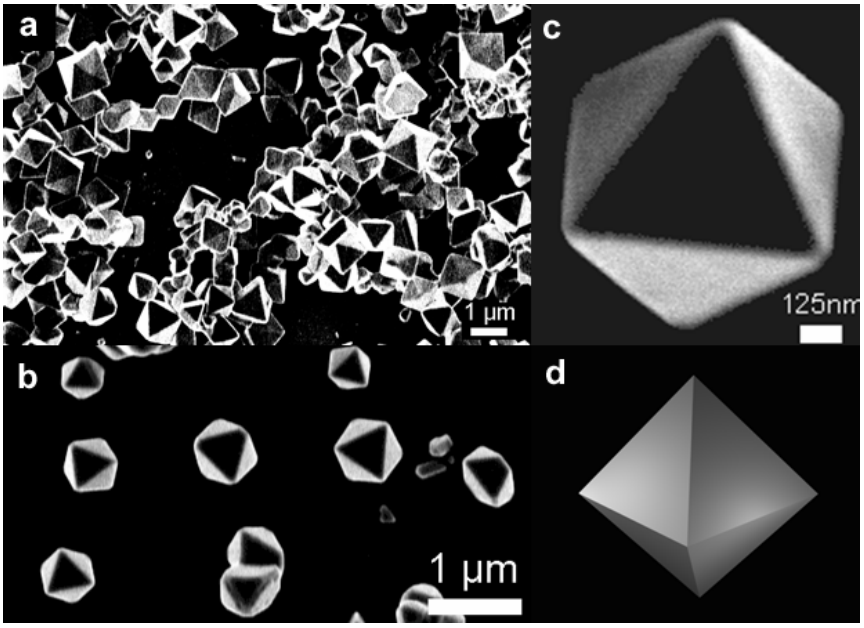

Figure 6.1: SEM images of bipyramidal GeTe nanoparticles (a-c) and simulated octahedral structure.

6.3.2 Heterostructured GeTe/Te Nanomaterials

Figure 6.2 shows the SEM images of GeTe-Te nanoparticle-nanorod heterostructures by reacting DPG and TOP-Te in the presence of 10% octanol. Branched and aligned Te nanorods were grown on the germanium telluride nanoparticles. The diameters of these Te nanorods range from 5 to 15nm and the lengths range from 100-500 nm. These Te nanorods were observed to grow epitaxially from the facet surface of GeTe nanoparticles as shown in figure 6.2 b-d.

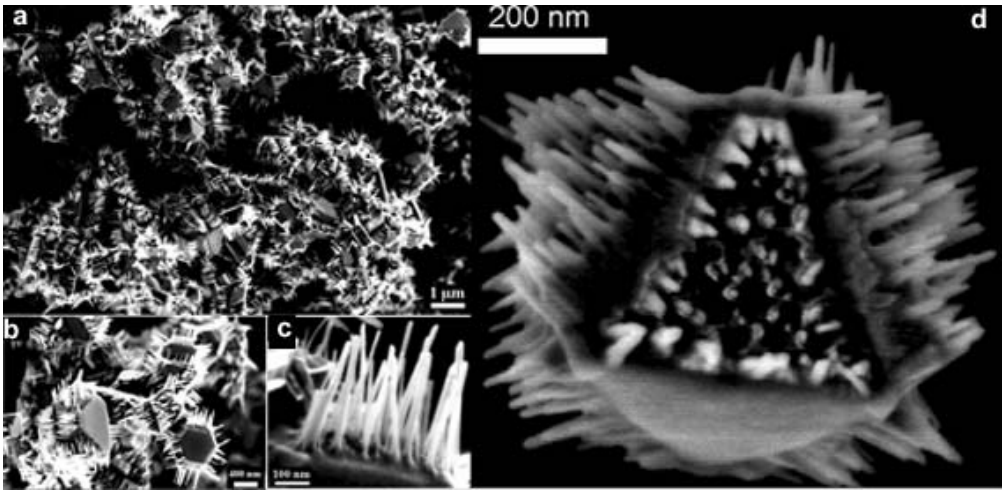

Figure 6.2: GeTe-Te nanoparticle-nanorod heterostructure synthesis by adding 10% octanol in a reaction. The Te nanorods were grown epitaxially on some facet planes of GeTe particles.

Figure 6.3 shows the TEM images of GeTe-Te heterostructures. Te nanorods were grown on the facet GeTe surface (Figure 6.3 b); however, the big thickness of GeTe particles and 3D spacial distribution of the Te nanorod on the GeTe surfaces make interfacial heterojunction of crystal lattice imaging between GeTe particle and Te nanorods very hard. Te nanorods are single crystalline with hexagonal crystallographic structure (Figure 6.5) and the morphology of tips are semi-sphere. Nanobeam electron dispersive spectroscopy (EDS) (Figure 6.4) of a particle and a rod, respectively, shows strong Ge and Te siganal on the particle and manily Te siganal with trace of Ge signal on the rod. The Ge signal shows Te nanorods were slightly doped while nanorod growth.

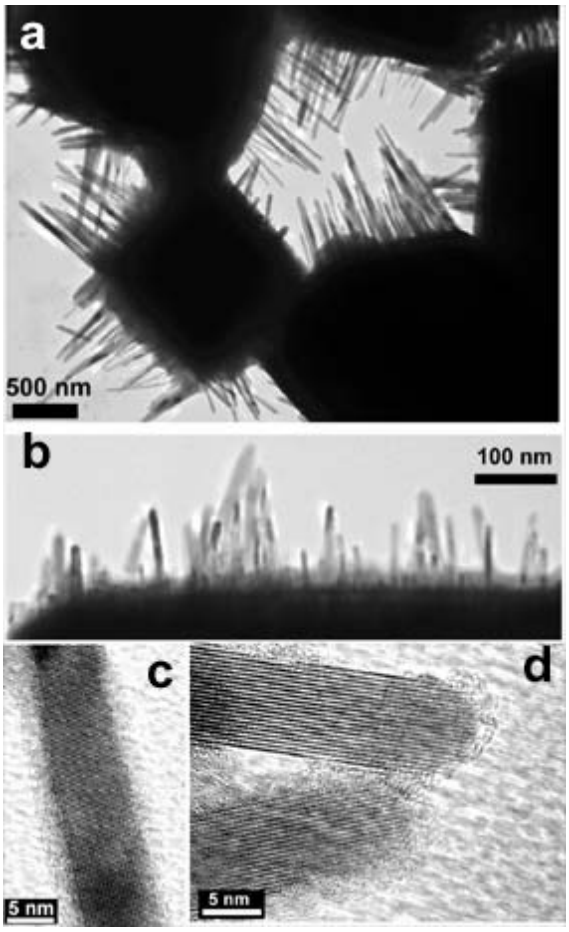

Figure 6.3: HRTEM of GeTe/Te heterostructures.

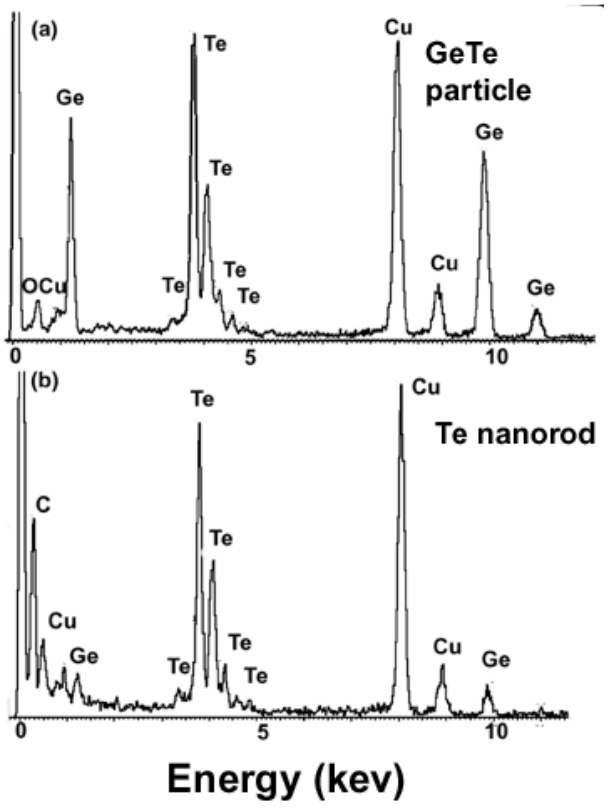

Figure 6.4: EDS of (a) GeTe particles and (b) Ge-doped Te nanorods.

X-ray diffraction pattern (figure 6.5) shows the crystallographic structure of Te nanorods is hexagonal – a kind of crystallographic structures with different surface energy on crystal faces. These kinds of materials tend to undergo anisotropic growth because the surfaces with higher surface energy grow much faster than the surfaces with lower surface energy.

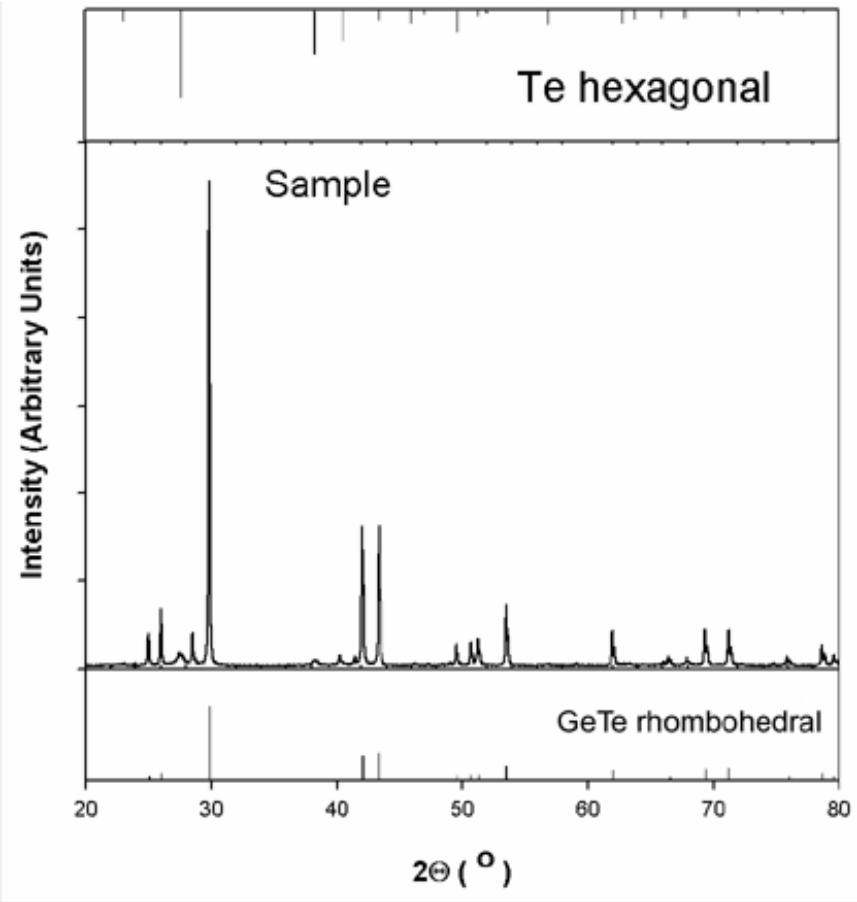

Figure 6.5: X-ray diffraction pattern of as GeTe/Te heterostructures.

6.3.3 The Role of Octanol on GeTe/Te Heterostructure Synthesis

Figure 6.6 shows scanning electron microscopy (SEM) images of Te nanorods growth on the facet GeTe nanocrystals by increasing concentration of octanol from 0% (figure 6.6 a) to 5% (figure 6.6b), 10% (figure 6.6c) and 20% (figure 6.6d), respectively. From the observation of SEM images, octanol were found to play two roles in the GeTe-Te heterostructure synthesis: (1) octanol can change the surface energy of facet surfaces of GeTe nanoparticles. When octanol adsorbs and stabilizes a certain surface by selective adhesion, the growth rate of each plane was different compared with the growth rate of each plane without surfactant added in. The bipyramidal shape of GeTe nanoparticles were changed to other facet shapes. (2) octanol can initiate Te naoorod growth on the facet plane of GeTe nanoparticles. No Te nanorods were observed without adding octanol (figure 6.6a) and were observed to grow in the presence of octanol (figure 6.6 b-d). Nanorod density increases proportionally to the concentration of octanol which demonstrates that octanol can increases reactivity and growth sites for Te nanorod growth on the GeTe nanocrystals. 10% of octanol gave the best quality of Te nanorods. While octanol concentration increases to 20%, limited space of facet GeTe particles can not allow too many Te nanorods nucleate on the surfaces and dense and short Te nanorods with bad morphology were grown.

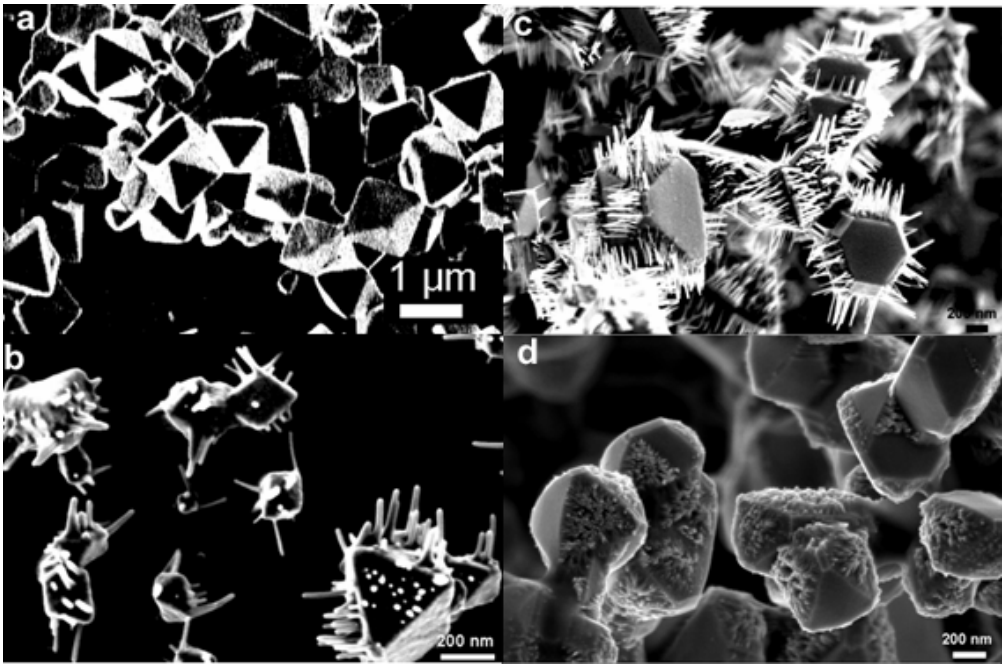

Figure 6.6: SEM images of synthesis result of GeTe/Te heterostructure by adding (a) 0% (b) 5% (c) 10%, and (d) 20% octanol.

6.3.4 Surfactant Effect On GeTe/Te Heterostructure Synthesis

The influence of surfactans on Te nanorod growth was sutided. The synthesis results of four different surfactants, octanol, oleic acid, isoprene, and 1 hexadecanethiol were compared as shown in Figure 6.7. Te nanord growth is similar in the presence of octanol and oleic acid, perhaps because the OH and COOH groups have similar bind affinity to the GeTe surface. Isoprene gave short rods with diameter ranging from 50 – 100 nm. Unlike the selective adhesion of Te rods on the GeTe planes that was obtained in the present of octanol and oleic acid. Te nanorods grew on the all of the facets of the GeTe particles and the density of Te nanorods on

the GeTe planes was much lower. While in 1-hexdecanethiol, no Te nanorods were obtained and GeTe morphology changed to a spherical shape.

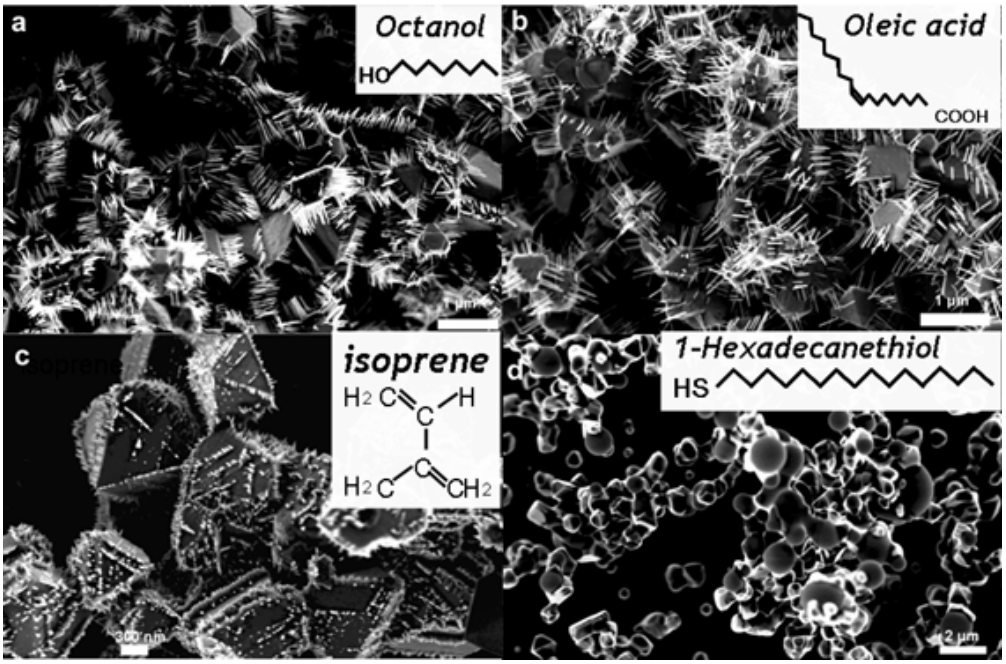

Figure 6.7: The synthesis result of GeTe/Te heterostructures using (a) octanol, (b) oleic acid, (c) isoprene, and (d) 1-hexadecanethiol.

6.4. CONCLUSIONS

Octahedral bipyramidal germanium telluride nanoparticles with diameters ranging from 300 nm to 1μm were synthesized by reacting DPG and TOP-Te at 460 ˚C at 13.7 MPa in supercritical hexane. GeTe/Te heterostructures; that is, well aligned Te nanorods grown on the facet surface of GeTe nanoparticles, were synthesized while adding octanol in the reaction. Octanol changes the bipyramidal shape of GeTe nanoparticles to other facet particles by modulating the surface energies of GeTe surfaces and the surface reactivity, allowing Te atoms nucleate on

the surface and grow in the form of nanorods. The best synthesis result of Te nanorods was obtained by adding10% of ocatnol in the reaction. Finally, different organic surfactants can induce various formations of GeTe/Te heterostructures.

6.5. REFERENCES

(1) Lauhon, L. J.; Gudiksen, M. S.; Wang, D.; Lieber, C. M. *Nature* **2002**, *420*, 57.

(2) Gudiksen, M. S.; Lauhon, L. J.; Wang, J.; Smith, D. C.; Lieber, C. M. *Nature* **2002**, *415*, 617.

(3) Lauhon, L. J.; Gudiksen, M. S.; Lieber, C. M. *Philos. Trans. R. Soc. London A* **2004**, *362*, 1247.

(4) Kuang, Q.; Jiang, Z. Y.; Xie, Z. X.; Lin, S. C.; Lin, Z. W.; Xie, S. Y.; Huang, R. B.; Zheng, L. S. *J. Am. Chem. Soc.* **2005**, *127*, 11777.

(5) Cui, Y.; Lieber, C. M. *Science* **2001**, *291*, 851.

(6) Wu, Y.; Fan, R.; Yang, P. D. *Nano Lett.* **2002**, *2*, 83.

(7) Bjork, M. T.; Ohlsson, B. J.; Sass, T.; Persson, A. I.; Thelander, C.; Magnusson, K.; Deppert, M. H.; Wallenberg, L.; Samulson, L. *Nano Lett.* **2002**, *2*, 87.

(8) Manna, L.; Scher, E. C.; Li, L. S.; Alivisatos, A. P. *J. Am. Chem. Soc.* **2002**, *124*, 7136.

(9) Wang, X. D.; Song, J. H.; Li, P.; Ryou, J. H.; Dupuis, R. D.; Summers, C. J.; Wang, Z. L. *J. Am. Chem. Soc.* **2005**, *127*, 7920.

(10) Ye, C. H.; Zhang, L. D.; Fang, X. S.; Wang, Y.; Yan, P.; Zhao, J. *Adv. Mater.* **2004**, *16*, 1019.

(11) Li, Q.; Wang, C. R. *J. Am. Chem. Soc.* **2003**, *125*, 9892.

(12) Wu, Y.; Xiang, J.; Yang, C.; Lu, W.; Lieber, C. M. *Nature* **2004**, *430*, 61.

(13) Li, Q.; Wang, C. R. *Appl. Phys. Lett.* **2003**, *82*, 1398.

(14) Hsu, Y. J.; Lu, S. Y. *Chem. Commun.* **2004**, 2102.

(15) Bu, W. B.; Hua, Z.; Chen, H. R.; Shi, J. L. *J. Phys. Chem. B* **2005**, *109*, 14461.

(16) Maynor, B. W.; Li, J. Y.; Lu, C. G.; Liu, J. *J. Am. Chem. Soc.* **2004**, *126*, 6409.

(17) Hu, J. Q.; Bando, Y.; Liu, Z. W.; Sekiguchi, T.; Golberg, D.; Zhan, J. H. *J. Am. Chem. Soc.* **2003**, *125*, 11306.

(18) Fu, L.; Liu, Z. M.; Liu, Y. Q.; Han, B. X.; Wang, J. Q.; Hu, P.; Cao, L. C.; Zhu, D. B. *J. Phys. Chem. B* **2004**, *108*, 13074.

(19) Wang, C. R.; Wang, J.; Li, Q.; Yi, G. C. *Adv. Funct. Mater.* **2005**, *15*, 1471.

(20) Jung, S. W.; Park, W. I.; Yi, G. C.; Kim, M. *Adv. Mater.* **2003**, *15*, 1358.

(21) Park, W. I.; Yi, G. C.; Kim, M.; Pennycook, S. J. *Adv. Mater.* **2003**, *15*, 526.

(22) Zhan, J. H.; Bando, Y.; Hu, J. Q.; Sekiguchi, T.; Golberg, D. *Adv. Mater.* **2005**, *17*, 225.

(23) Han, S.; Li, C.; Liu, Z. Q.; Lei, B.; Zhang, D. H.; Jin, W.; Liu, X. L.; Tang, T.; Zhou, C. W. *Nano Lett.* **2004**, *4*, 1241.

(24) Lei, B.; Li, C.; Zhang, D. H.; Han, S.; Zhou, C. W. *J. Phys. Chem. B* **2005**, *109*, 18799.

(25) Zhan, J. H.; Bando, Y.; Hu, J. Q.; Liu, Z. W.; Yin, L. W.; Golberg, D. *Angew. Chem., Int. Ed.* **2005**, *44*, 2140.

(26) Li, Y. B.; Bando, Y.; Golberg, D. *Adv. Mater.* **2004**, *16*, 93.

(27) Hu, J. Q.; Bando, Y.; Zhan, J. H.; Golberg, D. *Adv. Mater.* **2005**, *17*, 1964.

(28) Yin, Y.; Alivisatos, A. P. *Nature* **2005,** *437*, 664-670.

(29) Jun, Y. W.; Choi, J. S.; Cheon, J. *Angewandte Chemie-International Edition* **2006,** *45*, 3414-3439.

(30) Cozzoli, P. D.; Pellegrino, T.; Manna, L. *Chemical Society Reviews* **2006,** *35*, 1195-1208.

Chapter 7: Conclusions and Outlook

7.1 CONCLUSIONS

7.1.1 High Yield Silicon Nanowire Synthesis in Supercritical Benzene

Supercritical fluid-liquid-solid nanowire growth was demonstrated to be capable of high yields of silicon nanowires. The organic solvent was found to significantly affect the yield of Au-seeded SFLS Si nanowire synthesis. Silicon nanowire synthesis in supercritical benzene gave the largest amount of nanowires with 46.8 mg in a single reaction and a 63% yield. In toluene only 28.6 mg of Si nanowire were obtained, with a 38.4% yield. Only ~1 mg silicon nanowires with ~1.4% yield were produced in supercritical hexane. Silicon atoms result from MPS. Aromatic organic solvents such as benzene and toluene appear to speed the disproportionation reaction. Aliphatic solvents gave low conversion XRD of as-synthesized Si nanowire product matches with the crystallography of Si. SEM images show silicon nanowires with straight morphology. HRTEM images show synthesized Si nanowire were single crystalline.

7.1.2 Nanocrystal-Mediated Crystallization of Silicon and Germanium Nanowires in Supercritical Fluid: The Role of Catalysis and Solid-Phase Seeding

Since the most widely used metal, Au, traps electrons and holes in both Si and Ge and poses a serious contamination problem for nanowire integration with Si CMOS. Au-seeded Si and Ge nanowires are not desirable for microelectronic processing. Eight different nanocrystals, Co, Ni, CuS, Mn, Ir, $MnPt_3$, Fe_2O_3, and FePt, were used as seeds to synthesize Si and Ge nanowire in supercritical fluid. All of the nanocrystals produced nanowires at temperatures significantly below their bulk eutectic temperatures, so nanowires were crystallized from the seed nanoprticles via solid-phase diffusion as discussed in Chapter 4. Among eight nanoparticles used as seeds, Co gave the highest yield and quality of both Si and Ge nanowires. Ni nanocrystals also produced crystalline Si and Ge nanowires with good yield. CuS nanocrystals produced straight crystalline Si nanowires with slightly shorter lengths (3-10 μm) and Fe_2O_3 nanocrystals produced Ge nanowires with relatively high yield. Alloy nanoparticles can be found at the ends of Si and Ge nanowires and EDS analysis of the seed particles showed that they are silicides and germanides. <111> and <110> are two predominant growth directions of Si and Ge nanowires seeded with Ni, Co, Fe_2O_3 and CuS - different than Au-seeded Si and Ge nanowires with preferential growth in either the <111> (Si) or <110> (Ge) directions,in organic solvents.

Ni and Co also were also found to catalytically decompose octylsilane and trisilane to create Si atoms sufficient for Si nanowire growth which can not be achieved by using Au nanoparticles. Octylsilane and trisilane were heterogeneously

decomposition on the Ni and Co surface to form nanowires which is a different reaction route compared with that of decomposition of MPS which can undergo homogeneous disproportionation to silane and can then give rise to nanowire growth.

7.1.3 Germanium Nanowire Synthesis: An Example of Solid- Phase Seeded Growth with Nickel Nanocrystals

Using Ni-seeded germanium nanowires as an example, supercritical fluid-solid-solid (SFSS) nanowire growth mechanism, that is, nanowire growth occured by a *solid-phase* seeding process from the metal particle, was supported by five proofs. First, the melting point depression of used 5.9 nm Ni nanocrystals is only ~20%. The eutectic temperature of Ge and Ni only drops by about 100^{o}C, which is still over 200^{o}C higher than the nanowire growth temperature (~410 ˚C). A liquid alloy eutectic can not form at such low reaction temperature. Second, in SFSS, the shape of the $NiGe_x$ particles at the tips of the wires depended strongly on the nanowire diameter while the shapes of AuGex tips are all spherical in SFLS. $NiGe_x$ particles at the ends of Ge nanowires with diameters < 15 nm were hemispherical and were corresponding close to the shapes of starting Ni nanocrystal. In contrast, particles at the tips of nanowires with large diameters (>25nm) were irregularly shaped, consistent with solid-phase aggregated nanocrystals that had only partially coalesced. Third, much narrower size distribution of nanowires was obtained in Ni-seeded wires than that of Au-seeded wires. The Ni-seeded wires have an average

diameter of 14.5 nm and more than 80% of Ge nanowires were smaller than 20nm but the Au-seeded nanowires on the other hand are polydisperse and larger, with an average diameter of 54.8 nm. In SFSS, the aggregation of forming solid Ni-Ge alloy is much slower than that of liquid Au-Ge eutectic droplets in SFLS. Fourth, the growth rates of the Ni-seeded Ge nanowires appear to be limited by semiconductor diffusion through the metal seed particle with the size dependence of faster growth for smaller diameter wires. Finally, calculation of the solid-state diffusion rate that shows that nanowire growth was assisted by either core or surface-enhanced diffusion.

SFSS growth provides another example of nanowire growth route driven by thermodynamic equilibrium in addition to SFLS growth. Both nanowire growth approaches can produce high quality crystalline semiconductors. However, the fact that SFSS does not require a hot liquid eutectic formation for nanowire growth increases the number of metals available and range of potential operating conditions for metal-seeded type nanowire synthesis and is very important for future integration of nanowire device processing.

7.1.4 Silicon Nanowires and Silica nanotbues Seeded by Copper Sulfide Nanocrystals

CuS nanocrystals can induce the growth of silicon (Si) nanowires or silica (SiO_2) nanotubes in supercritical toluene at 500 $^{\circ}$C at 10.3 MPa using monophenylsilane (MPS) as a reactant. Silica nanotubes were seeded by copper

nanoparticles via a chemical approach to analogous to “VLS” nanowire growth. By inducing small amounts of water and oxygen, amorphous SiO_2 nanotubes were formed. Sulfur diffused out of the CuS very quickly when the seeds were in the reaction conditions and the remaining Cu nanoparticles become an active site for seeding Si nanowires. Like discussed in Chapter 4, the Si nanowires were grown several hundred degrees below the Cu:Si eutectic temperature and nanowire grow via supercritical fluid-solid-solid (SFSS) growth mechanism. SiO_2 nanotubes formed and 5% of silica nanotubes are helically coiled when oxygen and water were present in the reactions. Different metal nanoparticle yield vary results in silica nanotube synthesis. The difference of metal/silica interface morphology highly influences the yield of silica nanotubes produced. The “tear-drop” shape of Cu seeds has been observed at the end of Cu-seeded silica nanotbues and gave very high yield of silica nanotbue formation; however, Au seed particles were not observed with this shape and gold nanocrystals mostly seeded solid silica nanofibers with very few nanotubes in the presence of trace and oxygen. Besides, Cu can oxidize MPS to SiO_2 very effectively on the metal particle surface by both oxidation and reduction. Au only serves as a Si sink and seed to a Si nanowire that was then oxidized to SiO_2 when it evolves from the seed particle. In a future perspective, this transition-seeded silica nanotbue method can provide a general route to the formation of a wide range of metal oxide nanotubes.

7.1.5 Synthesis of Bipyramidal Germanium Telluride (GeTe) Particles and GeTe/Te Heterostructures

Germanium telluride particles were synthesized in supercritical fluid by using diphenylgermane (DPG) and Top-Te as precursors. When adding octanol in precursor solution, GeTe/Te heterstructures- branched and aligned Te nanorods were grown on the germanium telluride nanoparticles – were synthesized. HRTEM shows the Te nanorods are single crystalline and slightly Ge doped characterized by EDS. X-ray diffraction pattern (XRD) demonstrates that the synthesized products are GeTe and Te. Octanol (or all organic surfactants in the synthesis) plays two roles in the GeTe-Te heterostructure synthesis: (1) GeTe surface energy modulator, and (2) Te naoorod initiator. No Te nanorods were observed without adding octanol. However, too concentrated octanol results in dense and short Te nanorods with bad morphology because the limited area of facet GeTe particles can not allow too many Te nanorods nucleate on the surfaces. Four different organic surfactants, octanol, oleic acid, isoprene, and 1-hexadecanethiol were used to compare the surfactant effect on heterostructured GeTe/Te synthesis. Octanol and oleic acid gave similar morphology of GeTe/Te heterostructures. Isoprene produced short rods with diameter ranging from 50 – 100 nm were observed. Using 1-hexdecanethiol as a surfactant, on the other hand, no Te nanorods were synthesized and the morphology of GeTe nanoparticles was changed to sphere.

7.2 Recommendations

7.2.1. Gram-Scale Silicon Nanowire Synthesis

In our lab, a 250 ml parr reactor has been used to produce one gram germanium nanowires. Figure 7.1 shows the photograph and design of the 250 ml parr reactor. A continuous flow reaction was operated. A stir-bar was added in the reactor body for mixing the reactants and a temperature controller was used to control the reaction temperature and a pressure meter equipped with the stir bar was used to measure reactor pressure. In a typical reaction, a nitrogen-filled flask with precursor solution was directly connected to a HPLC pump. Reactants were injected into the reactor body by HPLC pump while the desired temperature and pressure were reached. A stir-bar was rotating during the reaction and the nanowire reaction became a CSTR-type reaction which the reactant concentration in the reactor kept constant when the reaction reached equilibrium. After a nanowire synthesis reaction, the stir-bar was removed and synthesized nanowires were deposited on the reactor walls and were collected by further treatment. Previous study of high yield silicon nanowire synthesis in supercritical benzene is promising for pushing the amount of produced Si nanowires to gram scale using this 250 ml Parr reactor. Benzene will be used to replace hexane as a reaction solvent since it can enhance the decomposition of MPS and reaction parameters might need to be re-adjusted for scale-up system.

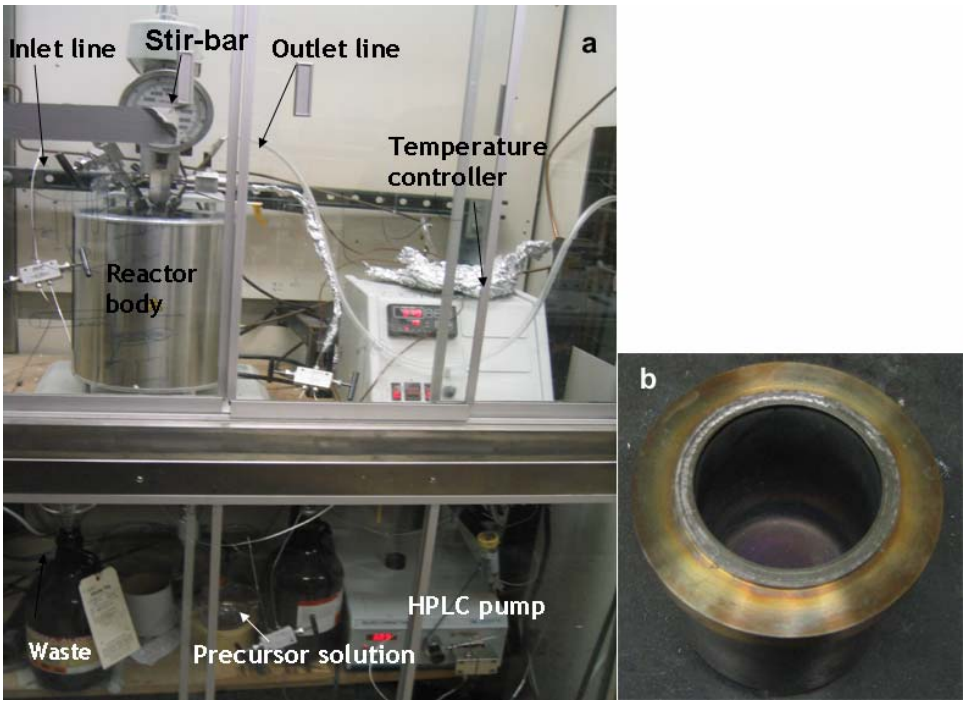

Figure 7.1. A 250 ml Parr reactor apparatus for scale-up supercritical fluid nanowire synthesis. (a) reactor design and (b) a 250 ml reactor cell.

7.2.2 Chemical Surface Passivation of Silicon Nanowires

The study of chemical surface passivation of silicon nanowires is very important for two reasons: (1) surface stability of Si nanowires highly affects their chemical and electronic property. (2) nanowire dispersibility in variety of organic solvents is critical for deposition processing methods such as spoin-coating, inkjet printing and imprint lithography for device fabrications. Hydrophobic organic surfactant capped-silicon nanowires were preferred since they can allow nanowires disperse in organic solvent and are with stable chemical and electronic properties. Alkenthiols (for example, dodecanethiol) and alkene (for example, hexene) are

suggested as organic ligands since they can form strong linkage with Si and the passivated silicon nanowires will be with hydrophobic characteristics. The surface states of Si nanowires will be characterized using X-ray photoelectron spectroscopy (XPS)

7.2.3 Germanium Telluride Nanowire Synthesis

Germanium Telluride (GeTe) has the characteristic of temperature-dependent phase transition behavior. Amorphous GeTe can be changed to crystalline by heating the temperature above glass transition temperature ~145 ˚C and converted back to amorphous by cooling the temperature. Using their different resistances in different states and the fast response conversion of crystal-amorphous state, GeTe can be used a material for next generation non-volatile memory, replacing current slow-response and high voltage driven flash drives. GeTe nanowire provides an ideal platform to study the device performance of non-volatile device made by one-dimensional nanomaterials. GeTe nanowire synthesis has been previously reported by Park et al, using Au nanoparticles to seed GeTe nanowires in chemical vapor deposition (CVD) technique. However, GeTe nanowire synthesis in solution phase has not been reported. I will recommend use Au or Bi nanoparitcles as seeds to synthesize GeTe nanowires using diphenylgermane and TOP-Te as precursors in supercritical fluid since Au-GeTe (480 ˚C) and Bi-GeTe (~300 ˚C) has relatively low eutectic temperature based on binary phase diagram.

Bibliography

A. Colli, S. Hofmann, A. C. Ferrari, C. Ducati, F. Martelli, S. Rubini, S. Cabrini, A. Franciosi, J. Robertson, Appl. Phys. Lett. 2005, 86, 153103.

A. Ghezelbash, B. A. Korgel, Langmuir 2005, 21, 9451.

A. I. Persson, M. W. Larsson, S. Stenstroem, B. J. Ohlsson, L. Samuelson, L. R. Wallenberg, Nature Mater. 2004, 3, 677.

Adachi, M.; Harada, T.; Harada, M. Langmuir 1999, 15, 7097-7100.

Ajayan, P. M.; Stephan, O.; Redlich, Ph.; Colliex, C. Nature 1995, 375, 564-567.

Amelinckx, S.; Zhang, X. B.; Bernaerts, D.; Zhang, X. F.; Ivanov, V.; Nagy, J. B. Science 1994, 265, 635-639.

B. A. Korgel, Science 2004, 303, 1308-1309.

Bakkers, E. P. A. M.; Verheigen, M. A. J. Am. Chem. Soc. 2003, 125, 3440-3441.

Baral, S.; Schoen, P. Chem. Mater. 1993, 5, 145-147.

Bethune, D. S.; Kiang, C. H.; de Vries, M. S.; Gorman, G.; Savoy, R.; Vazquez, J.;

Beyers, R. Nature 1993, 363, 605-607.

Binary Alloy Phase Diagram, 2nd ed,; ASM Internation: Materials Park OH. 1990; Vo.1.

Bird, R. B.; Stewart, W. E.; Lightfoot., E. N., Wiley, 2002.

Bjork, M. T.; Ohlsson, B. J.; Sass, T.; Persson, A. I.; Thelander, C.; Magnusson, K.; Deppert, M. H.; Wallenberg, L.; Samulson, L. Nano Lett. 2002, 2, 87.

Britz, D. A.; Khlobystov, A. N.; Porfyrakis, K.; Ardavan, A.; Briggs, G. A. D. Chem. Commun. 2005, 37-39.

Bu, W. B.; Hua, Z.; Chen, H. R.; Shi, J. L. J. Phys. Chem. B 2005, 109, 14461.

C. A. Stowell, B. A. Korgel, Nano Lett. 2005, 5, 1203.

C. B. Murray, S. Sun, H. Doyle, T. Betley, MRS Bull. 2001, 26, 985.

Castro, T.; Reifenberger, R.; Choi, E.; Andres, R. P. Phys. Rev. B 1990, 42, 8548-8556. Chem. Soc. 2001, 123, 7797-7803.

Chen, P.; Xie, S.; Ren, N.; Zhang, ,Y.; Dong, A.; Chen, Y.; Tang, Y. J. Am. Chem. Soc. 2006, 128, 1470-1471.

Chopra, N. G.; Luyken, R. J.; Cherrey, K.; Crespi, V. H.; Cohen, M. L.; Louie, S. G.; Zettl, A. Science 1995, 269, 966-967.

Colder, A.; Huisken, F.; Trave, E.; Ledoux, G.; Guillois, O.; Reynaud, C.;

Hofmeister, H.; Pippel, E. Nanotechnology, 2004, 15, L1-L4.

Coutant RW, Levy A., A Aerospace Research laboratories, 69-215 Oct 1965

Cozzoli, P. D.; Pellegrino, T.; Manna, L. Chemical Society Reviews 2006, 35, 1195-1208.

CRC Handbook of Chemistry and Physics 85th, edited by David R. Lide, 2004).

Cui, Y.; Lieber, C. M. Science 2001, 291, 851-853.

Cui, Y.; Wei, Q.; Park, H.; Lieber, C. M. Science 2001, 293, 1289-1292.

D. C. Lee, B. A. Korgel, Mol. Simul. 2005, 31, 637.

D. C. Lee, F. V. Mikulec, B. A. Korgel, J. Am. Chem. Soc. 2004, 126, 4951-4957.

D. C. Lee, T. Hanrath, B. A. Korgel, Angew. Chem. Int. Ed. 2005, 44, 3573.

D. D. Fanfair, B. A. Korgel, Cryst. Growth & Des. 2005, 5, 1971-1976.

D. Fanfair, B. A. Korgel, Cryst. Growth & Des. 2005, 5, 1971-1976.

D. W. Wang, H. J. Dai, Angew. Chem. Intl. Ed. 2002, 41, 4783-4786.

Daiguji, H.; Yang, P.; Szeri, A. J.; Majumdar, A. Nano Letters 2004, 4, 2315-2321.

Davidson, F. M., III; Schricker, A. D.; Wiacek, R. J.; Korgel, B. A. Adv. Mater. 2004, 16, 646-649.

Davidson, F. M., III; Wiacek, R.; Korgel, B. A. Chem. Mater. 2005, 17, 230-233.

Davidson, F. M.; Lee, D. C.; Fanfair, D. D.: Korgel, B. A. J. Phys. Chem. C 2007, 111, 2929-2935.

Dixon, D. J.; Johnston, K. P. In Encyclopedia of Separation;

Dloczik, L.; Engelhardt, R.; Ernst, K.; Fiechter, S.; Sieber, I.; Könenkamp, R. Appl. Phys. Lett. 2001, 78, 3687-3689.

Dong, Z. W.; Zhang, C. F.; Deng, H.; You, G. J.; Qian, S. X. Mater. Chem. Phys. 2006, 99, 160-163.

Duan, X. F.; Niu, C. M.; Sahi, V.; Chen, J.; Parce, J. W.; Empedocles, S.; Goldman, J. L. Nature 2003, 425, 274-278.

E. Tutuc, S. Guha, J. O. Chu, Appl. Phys. Lett. 2006, 88, 043113.

Fan, R.; Karnik, R.; Yue, M.; Li, D.; Majumdar, A.; Yang, P. Nano Letters 2005, 5, 1633-1637

Fan, R.; Wu, Y.; Li, D.; Yue, M.; Majumdar, A.; Yang, P. J. Am. Chem. Soc. 2003, 125, 5254-5255.

Fu, L.; Liu, Z. M.; Liu, Y. Q.; Han, B. X.; Wang, J. Q.; Hu, P.; Cao, L. C.; Zhu, D. B. J. Phys. Chem. B 2004, 108, 13074.

Gasparac, R.; Kohli, P.; Mota, M. O.; Trofin, L.; Martin, C. R. Nano Lett. 2004, 4, 513-516.

Geng, B.; Meng, G.; Zhang, L.; Wang, G.; Peng, X. Chem. Commun. 2003, 2572-2573.

Gerion, D.; Zaitseva, N.; Saw, C.; Casula, M. F.; Fakra, S.; Van Buuren, T.; Galli, G. Nano Lett. 2004, 4, 597-602.

Ghezelbash, A.; Korgel, B. A. Langmuir 2005, 21, 9451-9456.

Givargizov, E. I. J. Crystal Growth 1975, 31, 20-30.

Goldberger, J.; Fan, R.; Yang, P. Acc. Chem. Res. 2006, 39, 239-248.

Goldsmid, H. J. Diffusion in Semiconductors 1963, Inspec, London.

Gopalakrishnan, G.; Segura, J.-M.; Stamou, D.; Gaillard, C.; Gjoni, M.; Hovius, R.; Schenk, K. J.; Stadelmann, P. A.; Vogel, H. Angew. Chem. Int. Ed. 2005, 44, 4957-4960.

Gudiksen, M. S.; Lauhon, L. J.; Wang, J.; Smith, D. C.; Lieber, C. M. Nature 2002, 415, 617.

Gur, I.; Fromer, N. A.; Geier, M. L.; Alivisatos, A. P. Science 2005, 310, 462-465.

H. Adhikari, A. F. Marshall, C. E. D. Chidsey, P. C. McIntyre, Nano Lett. 2006, 6, 318-232.

H. akizawa ; Uheda, K.; Endo, T. Journal of Alloys and Compounds 2000, 305, 306-310.

H. J. Dai, J. Kong, C. W. Zhou, N. Franklin, T. Tombler, A. Cassell, S. S. Fan, M. Chapline, J. Phys. Chem. B 1999, 103, 11246-11255.

H. Yu, J. B. Li, R. A. Loomis, P. C. Gibbons, L. W. Wang, W. E. Buhro, J. Am. Chem. Soc. 2003, 125, 16168-16169.

H.-Y. Tuan, D. C. Lee, T. Hanrath, B. A. Korgel, Chem. Mater. 2005, 17, 5705.

H.-Y. Tuan, D. C. Lee, T. Hanrath, B. A. Korgel, Nano Lett. 2005, 5, 681.

Halls, M. D.; Schlegel, H. B. J. Phys. Chem. B 2002, 106, 1921-1925.

Han, S.; Li, C.; Liu, Z. Q.; Lei, B.; Zhang, D. H.; Jin, W.; Liu, X. L.; Tang, T.; Zhou, C. W. Nano Lett. 2004, 4, 1241.

Hanrath, T.; Korgel, B. A. Adv. Mater. 2003, 15, 437-440.

Hanrath, T.; Korgel, B. A. J. Am. Chem. Soc. 2002, 124, 1424-1429.

Hanrath, T.; Korgel, B. A. Small 2005, 1, 717-721.

Heath, J. R.; LeGoues, F. K. Chem. Phys. Lett. 1993, 208, 263-268.

Hofmann, S.; Sharma, R.; Ducati, C.; Du, G.; Mattevi, C.; Cepek, C.; Cantoro, M.; Pisana, S.; Parvez, A.; Cervantes-Sodi, F.; Ferrari, A. C.; Dunin-Borkowski,

R.; Lizzit, S.; Petaccia, L.; Goldoni, A.; Robertson, J. Nano Lett. 2007, 7, 602-608.

Holmes, J. D.; Johnston, K. P.; Doty, R. C.; Korgel, B. A. Science 2000, 287, 1471-1473.

Holmes, J. D.; Lyons, D. M.; Ziegler, K. J. Chem. Eur. J. 2003, 9,2144-2156.

Holmes, J. D.; Ziegler, K. J.; Doty, R. C.; Pell, L. E.; Johnston, K. P.; Korgel, B. A. J. Am. Chem. Soc. 2001, 123, 3743-3748.

Hoyer, P. Langmuir 1996, 12, 1411-1413.

Hsieh, Y. F.; Chen, L. J.; Marshall, E. D.; Lau, S. S. Thin Solid Films 1988, 162, 287-294.

Hsu, Y. J.; Lu, S. Y. Chem. Commun. 2004, 2102.

Hu, J. Q.; Bando, Y.; Liu, Z. W.; Sekiguchi, T.; Golberg, D.; Zhan, J. H. J. Am. Chem. Soc. 2003, 125, 11306.

Hu, J. Q.; Bando, Y.; Zhan, J. H.; Golberg, D. Adv. Mater. 2005, 17, 1964.

Hu, J. T.; Odom, T. W.; Lieber, C. M. Acc. Chem. Res. 1999, 32, 435-445.

Hu, J.-Q.; Meng, X.-M.; Jiang, Y.; Lee, C.-S.; Lee, S. T. Adv. Mater. 2003, 15, 70-73.

Huang, Y.; Duan, X. F.; Lieber, C. M. Small 2005, 1, 142-147.

Hulteen, J. C.; Jirage, K. B.; Martin, C. R. J. Am. Chem. Soc.1998, 120, 6603-6604.

Huynh, W. U.; Dittmer, J. J.; Alivisatos, A. P. Science 2002, 295, 2425-2427.

Iijima, S. Nature 1991, 354, 56-58.

J. D. Holmes, K. P. Johnston, R. C. Doty, B. A. Korgel, Science 2000, 287, 1471-1473.

J. T. Hu, T. W. Odom, C. M. Lieber, Acct. Chem. Res. 1999, 32, 435-445.

J. W. Grebinski, K. L. Hull, J. Zhang, T. H. Kosel, M. Kuno, Chem. Mater. 2004, 16, 5260.

Jang, J.; Yoon, H. Adv. Mater. 2004, 16, 799-802.

Jayaraman, K.; Okamoto, K.; Son, S. J.; Luckett, C.; Gopalani, A. H.; Lee, S. B.; English, D. S. J. Am. Chem. Soc. 2005, 127, 17385-17392.

Jiang, X.; Mayers, B.; Herricks, T.; Xia, Y. Adv. Mater. 2003, 15, 1740-1743.

Jun, Y. W.; Choi, J. S.; Cheon, J. Angewandte Chemie-International Edition 2006, 45, 3414-3439.

Jung, J. H.; Lee, S.-H.; Yoo, J. S.; Yoshida, K.; Shimizu, T.; Shinkai, S. Chem. Eur. J. 2003, 9, 5307-5313.

Jung, J. H.; Shinknai, S.; Shimizu, T. Chem. Mater. 2003, 15, 2141-2145.

Jung, J. H.; Yoshida, K.; Shimizu, T. Langmuir 2002, 18, 8724-8727.

Jung, S. W.; Park, W. I.; Yi, G. C.; Kim, M. Adv. Mater. 2003, 15, 1358.

K. A. Dick, K. Deppert, T. Mrtensson, B. Mandl, L. Samuelson, W. Seifert, Nano Lett. 2005, 5, 761.

Kamins, T. I.; Williams, R. S.; Basile, D. P.; Hesjedal, T.; Harris, J. S. J. Appl. Phys. 2001, 89, 1008-1016.

Kasuga, T.; Hiramatsu, M.; Hoson, A.; Sekino, T.; Niihara, K. Langmuir 1998, 14, 3160-3163.

Khlobystov, A. N.; Britz, D. A.; Briggs, G. A. D. Acc. Chem. Res. 2005, 38, 901-909.

Kohno, H.; Takeda, S. Jpn. J. Appl. Phys. 2002, 41, 577-578.

Korgel, B. A.; Hanrath, T.; Davidson, F. M. in Encyclopedia of Chemical Processing 1(1) (ed Lee, S. K. B.) 3191-3203 (Marcel Dekker, 2006).

Korgel, B. A.; Lee, D. C.; Hanrath, T.; Yacaman, M. J.; Thesen, A.; Matijevic, M.; Kiaas, R.; Kisielowski, C.; Diebold, A. C., IEEE Transactions on Semiconductor Manufacturing 2006, 19, 391-396.

Kuang, Q.; Jiang, Z. Y.; Xie, Z. X.; Lin, S. C.; Lin, Z. W.; Xie, S. Y.; Huang, R. B.;

Zheng, L. S. J. Am. Chem. Soc. 2005, 127, 11777.

Lakshmi, B. B.; Dorhout, P. K.; Martin, C. R. Chem. Mater. 1997, 9, 857-862.

Lauhon, L. J.; Gudiksen, M. S.; Lieber, C. M. Philos. Trans. R. Soc. London A 2004, 362, 1247.

Lauhon, L. J.; Gudiksen, M. S.; Wang, D.; Lieber, C. M. Nature 2002, 420, 57.

Law, M.; Goldberger, J.; Yang, P. Annu. Rev. Mater. Res. 2004, 34, 83-122.

Law, M.; Greene, L. E.; Johnson, J. C.; Saykally, R.; Yang, P. D. Nature Mater. 2005, 4, 455-459.

Lee, D. C.; Hanrath, T.; Korgel, B. A. Angew. Chem. Int. Ed. 2005, 44, 3573-3577.

Lee, D. C.; Korgel, B. A. Mol. Simul. in press.

Lee, D. C.; Mikulec, F. V.; Korgel, B. A. J. Am. Chem. Soc. 2004, 126, 4951-4957.

Lee, S. B.; Mitchell, D. T.; Trofin, L.; Nevanen, T. K.; Soderlund, H.; Martin, C. R. Science 2002, 296, 2198-2200.

Lei, B.; Li, C.; Zhang, D. H.; Han, S.; Zhou, C. W. J. Phys. Chem. B 2005, 109, 18799.

Levy A, Coutant R.W., Maeryman E.L., Trent D.E., Aerospace Research laboratories, 65-64 1965 April

Li, C.; Liu, Z.; Gu, C.; Xu, X.; Yang, Y. Adv. Mater. 2006, 18, 228-234.

Li, J. Y.; Chen, X. L.; Qiao, Z. Y.; Cao, Y. G.; Li, H. J. Mater. Sci. Lett. 2001, 20, 1987-1988.

Li, Q.; Wang, C. R. Appl. Phys. Lett. 2003, 82, 1398.

Li, Q.; Wang, C. R. J. Am. Chem. Soc. 2003, 125, 9892.

Li, X.; Li, Y.; Li, S.; Zhou, W.; Chu, H.; Chen, W.; Li, I. L.; Tang, Z. Crystal Growth & Design 2005, 5, 911-916.

Li, Y. B.; Bando, Y.; Golberg, D. Adv. Mater. 2004, 16, 93.

Liang, C.; Shimizu, Y.; Sasaki, T.; Umehara, H.; Koshizaki, N. J. Mater. Chem. 2004, 14, 248-252.

Liu, J. S.; Tanaka, T.; Sivula, K.; Alivisatos, A. P.; Frechet, J. M. J. Journal of the American Chemical Society 2004, 126, 6550-6551.

Lourie, O. R.; Jones, C. R.; Bartlett, B. M.; Gibbons, P. C.; Ruoff, R. S.; Buhro, W. E. Chem. Mater. 2000, 12, 1808-1810.

Lu, X. M.; Hanrath, T.; Johnston, K. P.; Korgel, B. A. Nano Letters 2003, 3, 93-99.

Lu, X.; Ziegler, K. J.; Ghezelbash, A.; Johnston, K. P.; Korgel, B. A. Nano Lett. 2004, 4, 969-974.

M. C. McAlpine, R. S. Friedman, S. Jin, K. H. Lin, W. U. Wang, C. M. Lieber, Nano Lett. 2003, 3, 1531-1535.

M. K. Sunkara, S. Sharma, R. Miranda, G. Lian, E. C. Dickey, Appl, Phys. Lett. 2001, 79, 1546.

M. Law, J. Goldberger, P. Yang, Annu. Rev. Mater. Res. 2004, 34, 83.

Ma, Y. W.; Huo, K. F.; Wu, Q.; Lu, Y.N.; Hu, Y. M.; Hu, Z.; Chen, Y. J. Mater. Chem. 2006, 16, 2834-2838.

Macak, J. M.; Tsuchiya, H.; Taveira, L.; Aldabergerova, S.; Schmuki, P. Angew. Chem. Int. Ed. 2005, 44, 7463-7465.

Manna, L.; Scher, E. C.; Li, L. S.; Alivisatos, A. P. J. Am. Chem. Soc. 2002, 124, 7136.

Mantl, S.; Rothman, S. J.; Nowicki, L. J.; Lerner, J. L. J. Phys. F: Metal Phys. 1983, 13, 1441-8.

Mao, Y.; Banerjee, S.; Wong, S. S. Chem. Commun. 2003, 408-409.

Martin, C. R. Science 1994, 266, 1961-1966.

Maynor, B. W.; Li, J. Y.; Lu, C. G.; Liu, J. J. Am. Chem. Soc. 2004, 126, 6409.

Mayya, K. S.; Gittins, D. I.; Dibaj, A. M.; Caruso, F. Nano Lett. 2001, 1, 727-730.

McIlroy, D. N.; Zhang, D.; Kranov, Y.; Norton, M. G. Appl. Phys. Lett. 2001, 79, 1540-1542.

Mitchell, D. T.; Lee, S. B.; Trofin, L.; Li, N. C.; Nevanen, T. K.; Soderlund, H.; Martin, C. R. J. Am. Chem. Soc. 2002, 124, 11864-11865.

Miyaji, F.; Davis, S. A.; Charmant, J. P. H.; Mann, S. Chem. Mater. 1999, 11, 3021-3024.

Morales, A. M. and Lieber, C. M., Science 1998, 279, 208-211.

Murr, E. L. Interfacial Phenomena in Metals and Alloys, Addison-Wesley, Reading, 1975.

Murray, C. B.; Norris, D. J.; Bawendi, M. G. Journal of the American Chemical Society 1993, 115, 8706-8715.

Murray, C. B.; Sun, S.; Doyle, H.; Betley, T. MRS Bull. 2001, 26, 985-991.

Nakamura, H.; Matsui, Y. J. Am. Chem. Soc. 1995, 117, 2651-2652.

Nemetschek, V. Th.; Hofmann, U. Zeitschrift fur Naturforschung 1953, 8b, 410-412.

Ogihara, H.; Sadakane, M.; Nodasaka, Y.; Ueda, W. Chem. Mater. 2006, 18, 4981-4983.

P. Nguyen, H. T. Ng, M. Meyyappan, Adv. Mater. 2005, 17, 1773.

P. S. Shah, T. Hanrath, K. P. Johnston, B. A. Korgel, J. Phys. Chem. B 2004, 108, 9574-9587.

Park, W. I.; Yi, G. C.; Kim, M.; Pennycook, S. J. Adv. Mater. 2003, 15, 526.

Patolsky, F.; Zheng, G. F.; Lieber, C. M. Anal. Chem. 2006, 78, 4260-4269.

Patzke, G. R.; Krumeich, F.; Nesper, R. Angew. Chem. Int. Ed. 2002, 41, 2446-2461.

Pell, L. E.; Schricker, A. D.; Mikulec, F. V.; Korgel, B. A., Langmuir 2004, 20, 6546-6548.

Persson, A. I.; Larsson, M. W.; Stenstroem, S.; Ohlsson, B. J.; Samuelson, L.; Wallenberg, L. R. Nature Mater. 2004, 3, 677-681.

Qu, Y.; Carter, J. D.; Guo, T. J. Phys. Chem. B 2006, 110, 8296-8301.

R. S. Wagner, W. C. Ellis, Appl. Phys. Lett. 1964, 4, 89.

Rao, C. N. R.; Govindaraj, A.; Deepak, F. L.; Gunari, N. A.; Nath, M. Appl. Phys. Lett. 2001, 78, 1853-1855.

Rao, C. N. R.; Satishkumar, B. C.; Govindaraj, A.; Nath, M. ChemPhysChem 2001, 2, 78-105.

Rossi, M. P.; Ye, H. H.; Gogotsi, Y.; Babu, S.; Ndungu, P.; Bradley, J. C. Nano Lett. 2004, 5, 989-993.

Ruthven, D. M., Ed.; John Wiley: New York, 1997, pp 1544-1569.

S. Mathur, H. Shen, V. Sivakov, U. Werner, Chem. Mater. 2004, 16, 2449.

S. P. Ahrenkiel, O. I. Micic, A. Miedaner, C. J. Curtis, J. M. Nedeljkovic, A. J. Nozik, Nano Lett. 2003, 3, 833.

S. Sun, C. B. Murray, D. Weller, L. Folks, A. Moser, Science 2000, 287, 1989.

Satishkumar, B. C.; Govindaraj, A.; Vogl, E. M.; Basumallick, L.; Rao, C. N. R. J. Mater. Res. 1997, 12, 604-606.

Saunders, A. E.; Sigman, M. B., Jr.; Korgel, B. A. J. Phys. Chem. B 2004, 108, 193-199.

Savage, P. E.; Goplan, S.; Mizan, T. I.; Martino, C. J.; Brock, E. E. AIChE Journal 1995, 41, 1723-1778.

Schricker, A. D.; Joshi, S. V.; Hanrath, T.; Banerjee, S. K.; Korgel, B. A. Journal of Physical Chemistry B 2006, 110, 6816-6823.

Shah, P. S.; Hanrath, T.; Johnston, K. P.; Korgel, B. A. J. Phys. Chem. B 2004, 108, 9574-9587.

Smith, D. K.; Lee, D. C.; Korgel, B. A. Chem. Mater. 2006, 18, 3356-3364.

Sun, Y.; Wiley, B.; Li, Z.-Y.; Xia, Y. J. Am. Chem. Soc. 2004, 126, 9399-9406.

Sun, Y.; Xia, Y. Adv. Mater. 2004, 16, 264-268.

T. Hanrath, B. A. Korgel, Adv. Mater. 2003, 15, 437-440.

T. Hanrath, B. A. Korgel, Small 2005, 1, 717-721

T. Hyeon, S. S. Lee, J. Park, Y. Chung, H. B. Na, J. Am. Chem. Soc. 2001,123, 12798.

T. I. Kamins, R. S. Williams, D. P. Basile, T. Hesjedal, J. S. Harris, J. Appl. Phys. 2001, 89, 1008.

T. J. Trentler, K. M. Hickman, S. C. Goel, A. M. Viano, P. C. Gibbons, W. E. Buhro, Science 1995, 270, 1791.

Taylor, B. R.; Fox, G. A.; Hope-Weeks, L. J.; Maxwell, R. S.; Kauzlarich, S. M.; Lee, H. W. H. Mater. Sci. Eng. B 2002, B96, 90-93.

Tenne, R. Angew. Chem. Int. Ed. 2003, 42, 5124-5132.

Tenne, R.; Margulis, L.; Genut, M.; Hodes, G. Nature 1992, 360, 444-446.

Thaddeus, B. M.; Hiroaki, O.; Subramanian, P. R.; Linda, K. Binary Alloy Phase Diagram, , 2nd ed,; ASM Internation: Materials Park OH. 1990; Vo.1.

Trentler, T. J.; Hickman, K. M.; Goel, S. C.; Viano, A. M.; Gibbons, P. C.; Buhro, W. E. Science 1995, 270, 1791-1794.

Tuan, H.-Y.; Lee, D. C.; Hanrath, T.; Korgel, B. A. Chem. Mater. 2005, 17, 5705-5711.

Tuan, H.-Y.; Lee, D. C.; Hanrath, T.; Korgel, B. A. Nano Lett. 2005, 5, 681-684.

Tuan, H.-Y.; Lee, D. C.; Korgel, B. A. Angew. Chem. Int. Ed. 2006, 45, 5184-5187.

V. F. Puntes, D. Zanchet, C. K. Erdonmez, A. P. Alivisatos, J. Am. Chem. Soc. 2002, 124, 12874.

Van Bommel, K. J. C.; Friggeri, A.; Shinkai, S. Angew. Chem. Int. Ed. 2003, 42, 980-999.

Wagner, R. S.; Ellis, W. C. Appl. Phys. Lett. 1964, 4, 89.

Wang, C. R.; Wang, J.; Li, Q.; Yi, G. C. Adv. Funct. Mater. 2005, 15, 1471.

Wang, D.; Dai, H. Angew. Chem. Int. Ed. 2002, 41, 4783-4786.

Wang, F. D.; Dong, A. G.; Sun, J. W.; Tang, R.; Yu, H.; Buhro, W. E. Inorg. Chem. 2006, 45, 7511-7521.

Wang, L.; Major, D.; Paga, P.; Zhang, D.; Norton, M. G.; McIlroy, D. N. Nanotechnology 2006, 17, S298-S303.

Wang, N.; Zhang, Y. F.; Tang, Y. H.; Lee, C. S.; Lee, S. T. Applied Physics Letters 1998, 73, 3902-3904.

Wang, W.; Huang, J.; Ren, Z. Langmuir 2005, 21, 751-754.

Wang, X. D.; Song, J. H.; Li, P.; Ryou, J. H.; Dupuis, R. D.; Summers, C. J.; Wang, Z. L. J. Am. Chem. Soc. 2005, 127, 7920.

Wilcoxon, J. P.; Provencio, P. P.; Samara, G. A. Phys. Rev. B 2001, 64, 035417/1-035417/9.

Wilcoxon, J. P.; Samara, G. A.; Provencio, P. N. Phys. Rev. B 1999, 60, 2704-2714.

Wu, Q.; Hu, Z.; Liu, C.; Wang, X.; Chen, Y. J. Phys. Chem. B 2005, 109, 19719-19722.

Wu, Q.; Hu, Z.; Wang, X.; Lu, Y.; Chen, X.; Xu, H.; Chen, Y. J. Am. Chem. Soc. 2003, 125, 10176-10177.

Wu, Y.; Fan, R.; Yang, P. Nano Lett. 2002, 2, 83-86.

Wu, Y.; Xiang, J.; Yang, C.; Lu, W.; Lieber, C. M. Nature 2004, 430, 61.

Xiong, Y.; Mayers, B. T.; Xia, Y. Chem. Commun. 2005, 5013-5022.

Y. Cui, C. M. Lieber, Science 2001, 291, 851-853.

Y. Ding, P. X. Gao, Z. L. Wang, J. Am. Chem. Soc. 2004, 126, 2066.

Y. Ohno, T. Shirahama, S. Takeda, A. Ishizumi, Y. Kanemitsu, Appl. Phys. Lett. 2005, 87, 043105.

Yang, J.; Liu, Y.-C.; Lin, H.-M.; Chen, C.-C. Adv. Mater. 2004, 16, 713-716.

Ye, C. H.; Zhang, L. D.; Fang, X. S.; Wang, Y.; Yan, P.; Zhao, J. Adv. Mater. 2004, 16, 1019.

Yen, H.-M.; Jou, S.; Chu, C.-J. Mater. Sci. Eng. B 2005, 122, 240-245.

Yin, L. W.; Bando, Y.; Golberg, D.; Li, M. S. Appl. Phys. Lett. 2004, 85, 3869-3871.

Yin, L.-W.; Bando, Y.; Li, M.-S.; Golberg, D. Small 2005, 1, 1094-1099.

Yin, Y.; Alivisatos, A. P. Nature 2005, 437, 664-670.

Yue, L.; Gao, W.; Zhang, D.; Guo, X.; Ding, W.; Chen, Y. J. Am. Chem. Soc. 2006, 128, 11042-11043.

Zhan, J. H.; Bando, Y.; Hu, J. Q.; Liu, Z. W.; Yin, L. W.; Golberg, D. Angew. Chem., Int. Ed. 2005, 44, 2140.

Zhan, J. H.; Bando, Y.; Hu, J. Q.; Sekiguchi, T.; Golberg, D. Adv. Mater. 2005, 17, 225.

Zhang, D.; Alkhateeb, A.; Han, H.; Mahmood, H.; McIlroy, D. M.; Norton, M. G. Nano Lett. 2003, 3, 983-987.

Zhang, H.; Yang, D.; Ma, X.; Que, D. Nanotechnology 2005, 16, 2721-2725.

Zhang, J.; Xu, B.; Yang, Y.; Jiang, F.; Li, J.; Wang, X.; Wang, S. J. Non-Crystalline Solids 2006, 352, 2859-2862.

Zhang, M.; Bando, Y.; Wada, K.; Kurashima, K. J. Mater. Sci. Lett. 1999, 18, 1911-1913.

Zhu, Y.; Li, H.; Koltypin, Y.; Hacohen, Y. R.; Gedanken, A. Chem. Commun. 2001, 2616-2617.

Ziegler, K. J.; Doty, R. C.; Johnston, K. P.; Korgel, B. A. J. Am.

Zou, J.; Baldwin, R. K.; Pettigrew, K. A.; Kauzlarich, S. M. Nano Lett. 2004, 4, 1181-1186.

Zwilling, V.; Aucouturier, M.; Darque-Ceretti, E. Electrochim. Acta 1999, 44, 921.

Zygmunt, J.; Krumeich, F.; Nesper, R. Adv. Mater. 2003, 15, 1538-1541.

Vita

Hsing-Yu Tuan, the sixth and the youngest child of Chin-Hsin Tuang, was born on February 4, 1980 in Hsinchu, Taiwan. Hsing-Yu graduated from National HsinChu Senior High School in Hsinchu, Taiwan, in 1998. He pursed his Bachelor of Science degree in Chemical Engineering at National Tsing Hua University in Taiwan from 1998 to 2002 and graduated with the highest honor in the Engineering school. After graduation, he served one-month military service. In September of 2003, he entered graduate school at the University of Texas at Austin in the Department of Chemical Engineering and pursued hid Ph.D. under the supervision of Dr. Brian A. Korgel researching one-dimensional silicon, germanium, silica, and germanium telluride nanomaterials.

Permanent address: NO6, Lane51, Shida Rd., Hsinchu, Taiwan 300,R.O.C

This dissertation was typed by the author.